Chapter-V
New compounds of molybdenum with 2-pivaloylamino-6-phenacylisoxanthopterin and selected sulfur, nitrogen donating ancillary ligands

Abstract

Seven new molybdenum-ptarin complexes are reported in this chapter. They include one Mo(IV) complex with a metal:pterin ratio of 1:2. Mixed ligand molybdenum (IV) complexes have also been isolated using suitable ancillary ligands. Using elemental sulfur as the ancillary ligand, di-μ-sulfido bridged binuclear Mo(VI) complex could be isolated. Reaction of the Mo(IV) complex possessing no ancillary ligand, with Me_3NO afforded a μ-oxo bridged binuclear Mo(V) complex. Most of these compounds have been obtained from a Mo(VI) starting material ($Na_2MoO_4.2H_2O$), under carefully controlled conditions (e.g., dinitrogen atmosphere / darkness / dinitrogen flow as well as careful choice of ancillary ligands). Flash chromatographic purification led to the isolation of pure compounds. They have been characterized by elemental analysis, different spectroscopic methods as well as cyclic voltammetry. Reactivities of the Mo(IV) complexes with an enzyme substrate like Me_3NO have been studied and relevant kinetic parameters have been evaluated.

Introduction

Pterins (2-amino-4-oxopteridines) are present in a wide range of redox enzymes containing metals like Fe, Mo, W etc. The pyrazine moiety of this ligand (i.e., pterins) can exist in several oxidation state and thereby facilitates the biological redox activity. In this chapter as well, the prime interest centered on molybdenum in its biologically relevant oxidation states (VI,V,VI). Here a slight variation of the side chain of the pterin ligand is introduced and a series of new compounds have been synthesized. They have been used to study the reactivity towards the enzyme substrate like $Me_3N{\rightarrow}O$ or substrate analogue like PPh_3. The schematic structures of the tautomers of the pterin ligand [$H_2L^3.H_2O$] are depicted in Scheme (V-1) below.

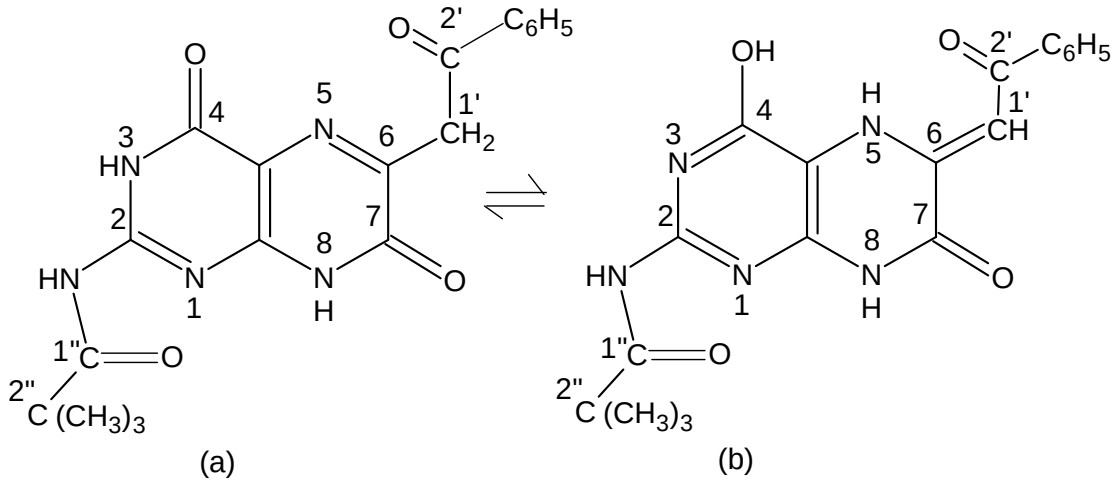

Scheme (V-1): Structural formulae of the two tautomeric forms of the pterin ligand [$H_2L^3.H_2O$].

The ancillary ligands used here are as follows (abbreviations used are given in the parenthesis):

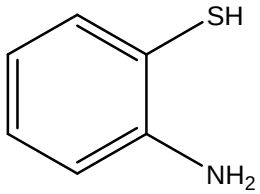

2-Aminothiophenol [H(atp), C_6H_7NS, F.W. 125.19];

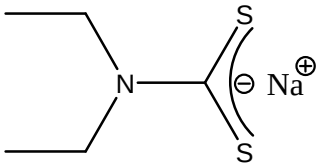

Sodium diethyldithiocarbamate [Na(dedtc).$3H_2O$, $C_5H_{17}NS_2O_3Na$, F.W. 208.27)

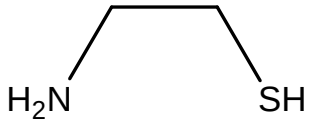

2-Aminoethanethiol [H(aet), C_2H_7NS, F.W. 77.15]

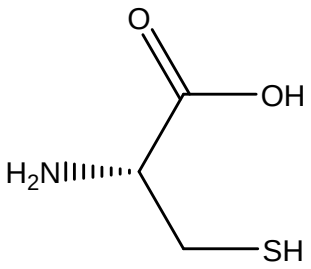

L-cysteine [H_2(cys), $C_3H_7NO_2S$, F.W. 121.16].

Scheme (V-2)

Experimental

Materials

Extra pure AR grade solvents were used as received. Pivalic anhydride, trimethylamine N-oxide and triphenyl phosphine were obtained from Aldrich, USA and Riedel – Hannover respectively. 8-Hydroxyquinoline (oxine), 2-aminothiophenol, L-cysteine were purchased from reliable chemical companies. Silica gel (230-400 mesh) for flash chromatography (dried at 453K for 6 h before use) and silica gel (GF254) for TLC were procured from SRL, Mumbai.

Methods

All the synthetic steps were carried out under the dinitrogen atmosphere using the Schlenk procedure [Fig. (III-1)]; the flash chromatography was performed under the dinitrogen flow as well [Fig. (III-2)] [42,43]. A paraffin oil bath afforded controlled heating conditions.

Synthesis

2-pivaloylamino-6-phenacylisoxanthopterin monohydrate (H_2L^3. H_2O)

The starting material 6-phenacyl-isoxanthopterin was obtained in 78% yield by modifying its original synthetic method in the light of subsequent developments (e.g., darkness, dinitrogen atmosphere) [24]. After that, the desired ligand (H_2L^3. H_2O) was prepared by boiling under reflux a mixture of 6-phenacyl-isoxanthopterin (0.50g, 1.68 mmol) and pivalic anhydride (9.3g, 50 mmol) in controlled conditions (6h, dinitrogen atmosphere, paraffin oil bath at 473K) [1(a), 25]. The reaction mixture was evaporated in a rotary evaporator (363 K, 15 mm Hg), the deep

brown crude product was purified by the flash chromatography using CH_2Cl_2:CH_3OH (9:1 v/v) as eluant, the final product was recovered through the evaporation of solvent, and dried in vacuo over P_4O_{10} ; yield 70%. Its purity was checked through TLC (UV lamp). (Found: C, 57.5; H, 5.0; N, 17.6; $C_{19}H_{21}N_5O_5$ (399.4) calcd.: C, 57.1; H, 5.3; N, 17.5%) UV/VIS (CH_3OH) [λ_{max}/nm (log ε)]: 242sh (4.20), 285sh (4.06), 338(3.89), 387(4.06), 431sh (3.83).

$[Mo^{IV}(L^3)_2].3CH_3OH$ (1)

A solution of the 2-pivaloylamino-6-phenacylisoxanthopterin monohydrate [$H_2L^3.H_2O$, 0.2g, 0.52 mmol] in CH_3OH (50 mL) was treated with a solution of $Na_2MoO_4.2H_2O$ (0.063 g, 0.26 mmol) in H_2O (5 mL), pH of the mixture was adjusted to 5.5 by the addition of 3N HCl and then the solution was boiled (paraffin oil bath) under reflux in the dark and dinitrogen atmosphere for 6h. The orange-yellow solution was evaporated in a rotary evaporator, the residue was purified through flash chromatography using CH_2Cl_2:CH_3OH (95:5 v/v) as eluant, the pertinent compound was obtained after evaporation of the solvent and dried in vacuo over P_4O_{10}; yield 29%. Its purity was checked through TLC (UV lamp). (Found: C, 51.7; H, 5.2; N, 14.3; $MoC_{41}H_{46}N_{10}O_{11}$(950.81) calcd,: C, 51.8; H, 4.9; N, 14.7%). It is diamagnetic. UV/VIS (CH_3OH) [λ_{max}/nm (log ε)]: 218(4.14), 261 (3.91), 311sh(3.61), 325sh(3.52), 386(3.74), 439sh(3.27). Λ_M ($ohm^{-1}cm^2mol^{-1}$) = 6.5(CH_3OH) at 293K is consistent with the formulation as noneletrolyte [21]. The schematic structure of the complex is shown below in Scheme (V-3).

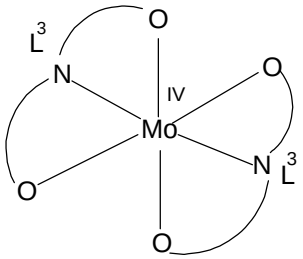

Scheme (V-3)

$(PPh_4)[Mo^{IV}(L^3)_2(dedtc)].CH_3OH$ (2)

To an aqueous solution (10 ml) of $Na_2MoO_4.2H_2O$ (0.06g, 0.25 mmol), a methanolic solution (60 ml) of 2-pivaloylamino-6-phenacylisoxanthopterin monohydrate [$H_2L^3.H_2O$, 0.2g, 0.5 mmol] was added; pH was adjusted to 5.3 by 3N HCl. It was refluxed at 345K under dinitrogen and darkness for 6h. The solvents were removed in a rotary evaporator. After

redissolving it in methanol, sodium diethyldithiocarbamate [Na(dedtc).3H_2O, 0.058g, 0.26 mmol] was added; warmed at 315K and stirred for 1h under dinitrogen and darkness. Then tetraphenyl phosphonium bromide [PPh_4Br, 0.105 g, 0.25 mmol] was added and stirred for 1h under the same condition. Solvent was removed in a rotary evaporator and the crude product was subjected to flash chromatography for purification. Desired product was obtained by using the eluant CH_2Cl_2 : CH_3OH (98:2 v/v). The final orange red product was obtained by removing the solvent in a rotary evaporator and dried over P_4O_{10} in vacuo. Purity was checked by TLC (UV lamp). Yield 50%. (Found C, 59.78; H, 5.0; N 11.10; $MoC_{68}H_{68}N_{11}O_9S_2P$ (1374.39) calcd.: C, 59.43; H, 4.99; N 11.21). It is diamagnetic. UV/VIS (CH_3OH) [λ_{max}/nm (log ε): 255(4.52), 288sh(4.21), 388(4.14), and 450sh(3.69). The compound is fluorescent. The schematic structure of the complex is shown by Scheme (V-4) below.

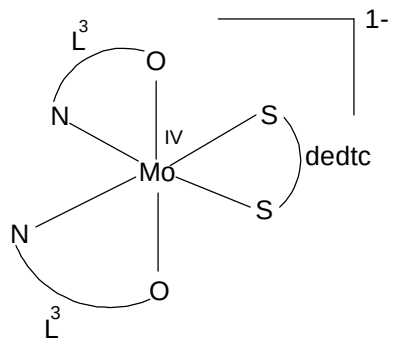

Scheme (V-4)

(PPh_4)[$Mo^{IV}(L^3)_2$(atp)].CH_3OH (3)

A methanolic solution (60 ml) of 2-pivaloylamino-6-phenacylisoxanthopterin monohydrate [$H_2L^3.H_2O$, 0.26 g, 0.66 mmol] was added to an aqueous solution (10ml) of $Na_2MoO_4.2H_2O$ (0.08g, 0.33 mmol) and pH of the resulting solution was adjusted to 5.3 by 3N HCl. Then it was boiled under reflux at 351K for 6h under darkness and dinitrogen atmosphere. The solvent was removed in a rotary evaporator. After dissolving this intermediate product in methanol, 2-aminothiophenol [H(atp), 0.041 g, 0.33 mmol] was added and stirred at 413K under darkness and dinitrogen atmosphere for 1h. Then tetraphenylphosphonium bromide [PPh_4Br, 0.138 g, 0.33 mmol] was added to reaction medium and stirred for 1.5h under the same condition. The crude product was obtained by evaporating the solvent in a rotary evaporator, purified through flash chromatography and the final reddish yellow product was obtained using the solvent CH_2Cl_2 : CH_3OH (98:2 v/v) as eluant. It was dried in vaccuo over P_4O_{10}. Purity was

checked by TLC (UV lamp). Yield 60%. (Found C, 61.78; H, 4.31; N 11.10; $MoC_{69}H_{64}N_{11}O_9SP$ (1350.29) calcd.: C, 61.37; H, 4.78; N, 11.41). It is diamagnetic. UV/VIS (CH_3OH) [λ_{max}/nm (log ε): 231 sh(3.98), 256 (3.95), 297 sh(3.77), 390 (3.34) and 483 sh (3.01). The schematic structure of the complex is shown in Scheme (V-5).

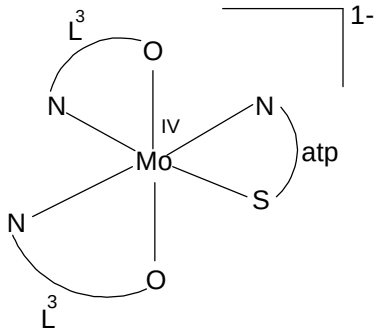

Scheme (V-5)

$(PPh_4)[Mo^{IV}(L^3)_2(aet)].CH_3OH$ (4)

A methanolic solution (60ml) of 2-pivaloylamino-6-phenacylisoxanthopterin monohydrate [$H_2L^3.H_2O$, 0.26 g, 0.66 mmol] was mixed with an aqueous solution (10 ml) of $Na_2MoO_4.2H_2O$ (0.08g, 0.33 mmol) and pH of the resulting solution was adjusted to 5.3 by 3N HCl. Then it was boiled under reflux at 345K for 6h under darkness and dinitrogen atmosphere. The solvent was removed in a rotary evaporator. After dissolving this intermediate product in methanol, 2-aminoethanethiol [H(aet), 0.025 g, 0.33 mmol] was added stirred at 299K under darkness and dinitrogen atmosphere for 1h. Then tetraphenylphosphonium bromide [PPh_4Br, 0.138 g, 0.33 mmol] was added to reaction medium and stirred for 1h at the same condition. The crude product was obtained by evaporating the solvent in a rotary evaporator purified through flash chromatography and the final reddish product was obtained using the solvent CH_2Cl_2 : CH_3OH (98:2 v/v) as eluant. It was dried in vaccuo over P_4O_{10}. Purity was checked by TLC (UV lamp). Yield 65%. (Found C, 60.23; H, 4.31; N 12.18; $MoC_{65}H_{64}N_{11}O_9SP$ (1302.24) calcd.: C, 59.95; H, 4.95; N, 11.83). It is diamagnetic. UV/VIS (CH_3OH) [λ_{max}/nm (log ε): 258 sh(4.18), 294 sh(4.05), 384.5 (4.02), and 460 sh(3.49). The schematic structure of the complex is shown by Scheme (V-6) below.

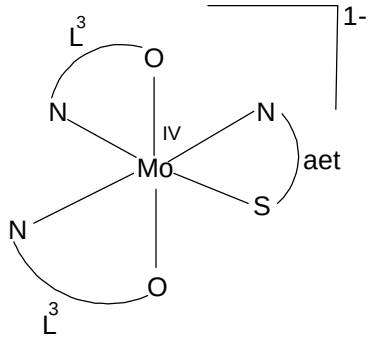

Scheme (V-6)

$(PPh_4)[Mo^{IV}(L^3)\ (HL^3)\ (cys)].CH_3OH$ (5)

To an aqueous solution (10 ml) of $Na_2MoO_4.2H_2O$ (0.08g, 0.33 mmol), methanolic solution (60ml) of 2-pivaloylamino-6-phenacylisoxanthopterin monohydrate [$H_2L^3.H_2O$, 0.26g, 0.66 mmol] was added, pH was adjusted to 5.3 by 3N HCl. It was refluxed at 345K under dinitrogen and darkness for 6h. Solvent was removed in a rotary evaporator. After dissolving it in methanol, L-cysteine [H_2(cys), 0.039g, 0.33 mmol) was added, warmed at 308K and stirred for 1h under dinitrogen and darkness. Then tetraphenylphosphonium bromide [PPh_4Br, 0.138 g, 0.33 mmol] was added and stirred for 1h under the same condition. Solvent was removed in a rotary evaporator and the crude product was subjected to flash chromatography for purification. The desired product was obtained by using the eluant of CH_2Cl_2 : CH_3OH (95:5 (v/v). The final brown product was obtained by removing the solvent in a rotary evaporator and dried over P_4O_{10} in vacuo. Purity was checked by TLC (UV lamp). Yield 60%. (Found C, 59.78; H, 4.45; N 11.62; $MoC_{66}H_{65}N_{11}O_{11}SP$ (1346.26) calcd.: C, 58.88; H, 4.79; N 11.44). It is diamagnetic. UV/VIS (CH_3OH) [λ_{max}/nm (log ε): 234 sh(3.83), 258 sh(3.55), 297 sh(3.39), 385 (3.36) and 470 sh(2.90). The schematic structure of the complex is shown in Scheme (V-7) below.

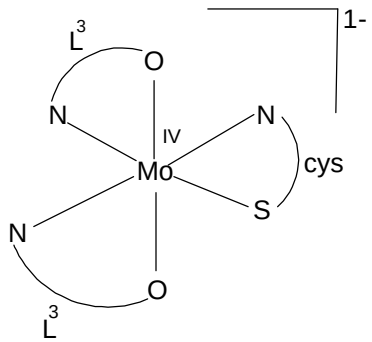

Scheme (V-7)

$[(CH_3O)_2(L^3)Mo^{VI}$-μ$(S)_2$- $Mo^{VI}(L^3)_2]$ (6)

A methanolic solution (60 ml) of 2-pivaloylamino-6-phenacylisoxanthopterin monohydrate [$H_2L^3.H_2O$, 0.26 g, 0.66 mmol] was mixed with an aqueous solution (10 ml) of $Na_2MoO_4.2H_2O$ (0.08g, 0.33 mmol) and pH of the resulting solution was adjusted to 5.3 by 3N HCl. Then it was boiled under reflux at 345K for 6h under darkness and dinitrogen atmosphere. The solvent was removed by a rotary evaporator. After dissolving this intermediate product in methanol, molecular sulphur [0.021 g, 0.66 mmol] was added stirred at 313K under darkness and dinitrogen atmosphere for 2h. The crude product thus obtained by evaporating the solvent by a rotary evaporator purified through flash chromatography and the final reddish product was obtained using the solvent mixture CH_2Cl_2 : CH_3OH (95:5 (v/v). It was dried in vaccuo over P_4O_{10}. Purity was checked by TLC (UV lamp). Yield 60%. (Found C, 48.40; H, 4.10; N 14.18; $Mo_2C_{59}H_{57}N_{15}O_{14}S_2$ (1456.19) calcd.: C, 48.66; H, 3.95; N, 14.43). It is diamagnetic. UV/VIS (CH_3OH) [λ_{max}/nm (log ε): 255(4.44), 260 sh(4.34), 294(4.14), 380(4.02) and 470 sh (3.57). The schematic structure of the complex is shown by Scheme (V-8) below.

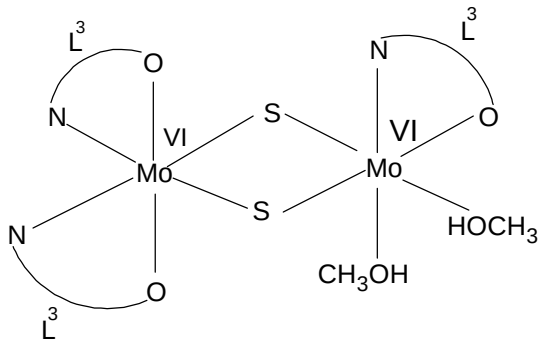

Scheme (V-8)

$[(L^3)_2Mo^V$-μ(O)-$Mo^V(L^3)_2]$. CH_3OH (7)

A solution of compound **(1)** (0.057 g, 0.06 mmol) in CH_3OH (60 mL) was stirred (in the dark) with trimethylamine N-oxide (0.0045 g, 0.06 mmol) for 60h (first 24h at 302K and the rest period at 313K); the gaseous product of the reaction, i.e., Me_3N (b.p. 276K) was driven off by a gentle flow of dry dinitrogen gas over the entire period into another flask containing a measured excess of perchloric acid in glacial acetic acid and the carrier gas escaped to the atmosphere through a silicone oil bubbler. Finally, the residual excess of perchloric acid was back titrated

using a standard sodium acetate solution [26]. For two moles of compound **(1)** added, ca. 0.85mol of Me_3N was recovered, indicating a reaction represented by Equation V-1 below.

2 compound **(1)** + $Me_3N{\rightarrow}O \rightleftharpoons$ [2 compound **(1)**.$Me_3N{\rightarrow}O$] $\longrightarrow$ Me_3N +

μ-oxoMo(V) compound **(7)**……Equation. (V-1)

The solution in the reaction flask was evaporated in a rotary evaporator; the residue was purified through flash chromatography using CH_2Cl_2:CH_3OH (93:7 v/v) as eluant. The relevant fraction (purity was checked through TLC) was evaporated once again and the residue was dried over P_4O_{10} in vacuo and the reddish-yellow final product was isolated. (Found: C, 52.4; H, 4.0; N,15.7; $Mo_2C_{77}H_{72}N_{20}O_{18}$ (1757.4) calcd : C, 52.6; H, 4.1;N, 15.9%). It is diamagnetic. UV/VIS (CH_3OH): [λ_{max}/nm (log ε)]: 210 (5.29), 249.5sh (5.22), 292sh (5.01), 346 (4.93), 383.5 (5.08), 445sh (4.28). The reaction pathway of the formation of compound **(7)** may be schematically represented by Scheme (V-9) below.

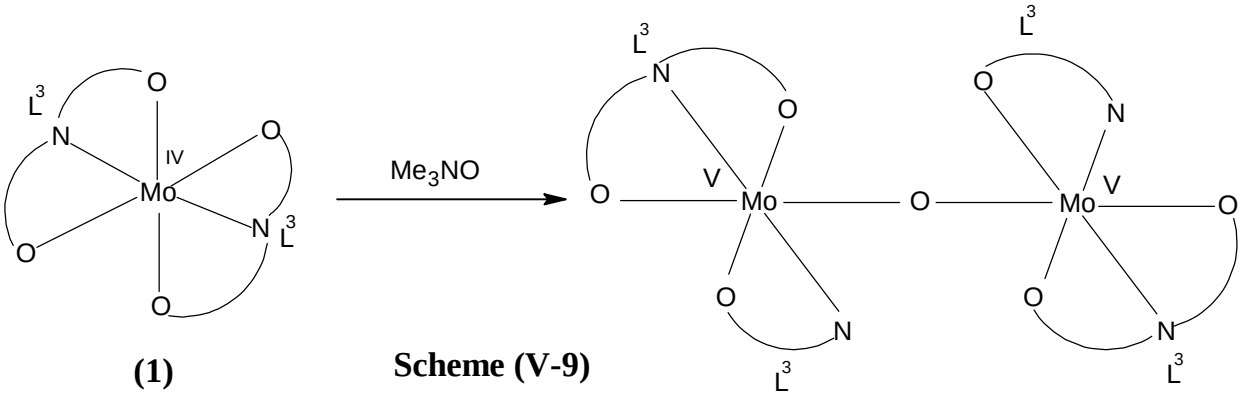

(1) **Scheme (V-9)** **(7)**

Results and Discussion

Here all the compounds, i.e., **1, 2, 3, 4, 5, 6** and **7** have been synthesized in dinitrogen atmosphere [Schlenk system, Fig. (III-1)], under subdued light and controlled heating on a paraffin oil bath. They have been also purified through flash chromatography [Fig. (III-2)] using suitable solvent mixture as elutant. Microanalytical data as well as spectroscopic data satisfy the compositions of these compounds, represented in the Scheme (V-3) to (V-9). Although a Mo(VI) starting material (e.g., $Na_2MoO_4.2H_2O$) has been used in most cases, compounds **(1)** to **(5)** possess a Mo(IV) center; the pterin ligand (H_2L^3. H_2O) acts both as a reducing agent and a complex forming agent here. As delineated here in terms of ^{1}H-NMR and fluorescence spectral data, the pterin ligand residue $(L^3)^{2-}$ is in a oxidized/ aromatic state. Using elemental sulfur as a

reactant a di-μ-sulfido bridged binuclear Mo(VI) compound **(6)** could be obtained. Reaction of compound **(1)** with Me_3NO affords a μ-oxo bridged Mo(V) dimeric complex [compound **(7)**]

ESIMS data

Electrospray ionization mass spectra (ESIMS) involving a soft ionization technique, help to elucidate the structure of these compounds [11]. ESIMS data of $H_2L^3.H_2O$ shows the characteristic isotope distribution pattern [Fig. (V-1a)] of the $[M-H]^+$ or $[C_{19}H_{20}N_5O_5]^+$ peak around m/z=398 (most abundant isotopic mass), where M is the relevant molecular formula together with the water of crystallization; this assignment of the composition is verified through matching with the calculated distribution pattern [Fig. (V-1b)][11,18]. Architectural stability of $H_2L^3.H_2O$ containing two major substituents at the 2-and 6- positions of the pterin ring as well as existence of a strong hydrogen bonding between the pterin ligand (H_2L^3) and its associated water molecule in $H_2L^3.H_2O$, are indicated [11(a), 11(b)]. Presence of such hydrogen bonding has been verified through single crystal x-ray structure determination of a closely related pterin compound, e.g., 2-pivaloylamino-7-acetonylxanthopterin monohydrate, where the H_2O molecules is hydrogen bonded to the NH(2) group [the N(2)-H....O hydrogen bonding distance is 2.945 Å [86].

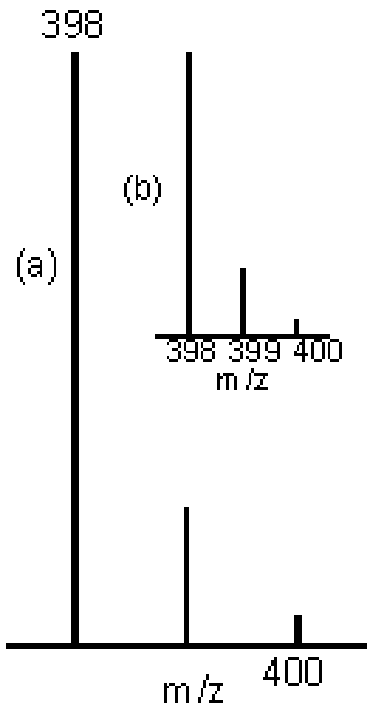

Fig. (V-1): (a) ESIMS data of the $H_2L^3.H_2O$ at the m/z(=398) region corresponding to the fragment $[M-H]^+$ or $[C_{19}H_{20}N_5O_5]^+$ where M represents the molecular formula of this compound and (b) (inset) the calculated isotope pattern.

In case of compound **(1)** [Fig.(V-2a)] the characteristic Mo isotopic distribution pattern for the essentially intact desolvated species $[M - 3CH_3OH - 3H]^+$ or $[MoC_{38}H_{31}N_{10}O_8]^+$ is observed at m/z=851, corresponding to its theoretical value [Fig. (V-2b)] [18].

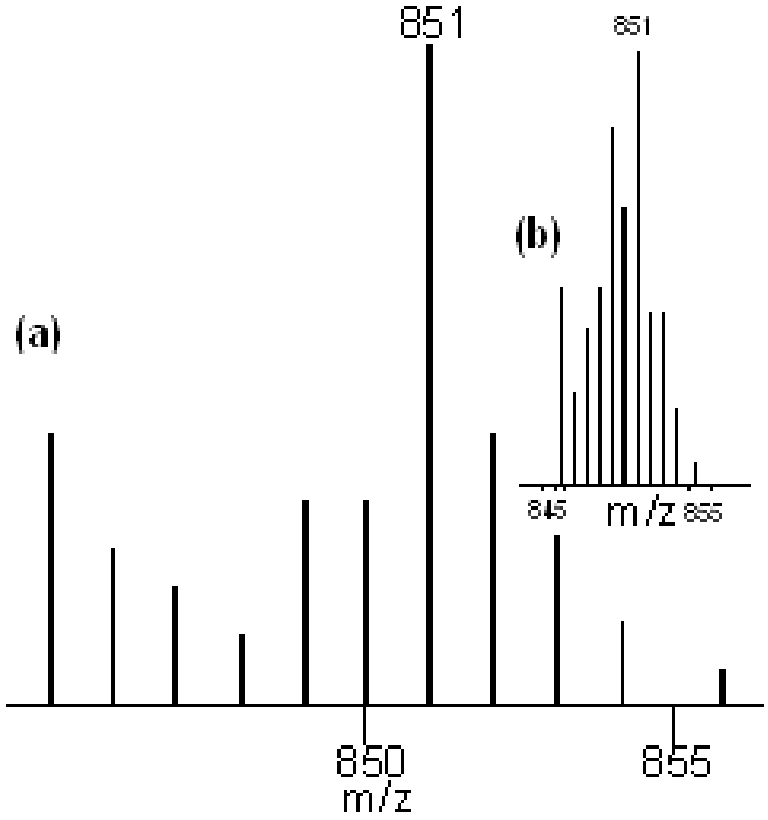

Fig. (V-2): (a) ESIMS data of the compound **(1)** at the m/z(=851) region corresponding to the fragment $[M - 3CH_3OH - 3H]^+$ or $[MoC_{38}H_{31}N_{10}O_8]^+$ where M represents the desolvated species of this complex and (b) (inset) the calculated isotope pattern.

The Fig. (V-3a) represents the ESIMS data of compound **(2)** at the m/z=(917) region. This may be assigned as $[M-(PPh_4+(CH_3)_3CCO)]^+$ or $[MoC_{38}H_{35}N_{11}O_7S_2]^+$ where M represents the desolvated species. The calculated isotope distribution pattern (most abundant isotopic peak) is presented in Fig. (V-3b). The difference between the experimental and calculated peak intensity is may be due to the ion-molecular interaction of the compound during the fragmentation process [11].

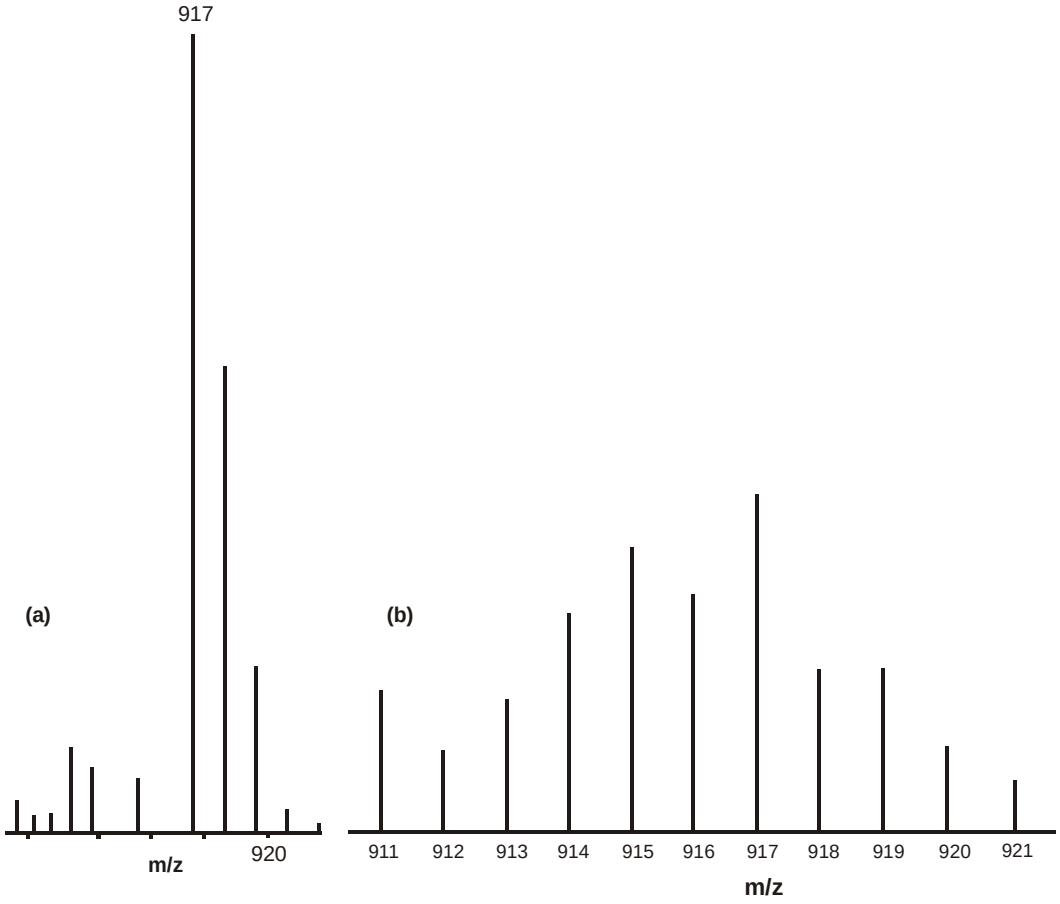

Fig. (V-3): (a) ESIMS data of the compound **(2)** at the m/z(=917) region corresponding to the fragment $[M-(PPh_4+(CH_3)_3CCO)]^+$ or $[MoC_{38}H_{35}N_{11}O_7\ S_2]^+$ where M represents the desolvated species of this complex and (b) the calculated isotope pattern.

For the compound **(3)** the ESIMS data at region m/z =979 is shown in the Fig. (V-4a). The Fig. (V-4b) represents the calculated isotopic distribution pattern at this region. The peak may be assigned as $[M- PPh_4]^+$ or $[MoC_{44}H_{40}N_{11}O_8S]^+$, where M represents the desolvated species of this compound. The slight variation between the theoretical and isolated peak pattern is due to the ion-molecular interaction during the fragmentation proess.

For compound **(4)** Fig. (V-5a) represents the ESIMS data at m/z =931 region of this compound corresponding to the fragment $[(M+ H)- PPh_4]^+$ or $[MoC_{40}H_{41}N_{11}O_8S]^+$, where M represents the desolvated species. Fig. (V-5b) corresponds to the theoretical isotope pattern. The ion-molecular interaction during the fragmentation process makes deviation from the calculated peak pattern.

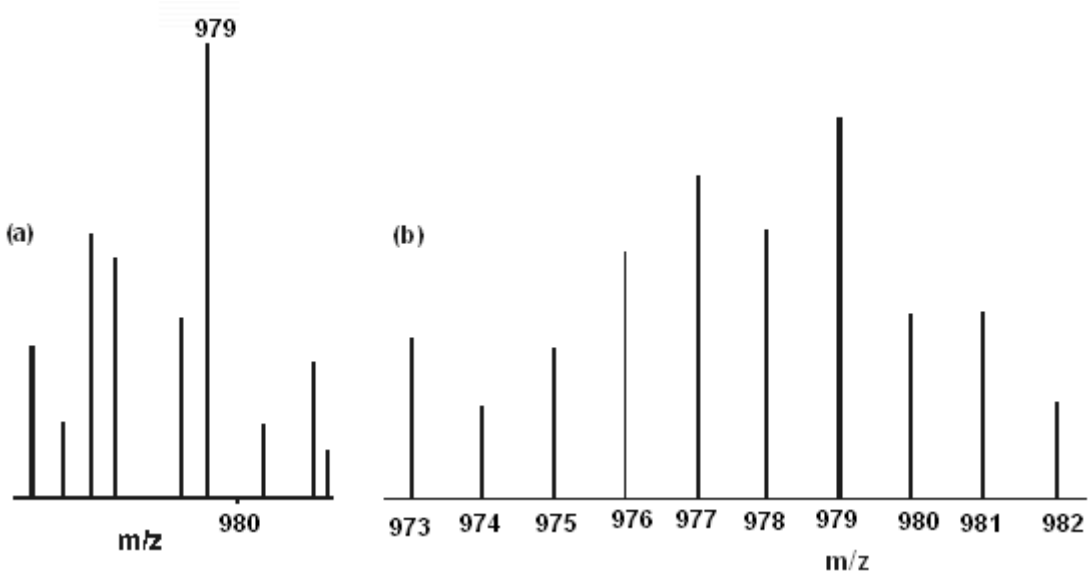

Fig. (V-4): (a) ESIMS data of the compound **(3)** at the m/z(=979) region corresponding to the fragment $[M-(PPh_4)]^+$ or $[MoC_{44}H_{40}N_{11}O_8S]^+$ where M represents the desolvated species of this complex and (b) the calculated isotope pattern.

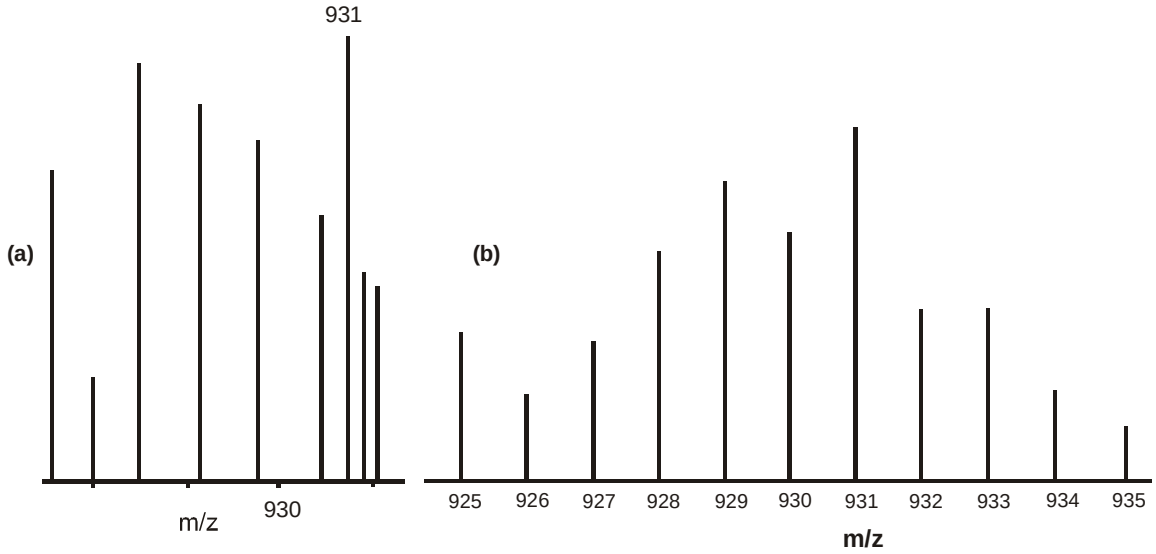

Fig. (V-5): (a) ESIMS data of the compound **(4)** at the m/z(=931) region corresponding to the fragment $[(M+ H)- PPh_4]^+$ or $[MoC_{40}H_{41}N_{11}O_8S]^+$ where M represents the desolvated species of this complex and (b) the calculated isotope pattern.

The ESIMS data of compound **(5)** represented in Fig. (V-6a), corresponding to the isotopic distribution pattern at the region m/z = 958, can be assigned as $[(M+H)-(PPh_4+H_2O)]^+$ or $[MoC_{41}H_{39}N_{11}O_9S]^+$, where M represents the desolvated species; Fig. (V-6b) corresponds to the calculated isotopic pattern.

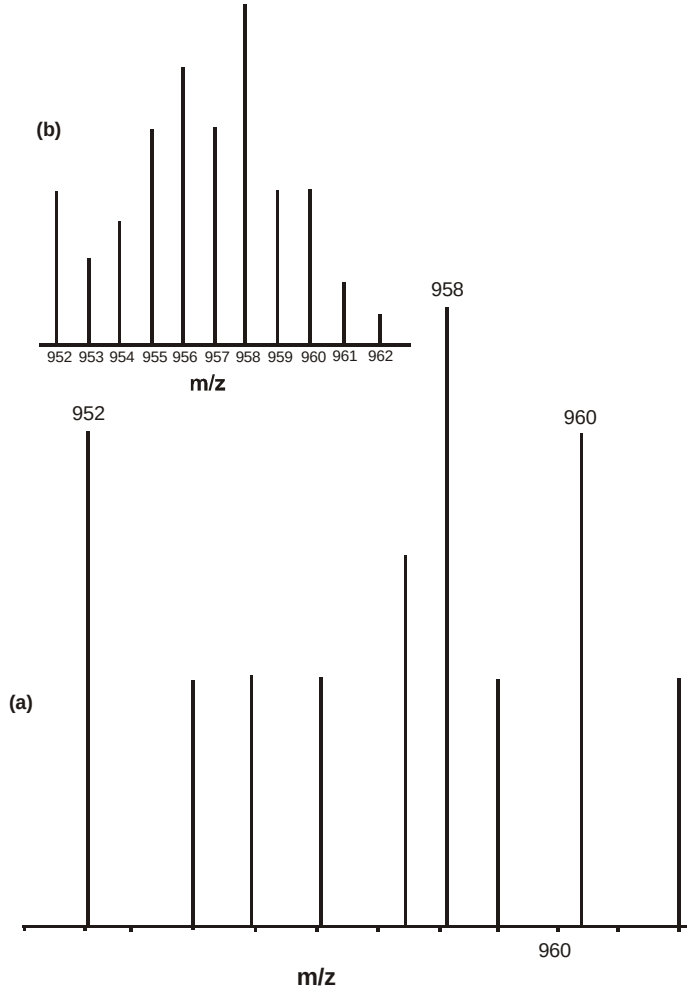

Fig. (V-6): (a) ESIMS data of the compound **(5)** at the m/z(=958) region corresponding to the fragment $[(M+H)-(PPh_4+H_2O)]^+$ or $[MoC_{41}H_{39}N_{11}O_9S]^+$ where M represents the desolvated species of this complex and (b) (inset) the calculated isotopic pattern.

For the compound **(6)** the presence of two Mo atoms can be reveled by the isotopic distribution pattern of the ESIMS data [Fig. (V-7a)]. The peak at the region m/z= 1108 corresponds to the $[M - (S+PhCO)]^+$ or $[Mo_2C_{38}H_{42}N_{15}O_{11}S]^+$, where M represents the desolvated binuclear species and Fig. (V-7b) represents the calculated isotopic pattern.

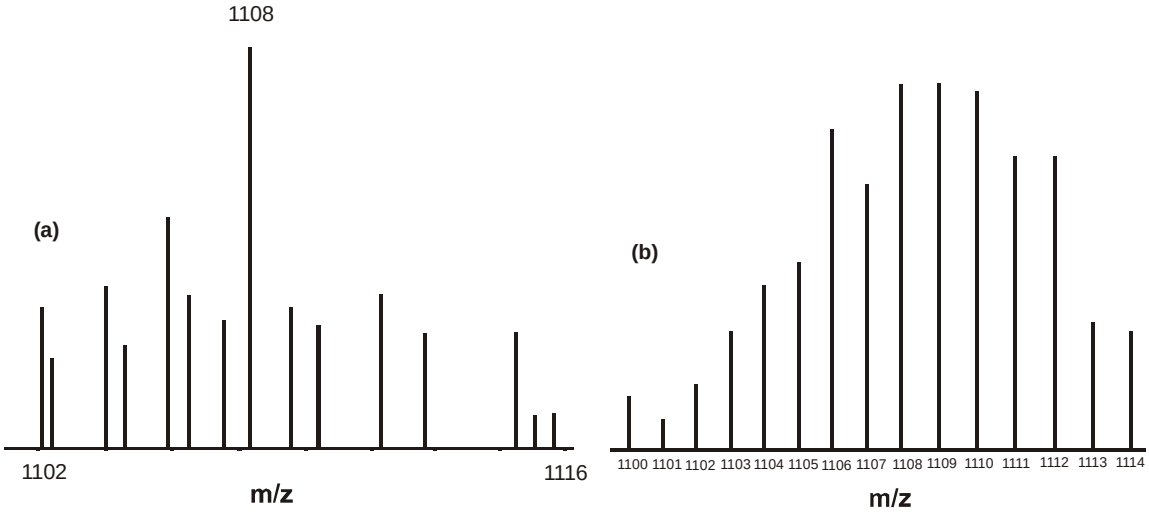

Fig. (V-7): (a) ESIMS data of the compound **(6)** at the m/z(=1108) region corresponding to the fragment $[M - (S+PhCO)]^+$ or $[Mo_2C_{38}H_{42}N_{15}O_{11}S]^+$ where M represents the desolvated species of this complex and (b) the calculated isotopic pattern.

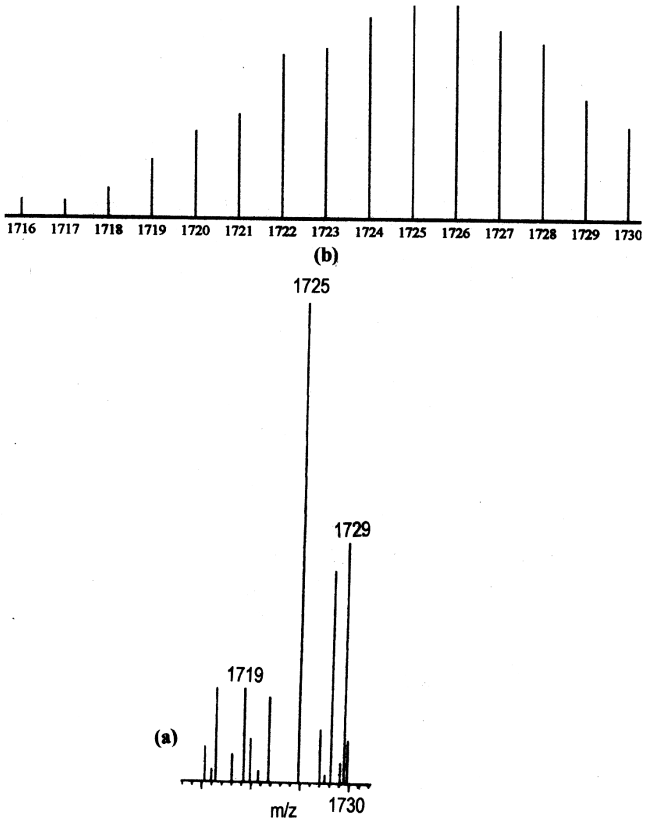

Fig. (V-8): (a) ESIMS data of the compound **(7)** at the m/z(=1725) region corresponding to the fragment $[M - CH_3OH]^+$ or $[Mo_2C_{76}H_{68}N_{20}O_{17}]^+$ where M represents the desolvated species of this complex and (b) the calculated isotope pattern.

ESIMS data of compound **(7)** helps to assign an important binuclear fragments through comparison of experimental and simulated isotope distribution patterns, e.g., the desolvated species $[M\text{-}CH_3OH]^+$ or $[Mo_2C_{76}H_{68}N_{20}O_{17}]^+$ at m/z=1725 [Fig. (V-8a) and Fig. (V-8b)]. The difference in intensity between the isotope peaks and calculated values in some of these cases is due to ion-molecule interaction, e.g. involving transfer of a hydrogen atom [11(a)]. The prominent m/z peaks of compound **1,2, 3, 4, 5, 6** and **7** along with probable fragmentation assignments are represented in Table (V-1).

IR spectroscopy

The IR spectrum of free ligand ($H_2L^3.H_2O$) is represented in Fig. (V-9) and on it comparing with that of compound **(1)** [Fig. (V-10b)], it is evident that the free ligand IR bands at 1346 cm^{-1} and 1261 cm^{-1} due to δ(O-H) and ν(C-O) + δ(O-H) vibrations respectively, of OH(4), undergo considerable modifications in compound **(1)** and a new strong band appears at 1261 cm^{-1} due to ν(C-O) mode of the corresponding phenoxide group[O(4)] [11(a)]. For the compounds **2, 3, 4, 5** and **6** [Fig. (V-11) to Fig. (V-15)] this band appears at 1261.4, 1261.4, 1253.6, 1257.5 and 1261.4 respectively. Besides these, most of the IR bands in the region 1600 – 1500 cm^{-1} of $H_2L^3.H_2O$ [where the ν(C=O)(1″), ν(C=O)(2′), ν(C=O)(7) modes as well as the ν(C=N) and ν(C=C) vibrations of the pterin and aromatic rings are present] undergo change (with respect to number, relative intensity and shape) in compounds **1, 2, 3, 4, 5, 6** and **7** due to tauomerism/ deprotonation/ electronic redistribution during the complex formation process involving the N(3)-C(4)-N(5)-C(6)-C(1′) system [Scheme V-1 and Scheme (V-10)]. In most cases the ν(C=O)(1″) mode (1681 -1676 cm^{-1}) remains essentially unchanged during this process. For the compounds **1, 2, 3, 4** and **5** no strong IR band assignable to the $\nu(Mo{=}O_t)$ mode could be located in the region 980 - 880 cm^{-1}. In case of compound **(7)**, a new intense IR band appears at 804 cm^{-1} corresponding to the $\nu(Mo\text{-}O_b\text{-}Mo)$ mode [9].

Table (V-1): The prominent ESIMS peaks (m/z) observed for the compounds (**1**) to (**7**) along with their assignments, Fig. (V-1) to (V-8).

Compound	m/z	Assigned fragmentation peak observed in the ESIMS data*
$H_2L^3.H_2O$	398	$[M-H]^+$
(1)	851	$[M - 3CH_3OH - 3H]^+$
(2)	917	$[M-(PPh_4+(CH_3)_3CCO)]^+$
(3)	979	$[M-(PPh_4)]^+$
(4)	931	$[(M+ H)- PPh4]^+$
(5)	958	$[(M+H)-(PPh_4+H_2O)]^+$
(6)	1108	$[M – (S+PhCO)]^+$
(7)	1725	$[M – CH_3OH]^+$

*M in each case indicates the relevant molecular formula of desolvated species.

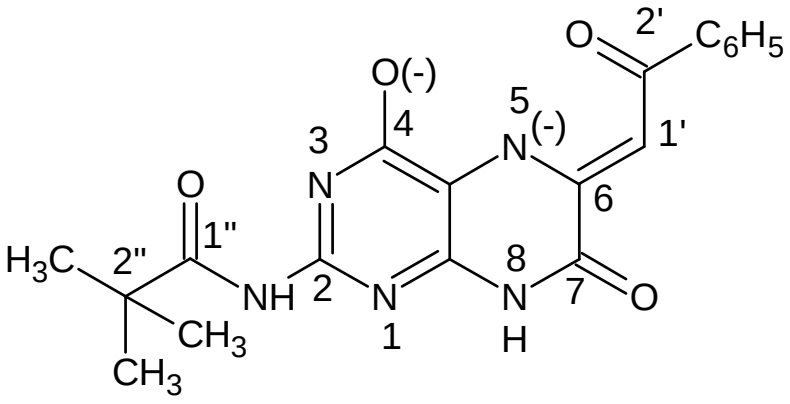

Scheme (V-10)

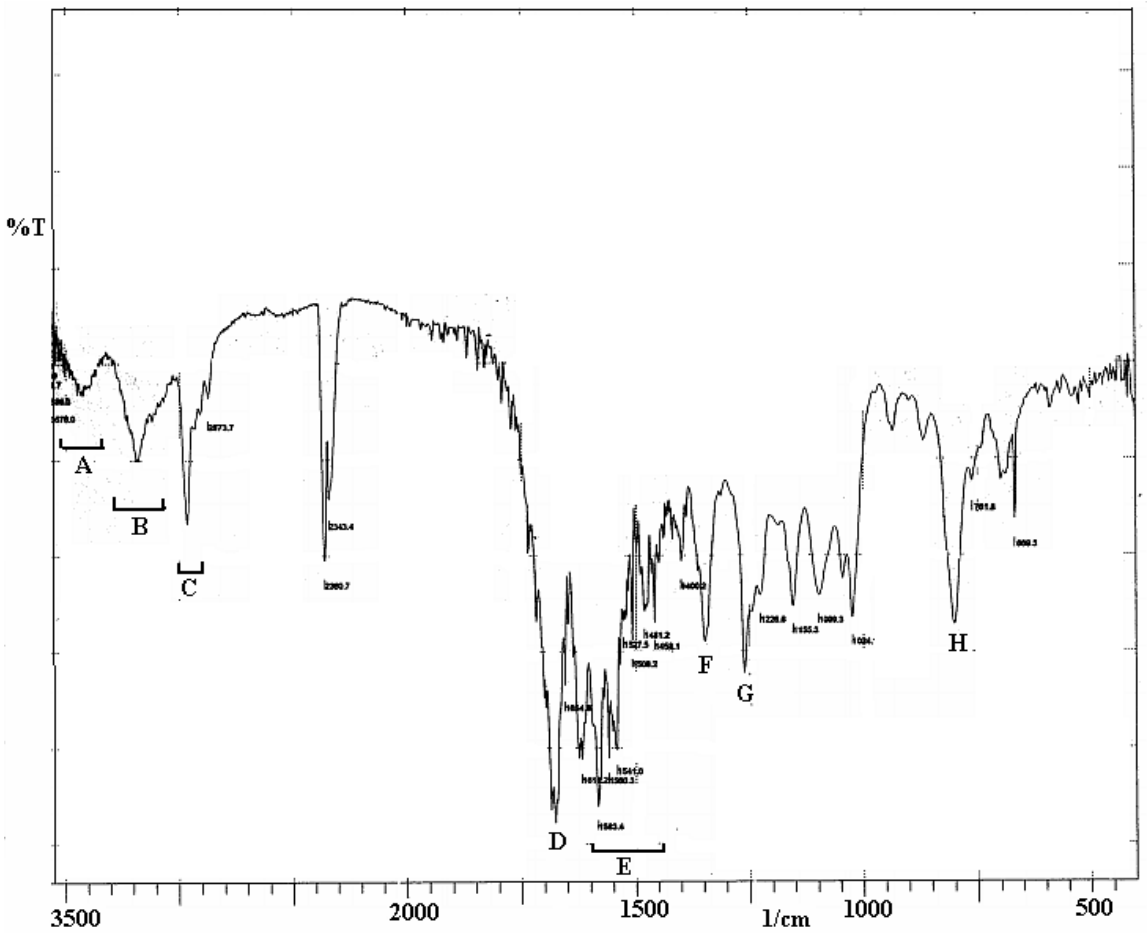

Fig.(V-9): FTIR spectrum (KBr) of ($H_2L^3.H_2O$)

A: the broad O-H stretching vibration of the hydrogen bonded 4(OH) group, indicating enolisation of the 4(oxo) group, at least partly, 3377 cm^{-1}.

B: the broad N-H stretching vibration, hydrogen bonded, 3180 cm^{-1}.

C: the C-H stretching vibrations, 2966, 2873 cm^{-1}.

D: the C=O stretching vibrations of the (C=O) (1′) and (C=O) (2′) groups, 1676 cm^{-1}.

E: the C⋯C and C⋯N ring stretching vibrations of the pterin ligand and C_6H_5 (2') group, 1654, 1618, 1560, 1541, 1481 cm^{-1}.

F: the δ (N-H) vibration of the NH(3), NH(5) groups, 1346 cm^{-1}.

G: the δ (N-H) + ν (C-N) vibrations of the NH(3), NH(5) groups, 1261 cm^{-1}.

H: out - of - plane C-H bending vibration, 802 cm^{-1}.

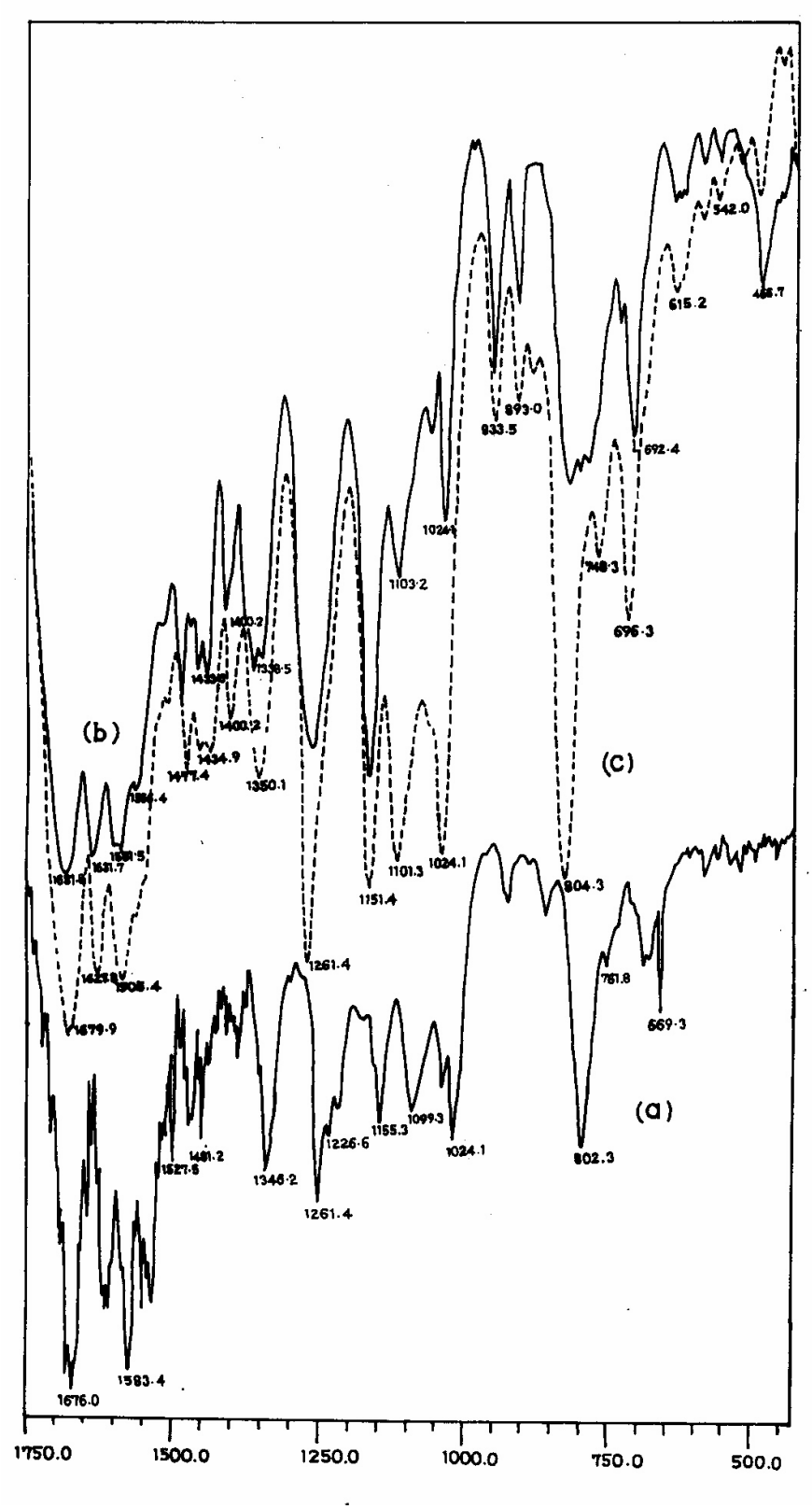

Fig. (V-10): FTIR spetrum. spectra (1750-400 cm^{-1}; KBr) of (a) the pterin ligand ($H_2L^3.H_2O$); (b) the compound **(1)**; (c) the compound **(7),** recovered after reaction with $Me_3N\rightarrow O$ and compound **(1)**.

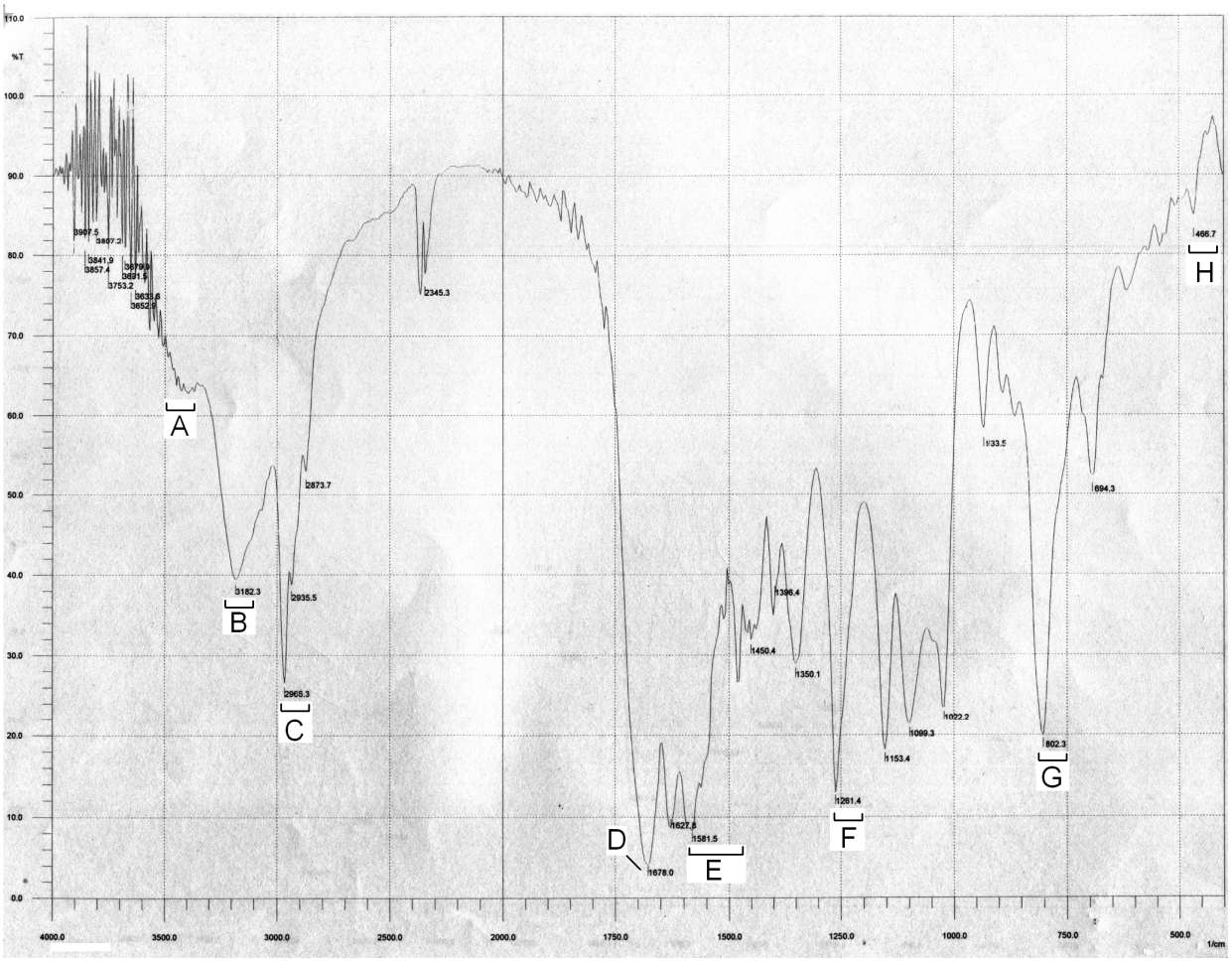

Fig.(V-11): FTIR spectrum (KBr) of compound **(2)**

A: the broad O-H stretching vibration, hydrogen bonded (CH_3OH), 3423 cm^{-1}.
B: the broad N-H stretching vibration, hydrogen bonded, 3182 cm^{-1}.
C: the C-H stretching vibrations 2966, 2935, 2873 cm^{-1}.
D: the C=O stretching vibrations of the (C=O) (1′) and (C=O) (2′) groups, 1676 cm^{-1}.
E: the C⋯C and C⋯N ring stretching vibrations of the pterin, 1581, 1450 cm^{-1}.
F: the ν (C-O) mode of the O(4) phenoxide group, 1261.4 cm^{-1}.
G: out - of - plane C-H bending vibration, 802.3 cm^{-1}.

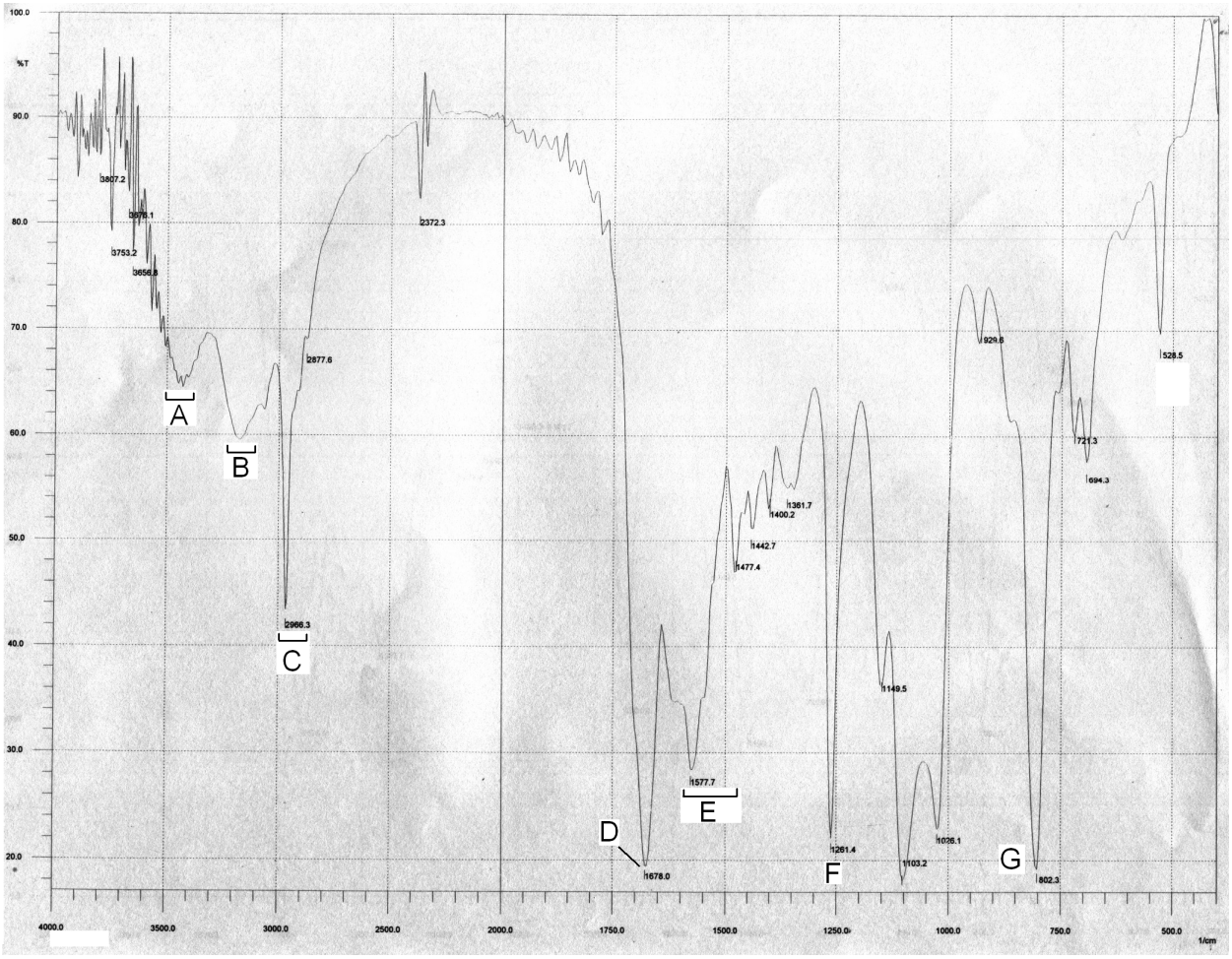

Fig.(V-12): FTIR spectrum (KBr) of compound **(3)**

A: the broad O-H stretching vibration, hydrogen bonded (CH_3OH), 3400 cm^{-1}.
B: the broad N-H stretching vibration, hydrogen bonded, 3150 cm^{-1}.
C: the C-H stretching vibrations 2966, 2877 cm^{-1}.
D: the C=O stretching vibrations of the (C=O) (1˝) and (C=O) (2′) groups, 1667 cm^{-1}.
E: the C⋯C and C⋯N ring stretching vibrations of the pterin 1577, 1477 cm^{-1}.
F: the ν (C-O) mode of the O(4) phenoxide group, 1261.4 cm^{-1}.
G: out - of - plane C-H bending vibration, 802.3 cm^{-1}.

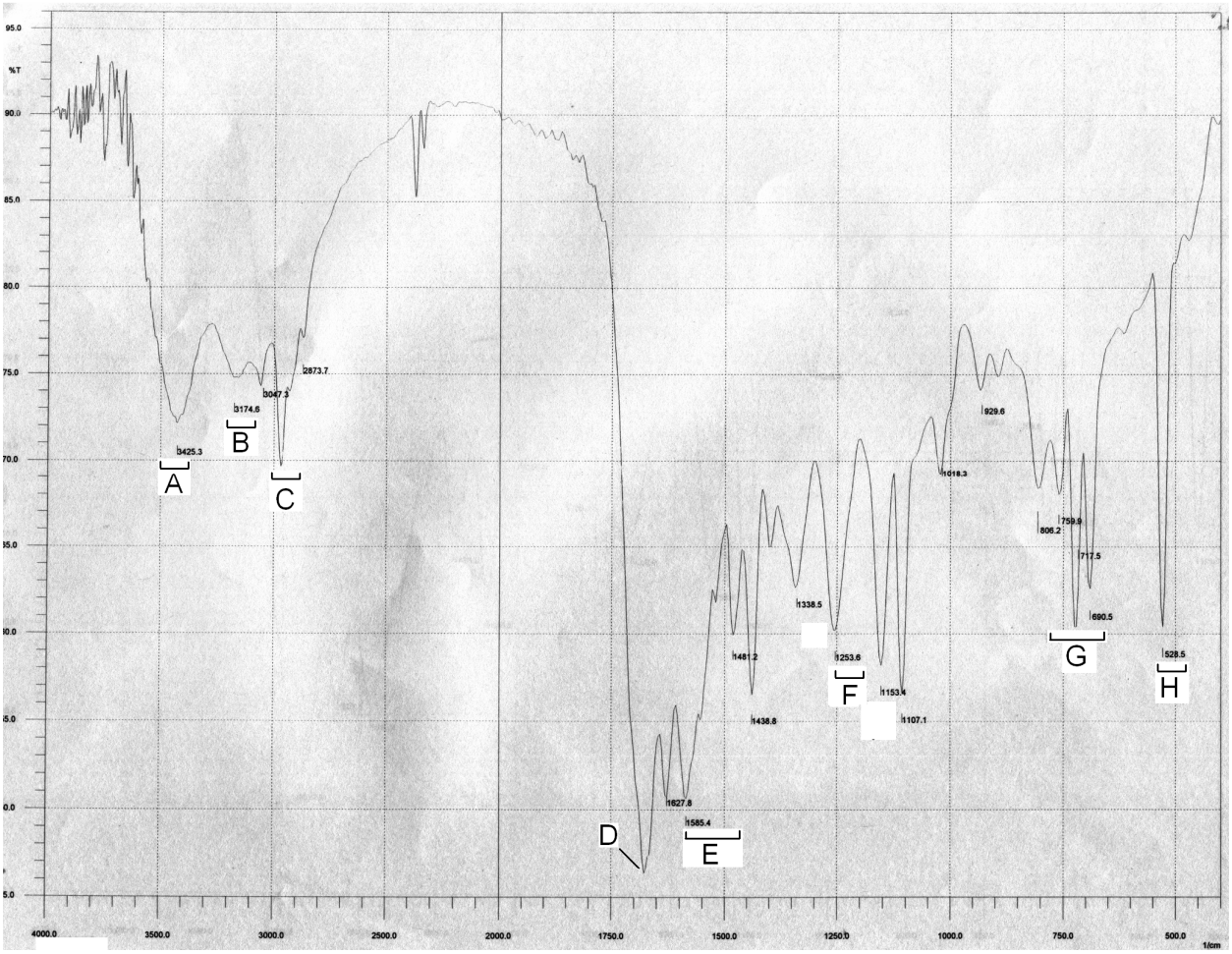

Fig.(V-13): FTIR spectrum (KBr) of compound **(4)**

A: the broad O-H stretching vibration, hydrogen bonded (CH_3OH), 3425 cm^{-1}.
B: the broad N-H stretching vibration, hydrogen bonded, 3174 cm^{-1}.
C: the C-H stretching vibrations 2968, 2873 cm^{-1}.
D: the C=O stretching vibrations of the (C=O) (1″) and (C=O) (2′) groups, 1662 cm^{-1}.
E: the C⋯C and C⋯N ring stretching vibrations of the pterin, $(aet)^{1-}$ 1585, 1482 cm^{-1}.
F : the ν (C-O) mode of the O(4) phenoxide group, 1253.6 cm^{-1}.
G: out - of - plane C-H bending vibration
H: the ν (C-S) mode related to the $(atp)^{1-}$ residue, 500-600 cm^{-1}.

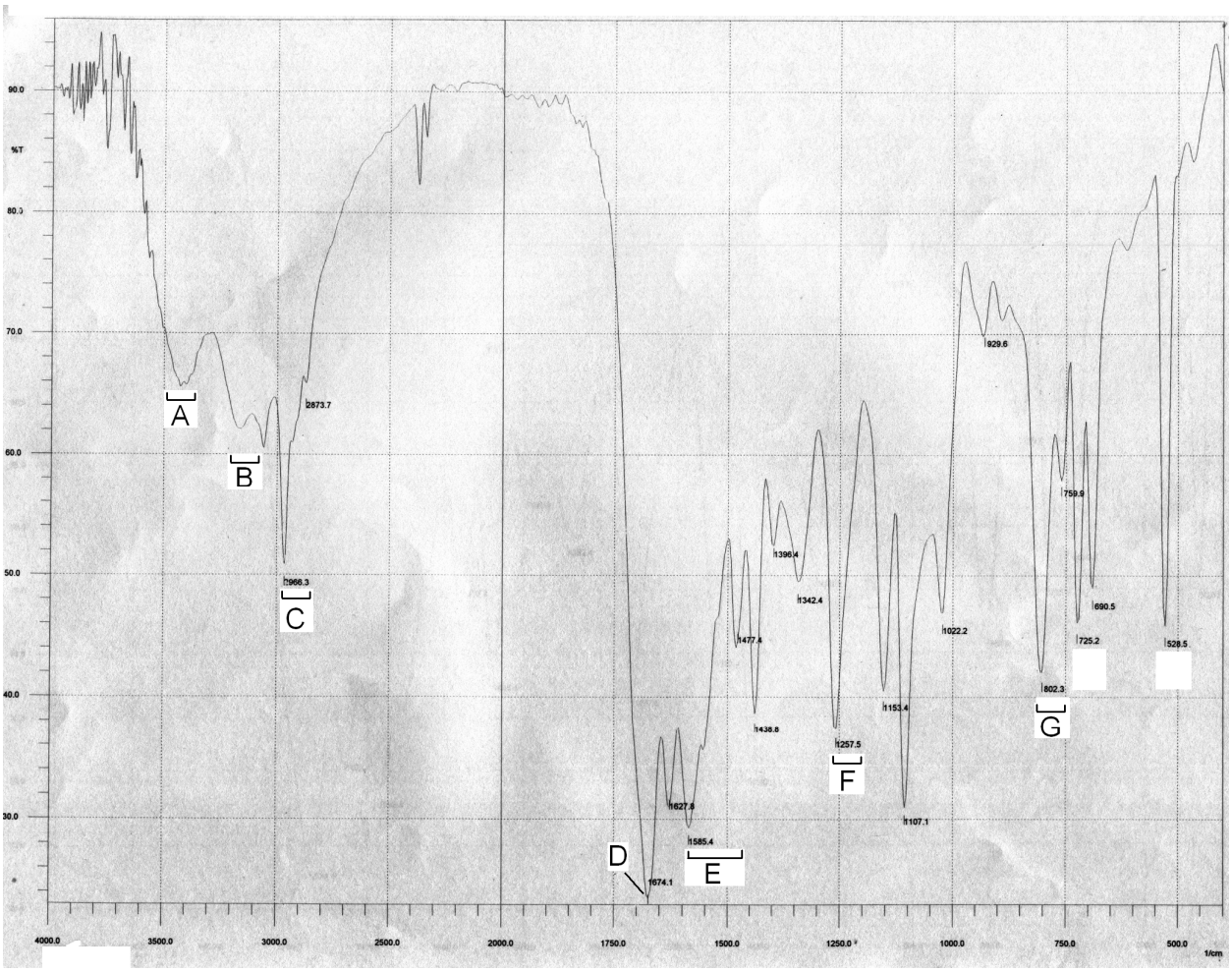

Fig.(V-14): FTIR spectrum (KBr) of compound **(5)**

A: the broad O-H stretching vibration, hydrogen bonded (CH_3OH), 3429 cm^{-1}.
B: the broad N-H stretching vibration, hydrogen bonded, 3154 cm^{-1}.
C: the C-H stretching vibration, 2966 cm^{-1}.
D: the C=O stretching vibrations of the (C=O) (1′) and (C=O) (2′) groups, 1664 cm^{-1}.
E: the C⋯C and C⋯N ring stretching vibrations of the pterin, 1585, 1477 cm^{-1}.
F: the ν (C-O) mode of the O(4) phenoxide group, 1257.5 cm^{-1}.
G: the out-of-plane C-H (aromatic) bending vibrations, 802.3 cm^{-1}

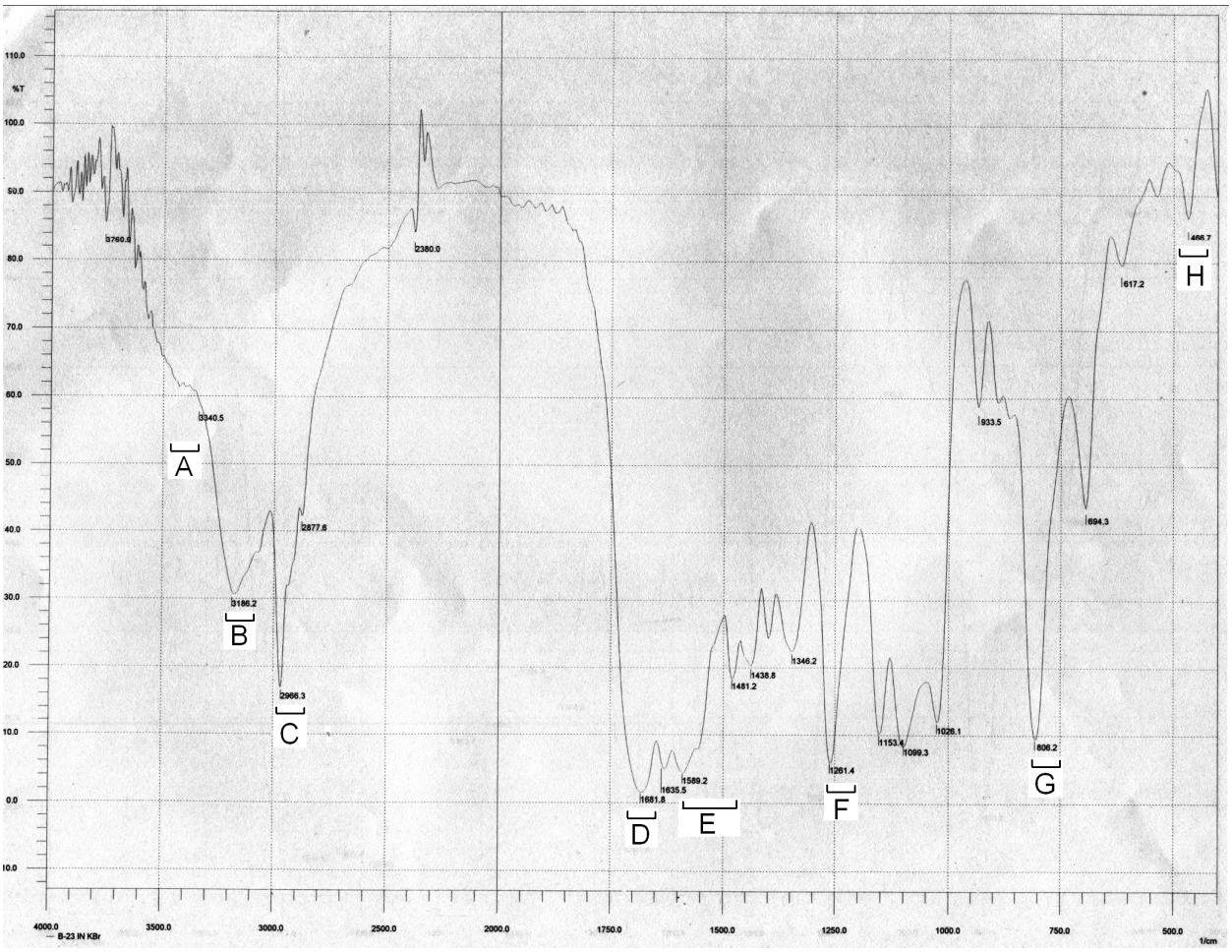

Fig.(V-15): FTIR spectrum (KBr) of compound **(6)**

A: the broad O-H stretching vibration of the CH_3OH

B: the broad N-H stretching vibration, hydrogen bonded, 3186 cm^{-1}.

C: the C-H stretching vibrations, 2966, 2877 cm^{-1}.

D: the C=O stretching vibrations of the (C=O) (1″) and (C=O) (2′) groups, 1681 cm^{-1}.

E: the C⋯C and C⋯N ring stretching vibrations of the pterin ligand and C_6H_5 (2') group, 1589, 1481 cm^{-1}.

F: the ν(C-O) mode of the O(4) phenoxide group, 1261.4 cm^{-1}.

G: the out-of-plane C-H (aromatic) bending vibrations, 802.3 cm^{-1}

H: the ν(M0-S_b) mode of vibration at 466.7

^{1}H-NMR spectra

Free ligand ^{1}H-NMR data in DMSO - d_6 (H_2L^3, H_2O):

This ligand exists in two tautomeric forms, in one of which the oxo group (4) is enolised [Scheme (V–1b)], as evident from the relevant OH(4) signal at δ13.25 (bs). The NH(5) and NH(8) signals appear at δ12.44 (bs) and δ10.90 (bs) respectively [Fig. (V–16)]. These assignments have been made on the basis of both 1D and 2D NMR data as well as protonic integration values of the former. These signals disappear when the ^{1}H-NMR spectrum is recorded afresh in CD_3OD, indicating their exchangeable nature [4c]. The phenyl ring (2′) protons appear at δ7.94 (2H, m) and δ7.56 (3H, m) and the cross peaks (^{1}H -^{1}H COSY) connect both of them to the CH(1′) signal at δ6.68 (1H) [Fig. (V-17)]. For the N(2)-pivaloyl substituent (i.e the 2-pivaloylamino group), two distinct signals characterize the NH(2) proton (δ4.20 q; δ3.96 q). They are connected by off-diagonal peaks (^{1}H – ^{1}H COSY data) to the two CH_3(2″) signals at δ1.202 (6H, double doublet) and δ1.046(3H, singlet) respectively [Fig. (V-18)]. 1D NMR data of some of the above – mentioned signals are shown in Fig. (V-19).

As evident from the ^{1}H-NMR data, the positions (δ, ppm) of the CH(1′) proton signal remains unchanged on complex formation with the [Mo(IV)] centre in most, as compared to the corresponding free ligand signal at δ6.68. This is in contrast to the behaviour of the ancillary ligands here [($dedtc^{-1}$), (aet^{2-}) etc.] as discussed below. Non participation of the carbonyl group in the 6- position substituent, i.e., the O(2′) atom in the coordination process, is indicated.

Again, the residual methyl signal (δ2.47, s) of DMSO-d_6 is related by off-diagonal peaks to the CH_3(2″) signal at δ1.202 as well as the NH(2) signal at δ4.20, indicating the existence of strong hydrogen bonding interaction between the ^{1}H-NMR solvent and the NH(2) group, with its influence (spin-spin interaction) extending all the way upto CH_3(2″) [Fig. (VI-18)]. This hydrogen bond restricts free rotation around the N(2) – C(1″) – C(2″) σ skeleton, leading to the appearance of two separate signals for both the NH(2) and CH_3(2″) type protons. ^{1}H-NMR data (1D and 2D) of ribavirin in DMSO-d_6 show that restricted rotation around a C-N bond can make even the two primary amide NH protons non-equivalent on the NMR time-scale [44].

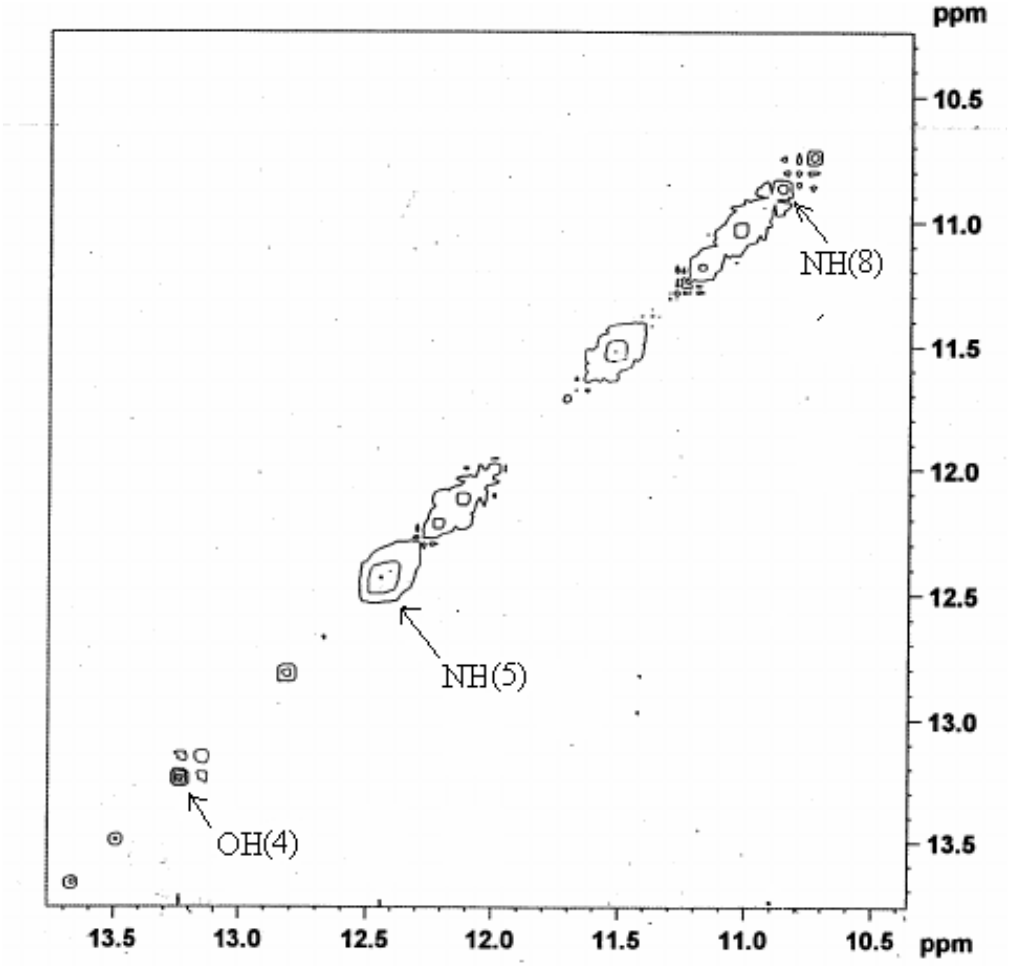

Fig.(V-16): ^{1}H-^{1}H COSY data (symmetrized) of ($H_2L^3.H_2O$) in DMSO-d_6 showing assignments of NH(8), NH(5) and OH(4) signals over the region δ 14.0 – 10.3.

The above observations about hydrogen bonding interactions are in line with the x-ray structural data on oxomolybdoenzymes, which establish that the pterin ring substituents like NH_2(2) and NH(8) groups link up with the electron transfer proteins (e.g., ferredoxin) through such interaction [34,45]. Intermolecular hydrogen bonding has also been implicated in the control of redox potential of a pterin derivative[46].

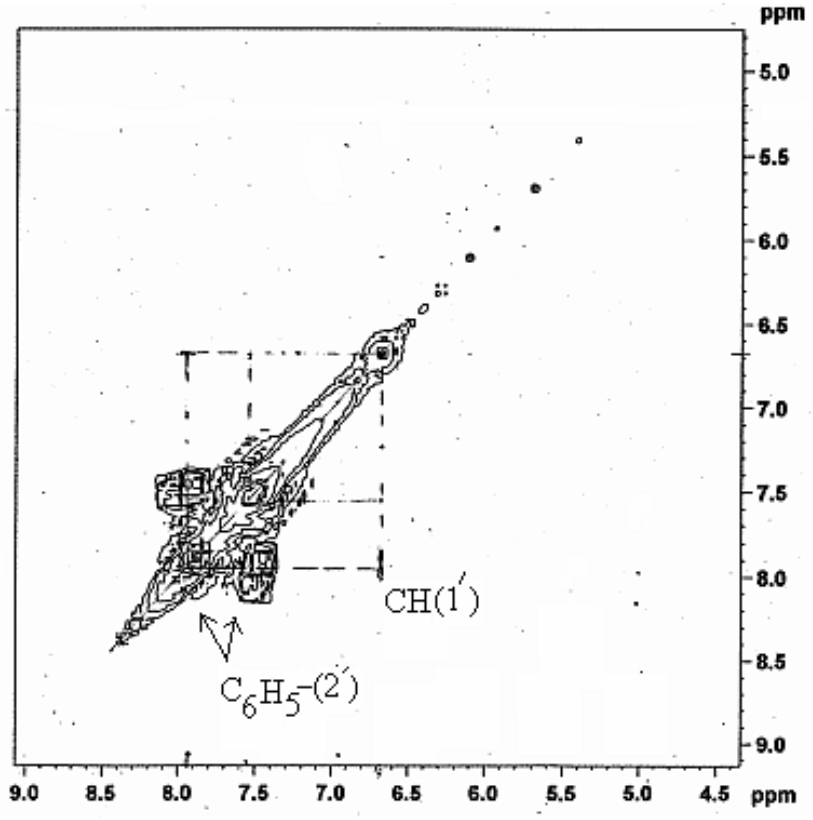

Fig.(V-17): ^{1}H-^{1}H COSY data (symmetrized) of ($H_2L^3.H_2O$) in DMSO-d_6, showing assignments of the CH(1′) and C_6H_5(2′) proton signals.

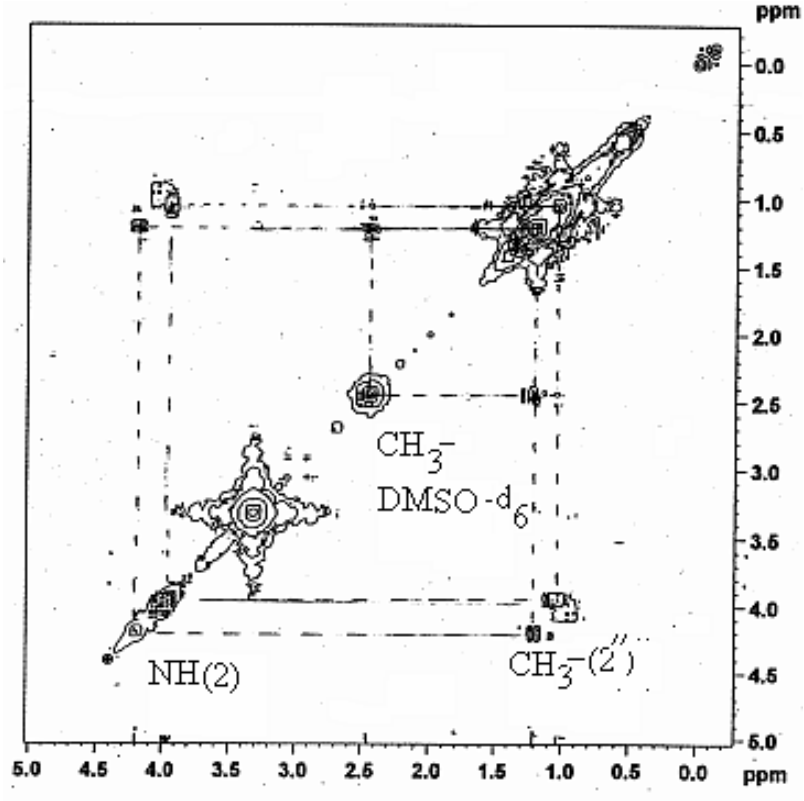

Fig.(V-18): ^{1}H-^{1}H COSY data (symmetrized) of ($H_2L^3.H_2O$) in DMSO-d_6, showing assignments of the $CH_3(2'')$ and NH(2) proton signals.

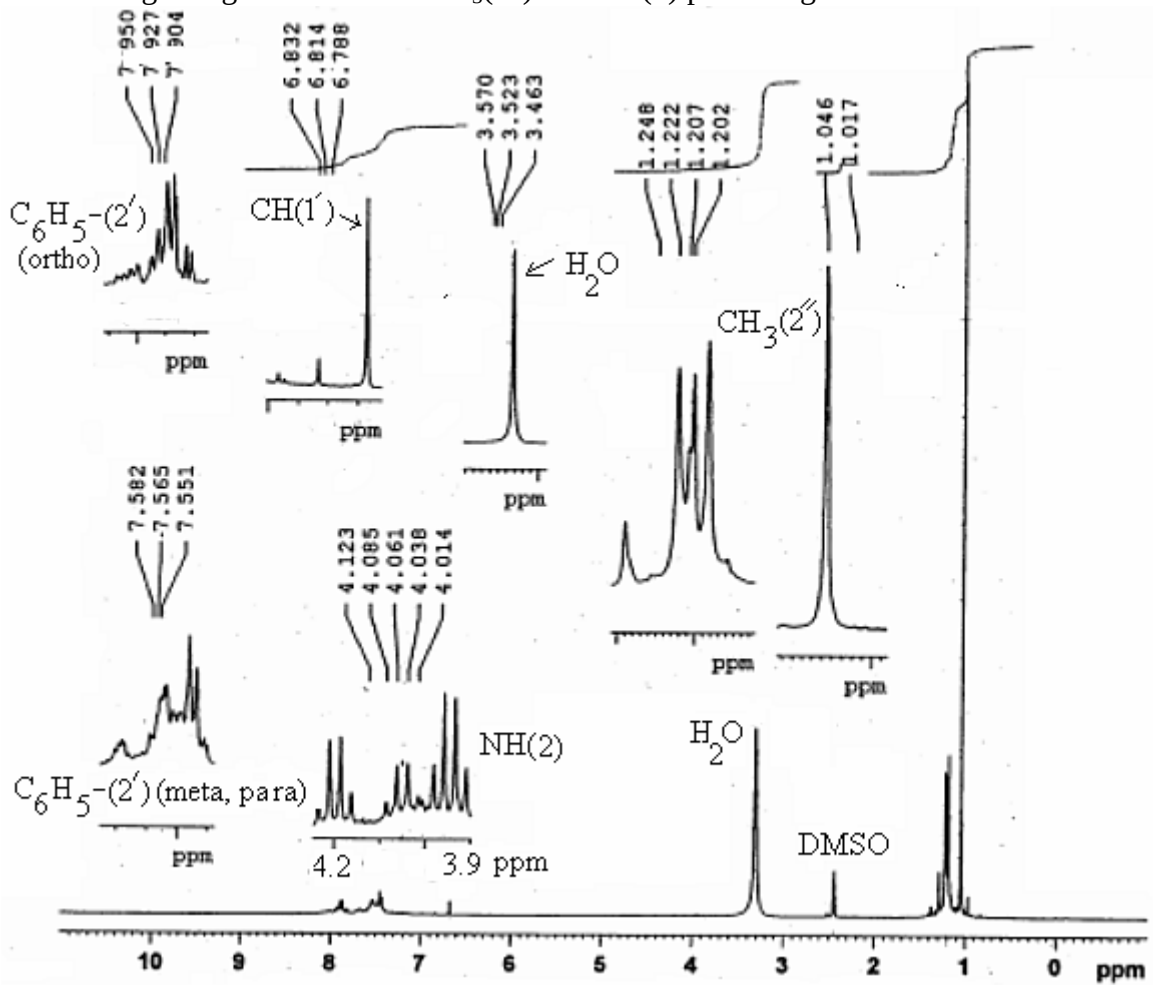

Fig.(V-19): 1D ^{1}H-NMR data of ($H_2L^3.H_2O$) in DMSO - d_6.

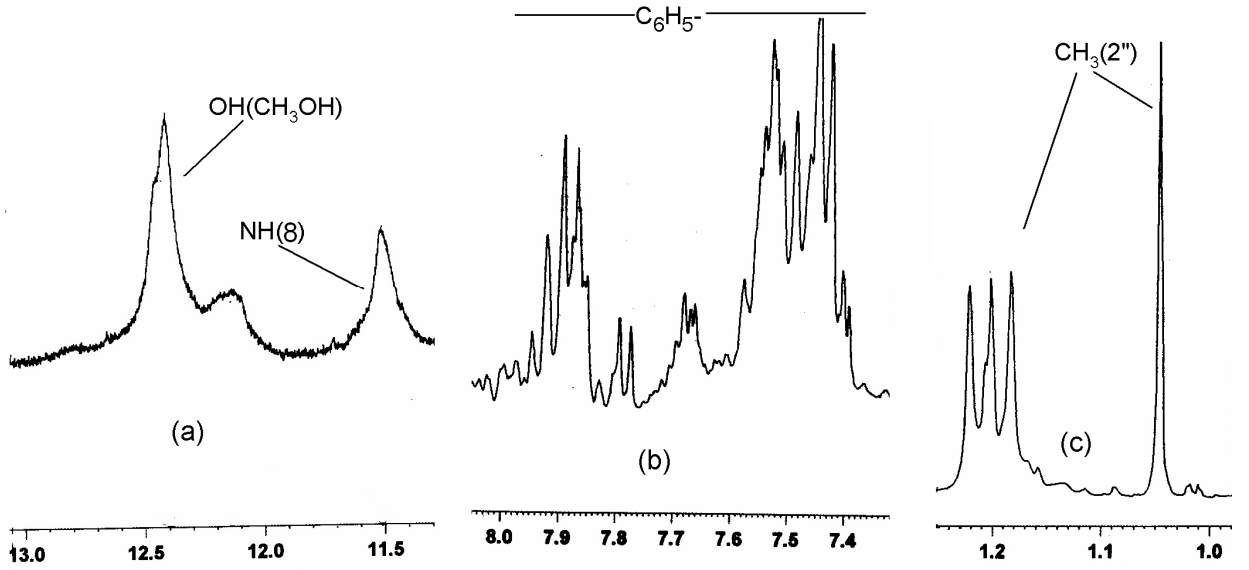

Fig.(V-20): ^{1}H-NMR data of compound **(1)** in DMSO-d_6 over the region (a) δ13.0-11.5; (b) δ8.0-7.4 and (c) δ1.2-1.0 (vide text for details).

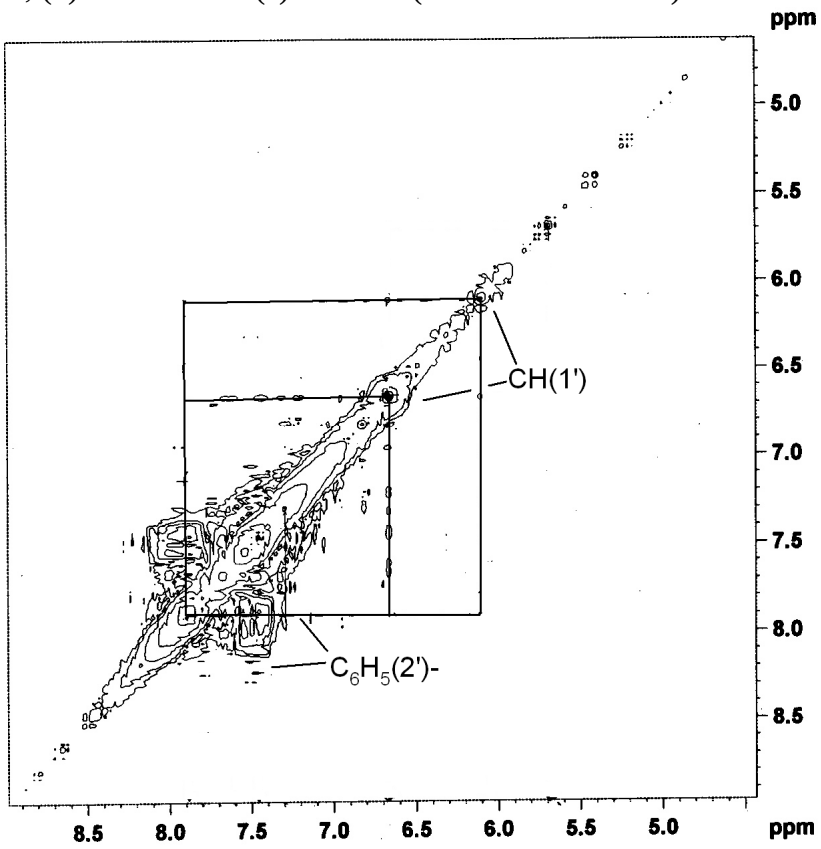

Fig. (V-21): ^{1}H-^{1}H COSY data (symmetrized) of compound **(1)** in DMSO-d_6 over the region δ9.0-5.0 (vide text for details).

The1D and 2D ^{1}H-NMR data of compound **(1)** [Fig. (V-20) and Fig. (V-21)], indicate that the phenyl(2′) ring protons appear at δ7.88(2H,m) and δ7.46(3H,m); the former is connected by cross peaks (in 2D spectrum) to the two separate CH(1′) signals appearing at δ6.67(s) and δ6.10(s). As stated later, the distorted octahedral geometry of compound **(1)** is responsible for the slightly different electronic environment (especially around the metal coordination zone) of the two unsymmetrical ligand residues, leading to the appearance of two separate signals for the CH(1′) proton. The proton signals of the 2-pivaloylamino substituent of ($H_2L^3.H_2O$) remain essentially unaffected through coordination to the metal atom in compound **(1)** [Fig. (V-20)] . From Fig. (V-20) it is evident that the NH(8) appears at δ11.50(wb) and phenyl ring protons at δ7.4-8.0.

A consideration of difference (Δδ ppm) in positions of the CH(1′) and NH(8) proton signals in ($H_2L^3.H_2O$) and compound **(1)** indicates that while the former signal is shielded (upto 0.98 ppm), the latter one is deshielded (to a limit of 0.60 ppm) during the coordination (to the

Mo atom) process. There is a increase in electron density around the Mo atom in compound **(1)** with electron depletion from the NH(8) region of its pterin ligand residues $(L^3)^{2-}$ [5]; this attribute is utilized by the metal centre of compound **(1)** in the reduction of $Me_3N \rightarrow O$ to Me_3N [4c].

^{1}H-NMR spectral data of compound **(2)** in DMSO-d_6 are shown in Fig.(V-22) to Fig. (V-25). Most of the 1D NMR signals [Fig.(V-22) and Fig.(V-23)] have been assigned on the basis of the corresponding 2D NMR data [Fig.(V-24) and Fig.(V-25)]. These results may be compared with those of [$H_2L^3.H_2O$] [Fig. (V-16) to Fig. (V-19)] and [Na(dedtc).$3H_2O$] shown Fig. (IV-20).

As indicated in [Fig.(V-23) and Fig.(V-25)] the NH(8) signal of the two pterin ligand residues appear at δ12.25(wb) and δ11.65(wb) respectively, indicating small differences between them on the NMR time scale. The OH(CH_3OH) signal is observed at δ12.50(ss). Beside these, a series of weaker signals are observed over the region δ11.00- δ14.5 arising from the contribution of smaller isomer/conformer of compound **(2)**. The phenyl signals of the $(Ph_4P)^+$ cation as well as the C_6H_5(2′) of $(L^3)^{2-}$ residue are also assigned in Fig.(V-23). They give overlapping signals in the corresponding 2D NMR data, Fig.(V-25). These intense aromatic signals somewhat dwarf the CH_2 signals of the $(dedtc)^{1-}$ residue of compound **(2)** at δ7.10. However, the corresponding 2D NMR data [Fig.(V-24)] stands in good stead for the unambiguous assignments of the CH_3 and $–CH_2-$ signals of the $(dedtc)^{1-}$ residue at δ3.55 and δ7.10 respectively. In the corresponding free ligand [Fig. (IV-20)], such signals appear at δ1.086 and δ4.0 respectively. The results are collected together in Table (V-2). The strong deshielding (Δ) of the proton signals, especially that of the $–CH_2-$ group of $(dedtc)^{1-}$ residue indicate exceptionally strong bonding with the metal [Mo(IV)] entre through the sulfur donor atoms; contributions from Lewis structures like the following cannot be ruled out[Scheme (V-11) [106]. This inference is in complete agreement with the x-ray structure data of oxomolybdoenzyme [Fig. (I-3)], indicating bonding of the molybdenum centre to the 6-substituted pterin (precisely pyranopterin) through the dithiolene sulphur donor atoms. Since this compound is a mononuclear one, the above aspect confers it some attributes of a close approach to a model system. That is, the minimal synthetic representation of the relevant enzyme action site. Besides this [Scheme (V-4)], the large Δ values [Table (V-3)] indicate considerable electron density build-up around the Mo(IV) centre which is utilized during reaction with an oxygen atom transfer reagent like Me_3NO.

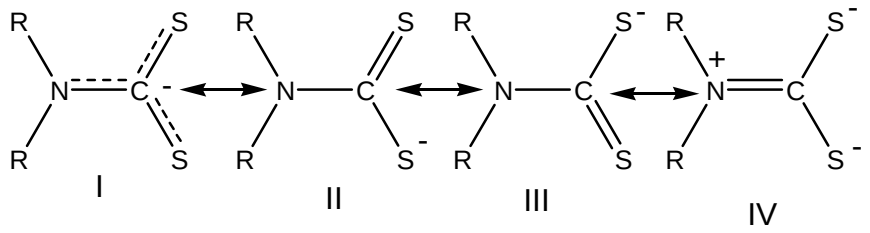

Scheme (V-11)

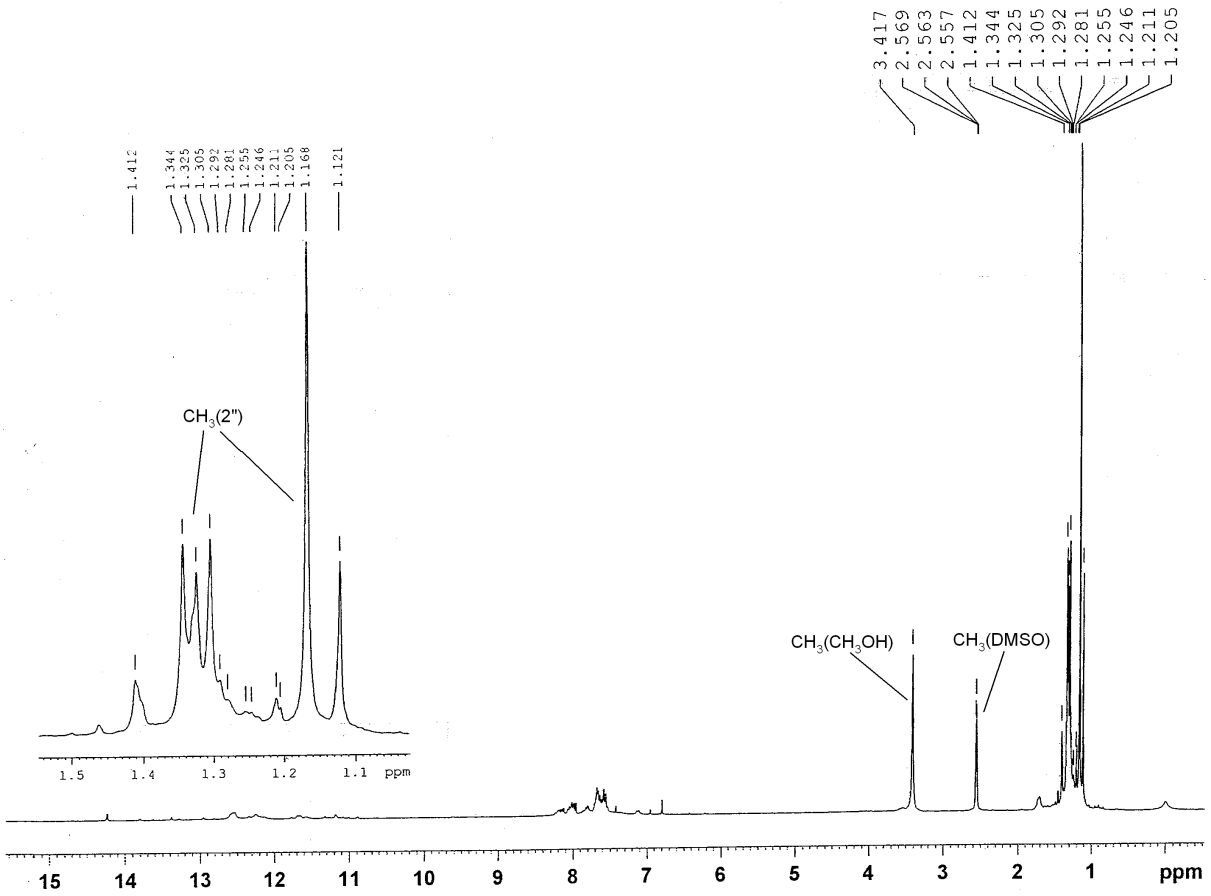

Fig.(V-22): ^{1}H-NMR data of compound **(2)** in DMSO-d_6 over the region δ16.0-0.0 (vide text for details).

The CH(1′) signal of $(L^3)^{2-}$ residue could be assigned at δ6.80[Fig.(V-23)]; it is associated with a weaker signal at δ6.98 assignable to a minor isomer, the major signal is hardly affected from its ligand position [Fig.(V-17)] at δ6.68 reflecting non-participation of the 2′ carbonyl group $(L^3)^{2-}$ residue] in complex formation process. That is this pterin ligand acts as a bidented O,N donor through O(4) and N(5) donor atoms, as inferred from IR data [Scheme (V-10)].

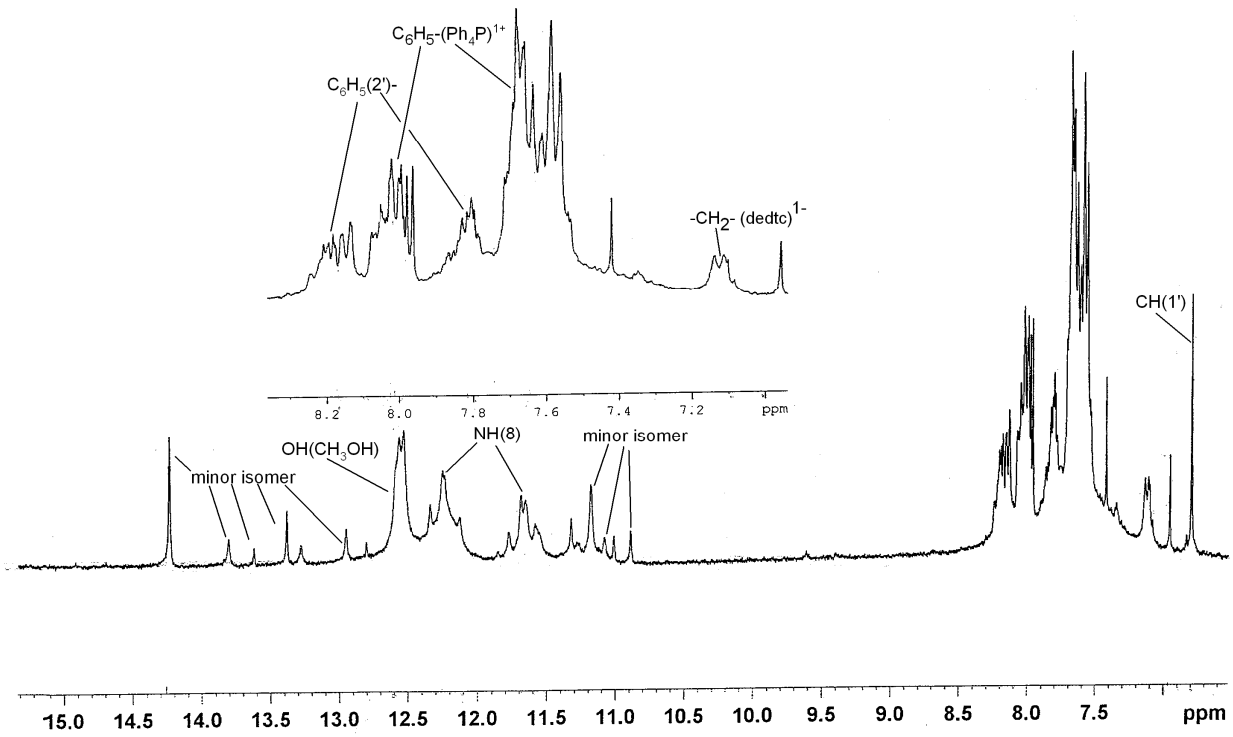

Fig.(V-23): ^{1}H-NMR data of compound **(2)** in DMSO-d_6 over the region δ16.0-7.0 (vide text for details).

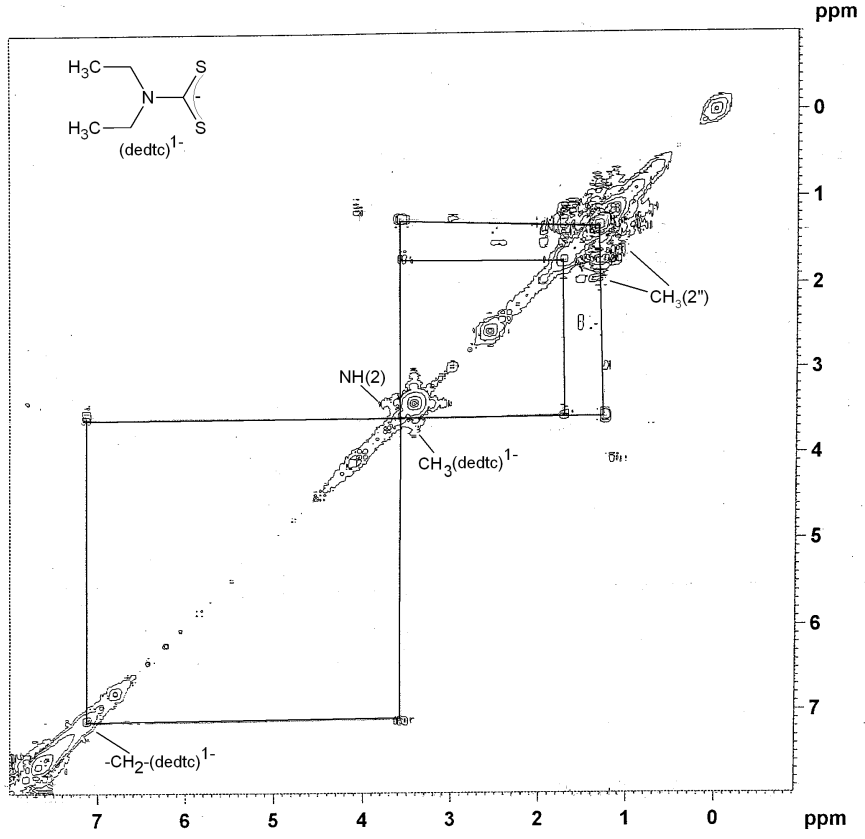

Fig. (V-24): ^{1}H-^{1}H COSY data (symmetrized) of compound **(2)** in DMSO-d_6 over the region δ8.0-0.0 (vide text for details).

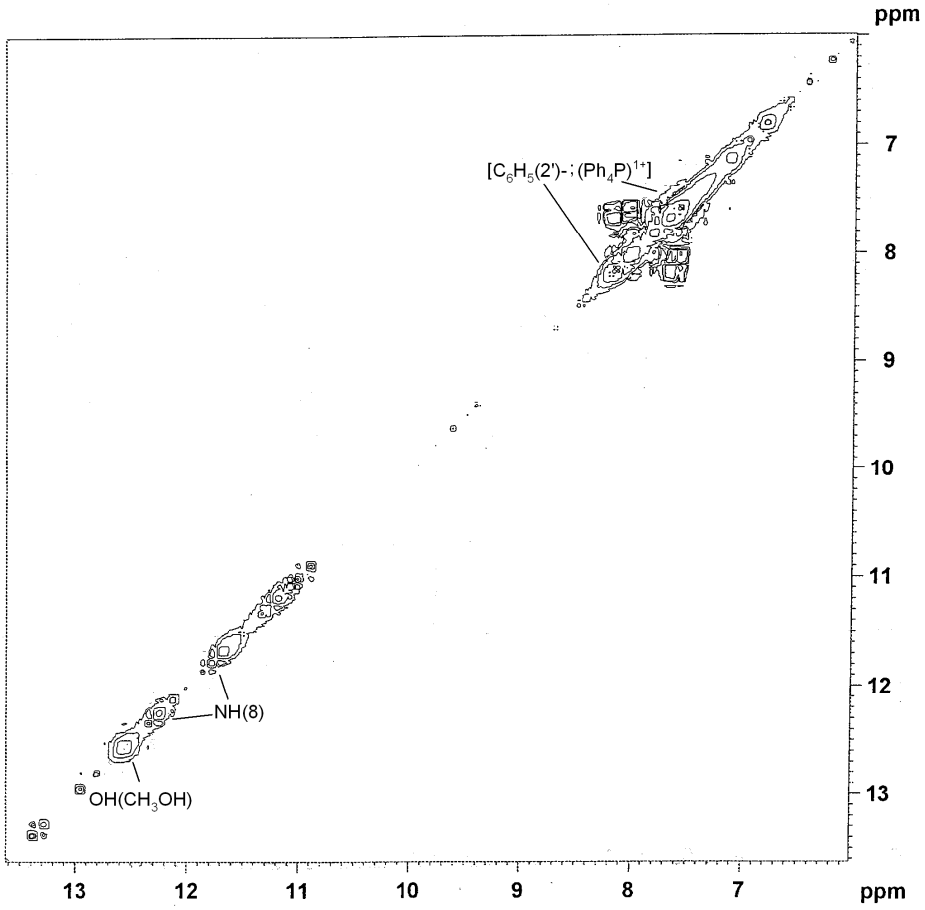

Fig. (V-25): ^{1}H-^{1}H COSY data (symmetrized) of compound **(2)** in DMSO-d_6 over the region δ13.0-6.0 (vide text for details).

Table (V-2): Comparison of CH_3 and $–CH_2$- signal in free ligand [Na_2(dedtc).$3H_2O$] and $(dedtc)^{1-}$residue in compound **(2)**.

	CH_3 signal	-CH_2- signal
Na(dedtc).$3H_2O$	δ 1.08(t)	δ 4.0(q)
$(dedtc)^{1-}$ in **(2)**	δ 3.55	δ 7.10
Δ*	δ 2.464	δ 3.10

*Δ= changeover in signal position through complex formation

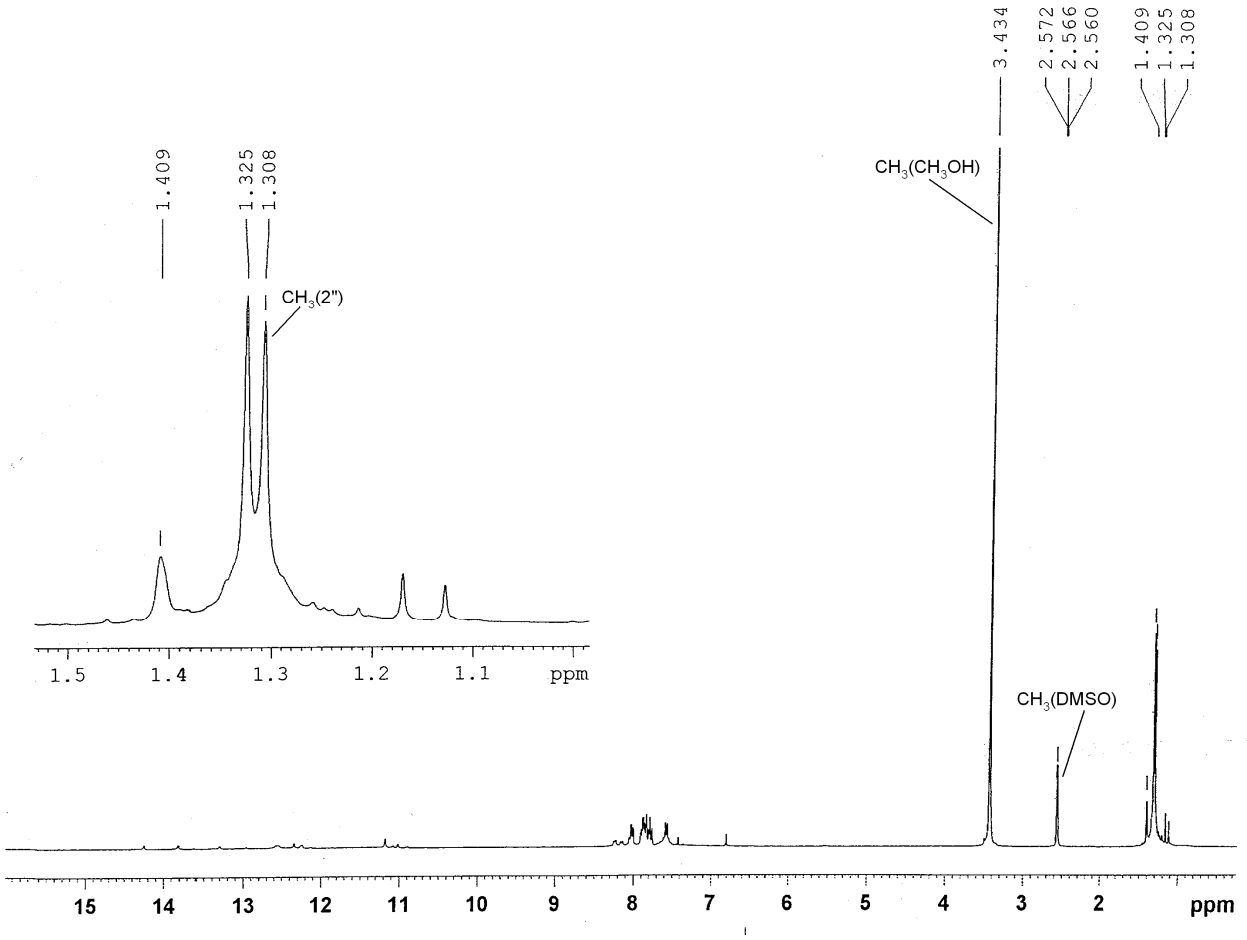

Fig.(V-26): ^{1}H-NMR data of compound **(3)** in DMSO-d_6 over the region δ16.0-0.0 (vide text for details).

Fig.(V-26) to Fig.(V-28) represent the 1D and 2D NMR data of compound **(3)**. Fig. (III-23) to Fig. (III-26) shows the corresponding data of ancillary ligand 2-aminothiophenol, H(atp) [Scheme (V-2)]. Assignments some of the relevant signals are indicated in the above figures. The CH(1′) signal is located at δ6.84 and it is only slightly modified from its free ligand position at δ6.68 indicating that the 2′ carbonyl group is not involved in the coordination process and the pterin ligand residue $(L^3)^{2-}$ acts as a bidented O,N donor as usual. Appearance of two separate sets of signals for the NH(8) signals indicate slight differences between the two pterin ligand residues on the NMR time scale. Both these signals are deshielded from their free ligand position at δ10.90, indication of considerable electron density withdrawal from the NH(8) position during the complex formation process. This is in agreement with a observation of Joule and coworker from synthetic and structural studies on pterin compounds [5b,5c]; this leads to electron density build up around the metal centre [Mo(IV)], which may be circulated even up to the ancillary

ligand $(atp)^{1-}$. For example, from 2D NMR data the NH_2 signal of $(atp)^{1-}$ could be located at δ3.25 [Fig. (V-28)], which is shielded from its free ligand position at δ4.8 [Fig. (III-23)]. Although the deprotonation of the adjacent –SH group (2-aminothiophenol) may contribute partly to this shielding process, distinct contribution from the electron density build up around the metal centre cannot be ruled out. The NH(2) signal of $(L^3)^{2-}$ residue also appears at δ3.25 as evident from the 2D NMR data, where a cross pick connects this signal to the $CH_3(2'')$ signal at δ1.32 [Fig. (V-28)].

The aromatic proton signals of $(L^3)^{2-}$, $(Ph_4P)^+$ and of $(atp)^{1-}$ are also indicated in the above figures. The above inferences are in agreement with the schematic structure of compound **(3)** as shown in Scheme (V-5), i.e., metal centre achieves a coordination no of six or octahedral coordination.

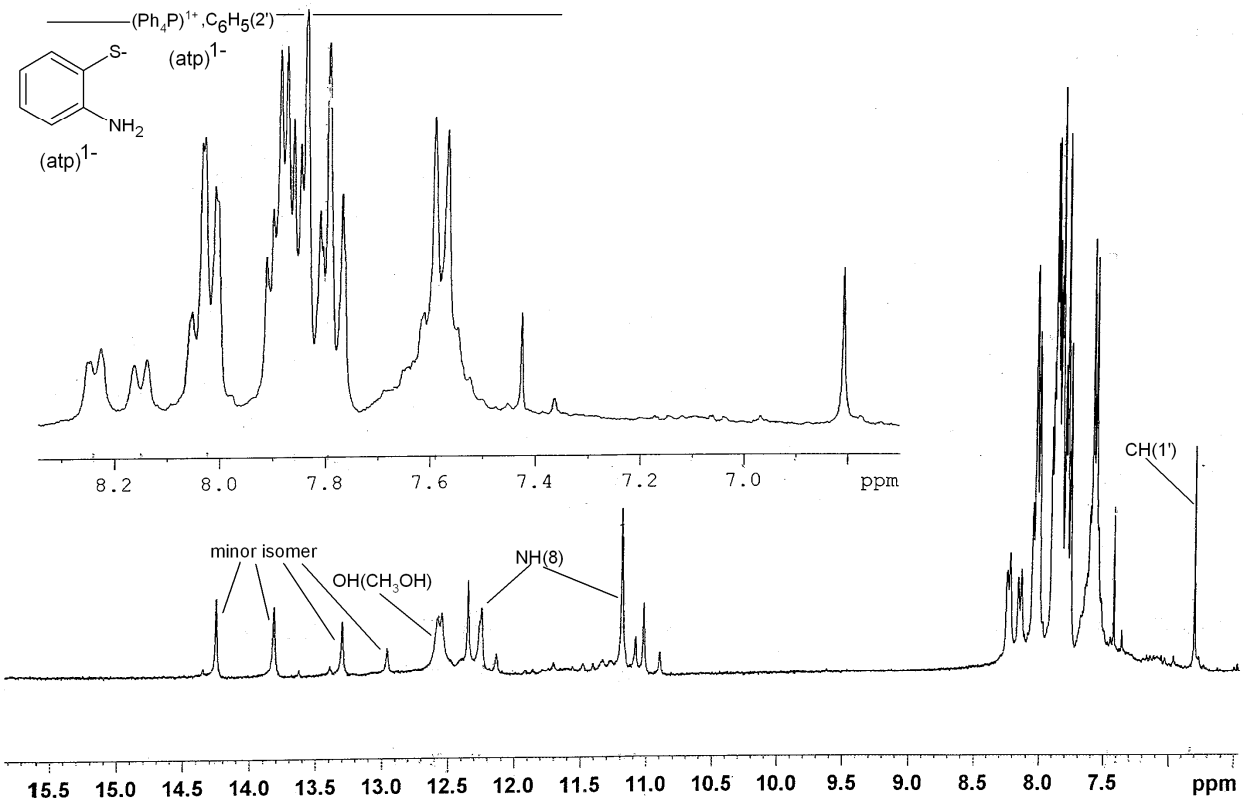

Fig.(V-27): ^{1}H-NMR data of compound **(3)** in DMSO-d_6 over the region δ15.5-6.0 (vide text for details).

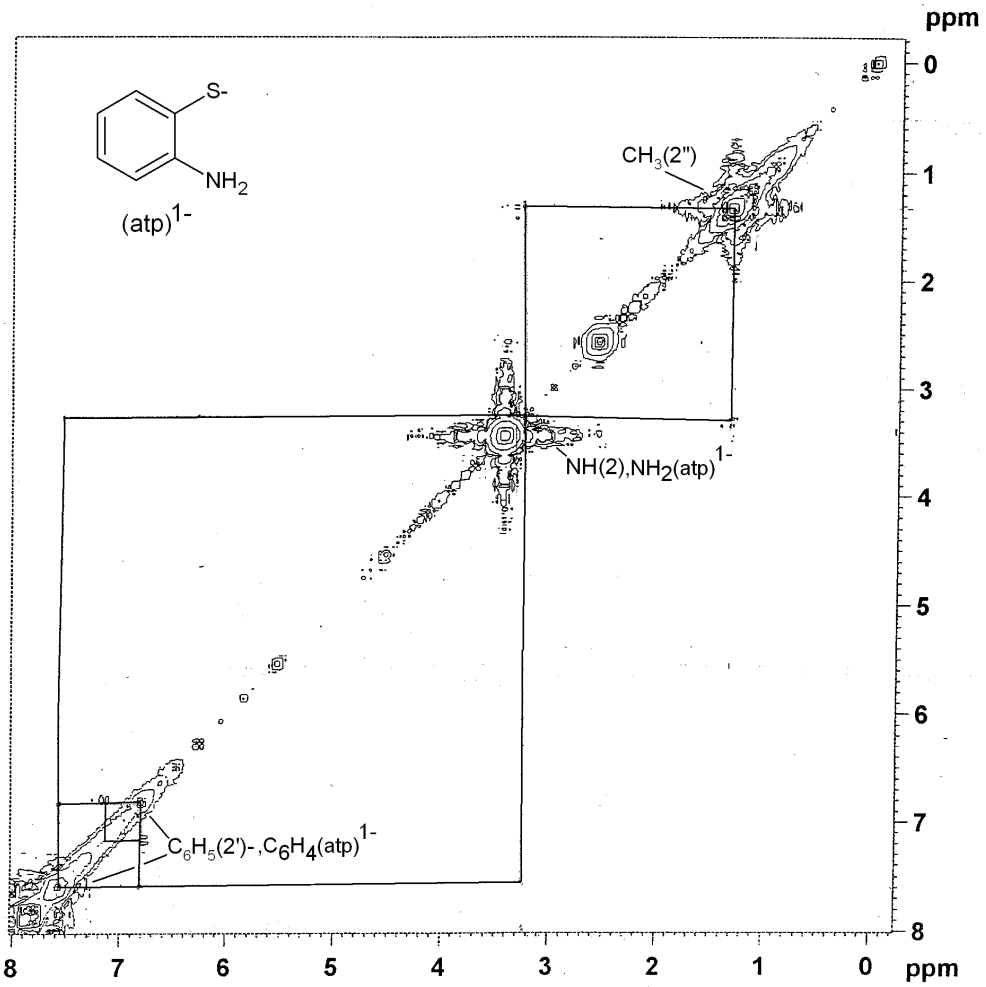

Fig. (V-28): ^{1}H-^{1}H COSY data (symmetrized) of compound **(3)** in DMSO-d_6 over the region δ8.0-0.0 (vide text for details).

The ^{1}H-NMR spectrum of the ancillary ligand 2-aminoethanethiol hydrochloride is shown in Fig. (III-33). Fig. (V-29) to Fig. (V-31) represent the 1D and 2D NMR spectral data of the compound **(4)**. As evident from Fig. (V-30) the CH(1′) signal appears at δ6.81(s), essentially unchanged from its free ligand position at δ6.68(s) and reflecting the non-participation of the 2′-carbonyl group in the metal coordination process; bidented O,N coordination nature of the pterin ligand residue $(L^{3})^{2-}$ is indicated. A minor signal at δ7.11(s) is due to the presence of minor isomer of compound **(4)**. Two separate signals are observed for the NH(8) group indicating the small differences between the two pterin ligands as in earlier cases. Both these signals are deshielded from the free ligand position at δ10.90(wb) indicating electron withdrawal from the NH(8) position during the complex formation process [5b,5c]. Assignment of the aromatic proton signals are indicated in Fig. (V-29). The CH_3(2″) signals appear around δ1.10 to δ1.14

[Fig. (V-29)]; the two sets of signal points out difference among the three $CH_3(2'')$ signals due to restricted rotation around NH(2) –C(1″) bond. The 2D NMR spectrum [Fig. (V-31)] gives a better insight into this aspect. The major $CH_3(2')$ signal at δ1.17 is connected by off-diagonal peaks to the NH(2) signal at δ4.02. The latter signal is only slightly affected from its free ligand position indicating little change in electron density around NH(2) group during the complex formation process unlike the electron depletion around NH(8). However in Chapter-II, the pterin ligand (H_2L^1) shows a different behaviour, e.g., there is building-up of electron density around the $NH_2(2)$ group [Fig. (II-8)] during the complex formation process, as evident from x-ray structural data. This involvement of either NH(2)/$NH_2(2)$ or NH(8) in electron transfer process, is also supported by the results of x-ray structural data on oxomolybdoenymes or tungstopterin enzymes. The electron transfer protein (Fe-S cluster) is H-bonded to either the NH(2) or the NH(8) group, depending on the functional aspect of the metal centre of such enzymes [Fig. (I-3)].

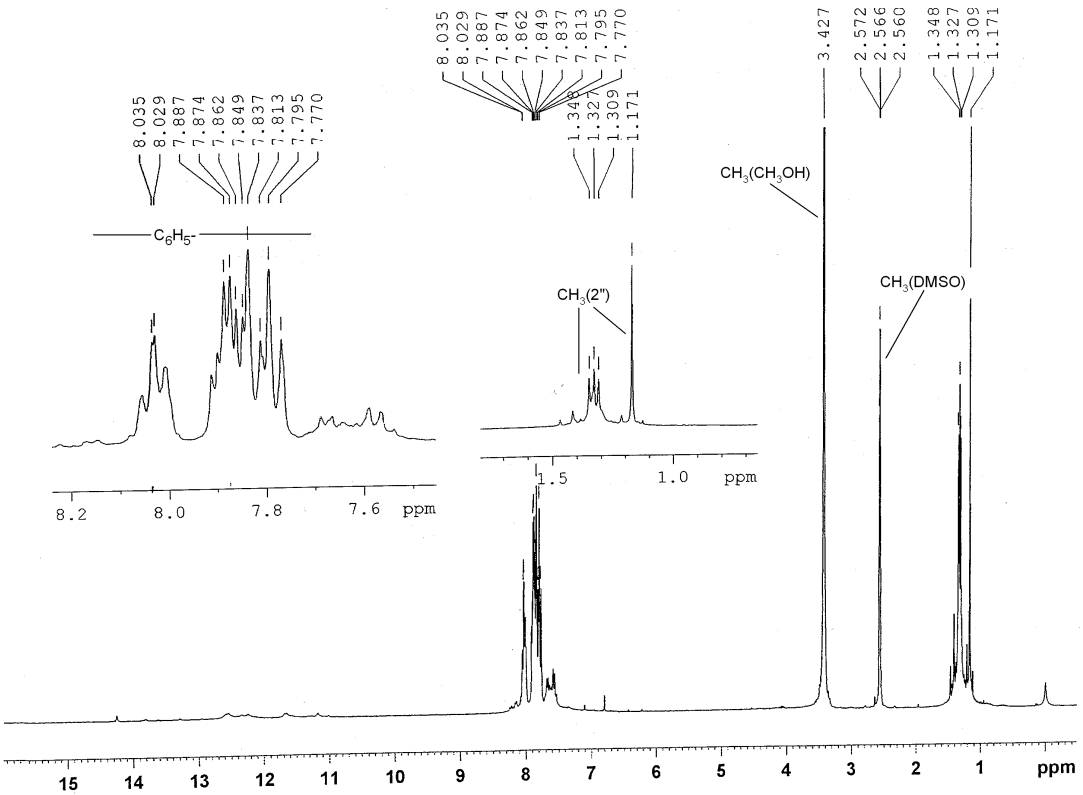

Fig.(V-29): ^{1}H-NMR data of compound **(4)** in DMSO-d_6 over the region δ16.0-0.0 (vide text for details).

The phenyl signals are assigned in 1D NMR data [Fig. (V-29)]; evidently the aromatic protons of $(L^3)^{2-}$ and $(Ph_4P)^+$ could not be differentiated. The proton signals of the $(aet)^{1-}$ residue

[CH_2(1)(aet); CH_2(2)(aet) and NH_2(aet)] appear at δ2.25, δ2.60 and δ3.29 respectively [Fig. (V-31)]. As compared to the free ligand data in hydrochloride from [Fig. (III-33)], they undergo shielding on complex formation. Loss of the HCl moiety as well as deprotonation of –SH group of the ancillary ligand (hydrochloride from) during chelation, leads to electron density enhancement around this ligand residue in compound **(4)**.

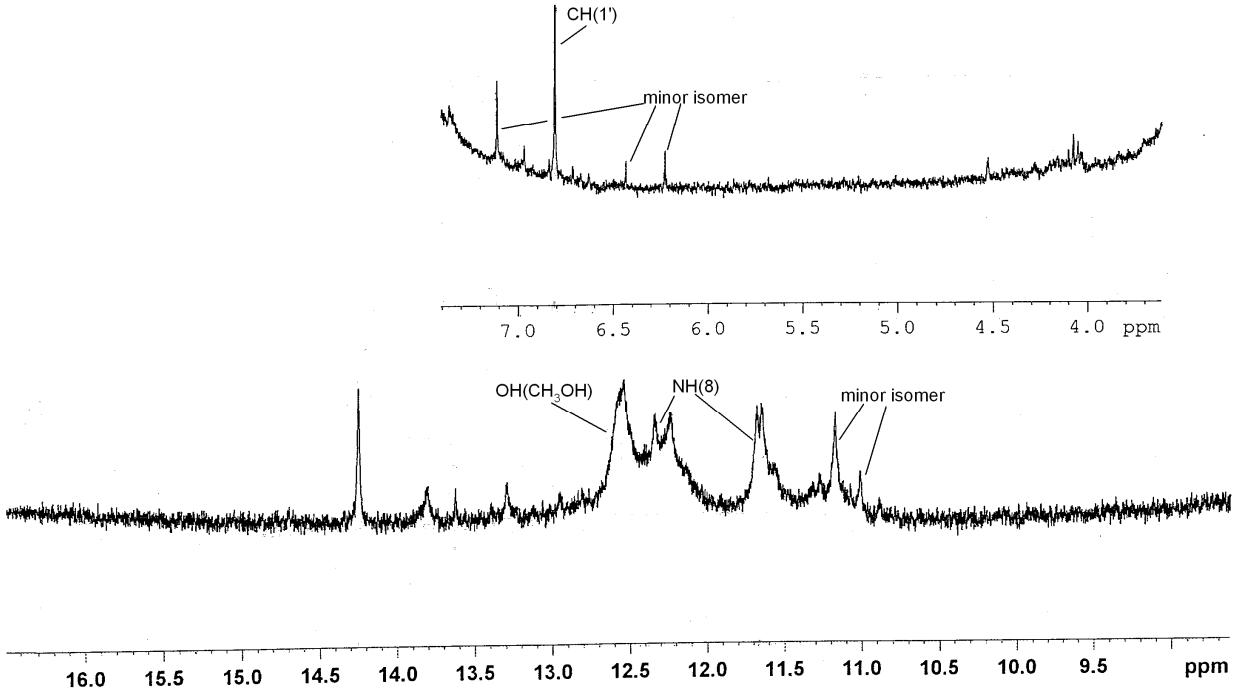

Fig.(V-30): ^{1}H NMR data of compound **(4)** in DMSO-d_6 over the region δ16.0-9.0 (vide text for details).

The relevant ^{1}H-NMR data of compound **(5)** are shown in [Fig. (V-32) to Fig. (V-34)]. The 2D NMR data of the ancillary ligand cysteine is shown in Fig. (III-38). As in earlier cases, the CH(1′) signal $(L^3)^{2-}$ residue appears at δ6.81(ss) indicating non-participation of the 2′-carbonyl group coordination process; $(L^3)^{2-}$ residue acts as bidented O,N donor involving the O(4), N(5) donor sites. The CH_3(2′) signals appear around δ1.20- δ1.50(m) with the band centre at δ1.32. The aromatic proton signals of the $(Ph_4P)^+$, $(L^3)^{2-}$ residues are observed over the region δ7.5- δ8.2 (m) both in the 1D and 2D spectra.. The –OH(CH_3OH) and NH(8) signals could be located at δ12.55(d), δ12.28 (bd) and δ11.69(bt) respectively. The NH(8) signals are deshielded from their free ligand position (δ10.9) as usual. Besides these, a few other signals could be observed over the region δ11.0- δ14.0 due to contribution from the minor isomers. The 2D NMR data helps to assign the NH(2) signals at δ4.06, which is connected by cross-peaks to the CH_3(2″) signal at δ1.20; the former signal is hardly affected from its free ligand position at

δ4.20. For the ancillary ligand residue $(cys)^{2-}$, the NH_2, CH(1) and CH_2(2) signals could be located at δ2.60, δ1.95 and δ1.32 respectively [Fig. (V-34)]. These signals are all shielded from their free ligand positions, as shown in Fig. (III-38). Deprotonation of the –SH group is partly responsible for this observation. Besides these the high electron density around the [Mo(IV)] centre may contribute to this aspect.

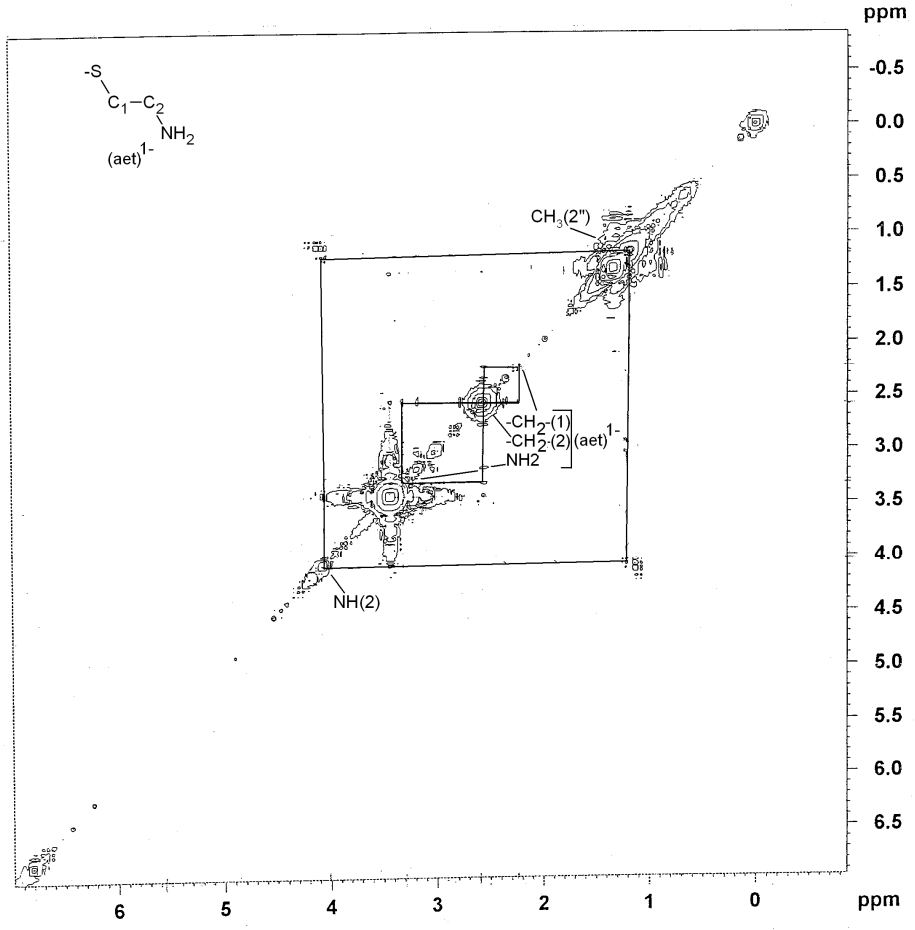

Fig. (V-31): ^{1}H-^{1}H COSY data (symmetrized) of compound **(4)** in DMSO-d_6 over the region δ6.0-0.0 (vide text for details).

The 1D and 2D ^{1}H- NMR data of compound **(6)** are represented in Fig. (V-35) to Fig. (V-37). From the 1D spectrum [Fig. (V-37)], the –OH(CH_3OH) is assignable at δ12.56(t); NH(8) group of the two $(L^3)^{2-}$ residue are seen at δ12.28 and δ11.58, indicating the deshielding of the NH(8) group from its free ligand position. The aromatic proton signals of -C_6H_5 group of the $(L^3)^{2-}$ residue appear at δ7.5- δ8.3(m) [Fig. (V-37)]. From the off-diagonal peaks of Fig. (V-35) two CH_3(2″) and NH(2) of two $(L^3)^{2-}$ residue are assigned at δ1.17, δ1.32 and δ4.07, δ4.38 respectively. From Fig. (V-36) only one of the CH(1′) group can be assigned at δ6.80, which is practically unchanged from the free ligand ($H_2L^3.H_2O$) position. The above observation indicates

the bidented nature of the pterin ligand during the metal coordination process. The contributions from minor isomer appear at δ11.25 and from δ1.0 to δ1.53.

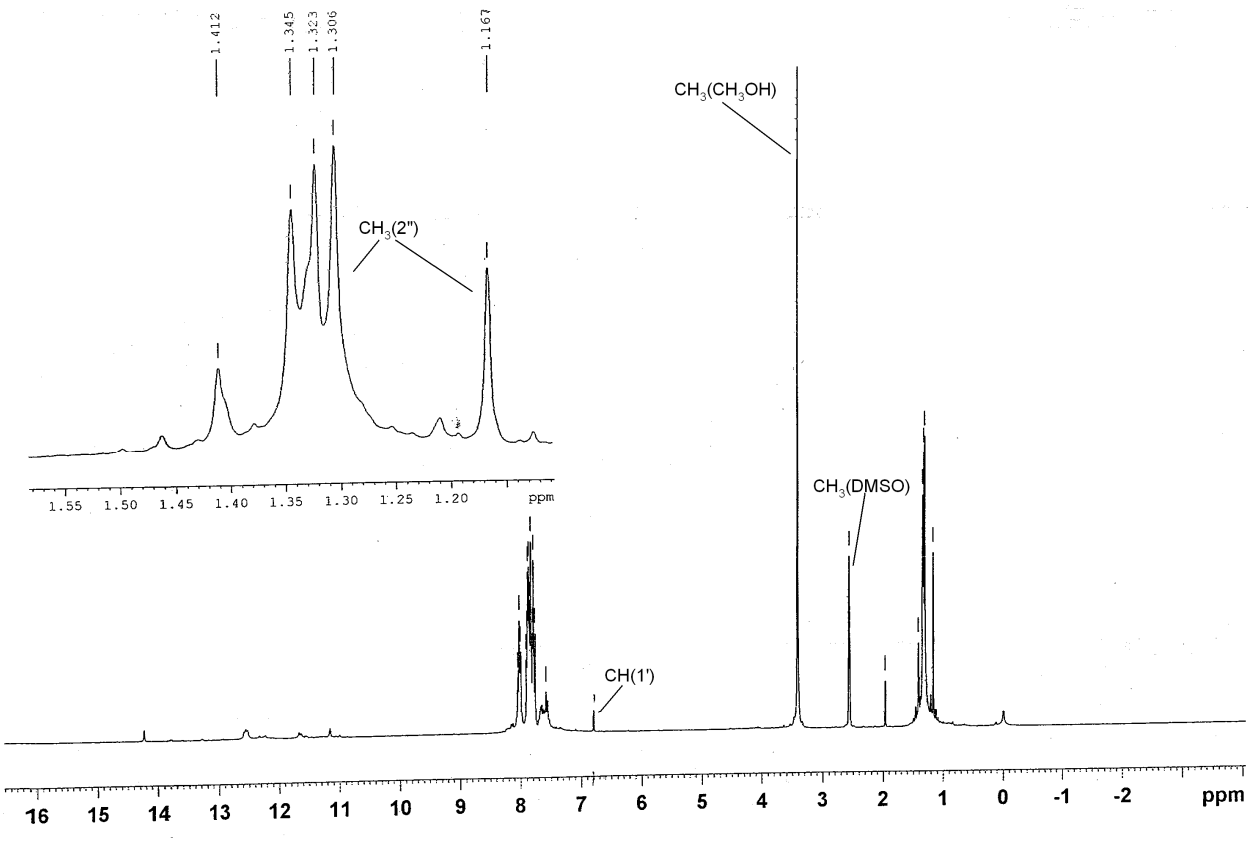

Fig.(V-32): ^{1}H-NMR data of compound **(5)** in DMSO-d_6 over the region δ16.0-0.0 (vide text for details).

In the ^{1}H-NMR spectrum of compound **(7)** (D_6-DMSO), the phenyl (2′) ring protons could be assigned at δ8.13 (2H, m) and δ7.55(3H, m) ; the three separate CH(1′) signals appear at δ7.37(s), δ6.98(s) and δ6.81(s) respectively. The three signals (bs) for the

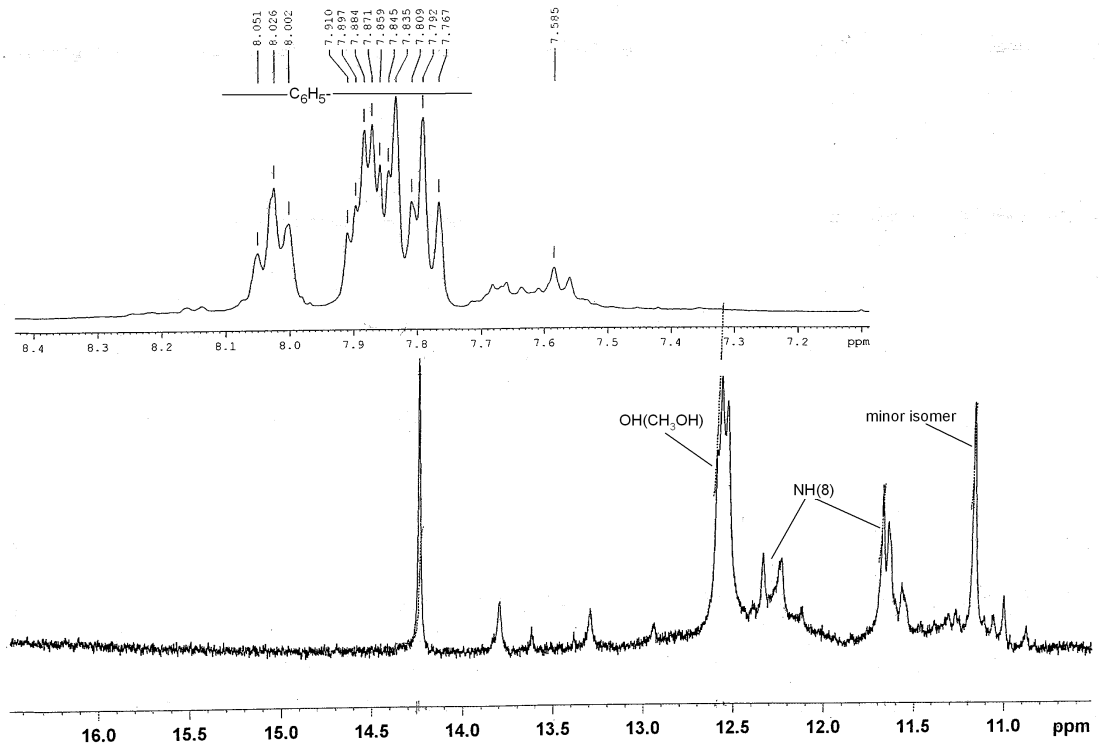

Fig.(V-33): ^{1}H-NMR data of compound **(5)** in DMSO-d_6 over the region δ16.0-11.0 (vide text for details).

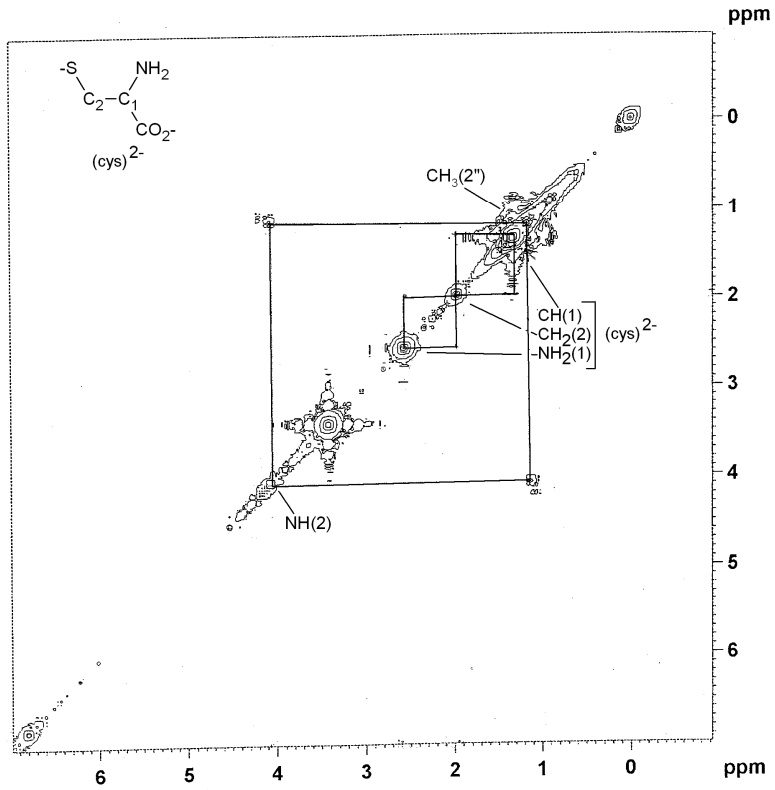

Fig. (V-34): ^{1}H-^{1}H COSY data (symmetrized) of compound **(5)** in DMSO-d_6 over the region δ6.0-0.0 (vide text for details).

NH(8) proton are characterized at δ12.28, δ11.78 and δ11.55. That is, all these proton signals are deshielded from their corresponding positions in compound **(1).** Reaction [Equation. (V-1) and Scheme (V-9)] between compound **(1)** and $Me_3N \rightarrow O$ involves transfer of electron density from the former to the later and the pterin ligand residues $(L^3)^{2-}$ act as the source of electrons here. Redox non-innocent behavior of the pterin ligand is highlighted here.

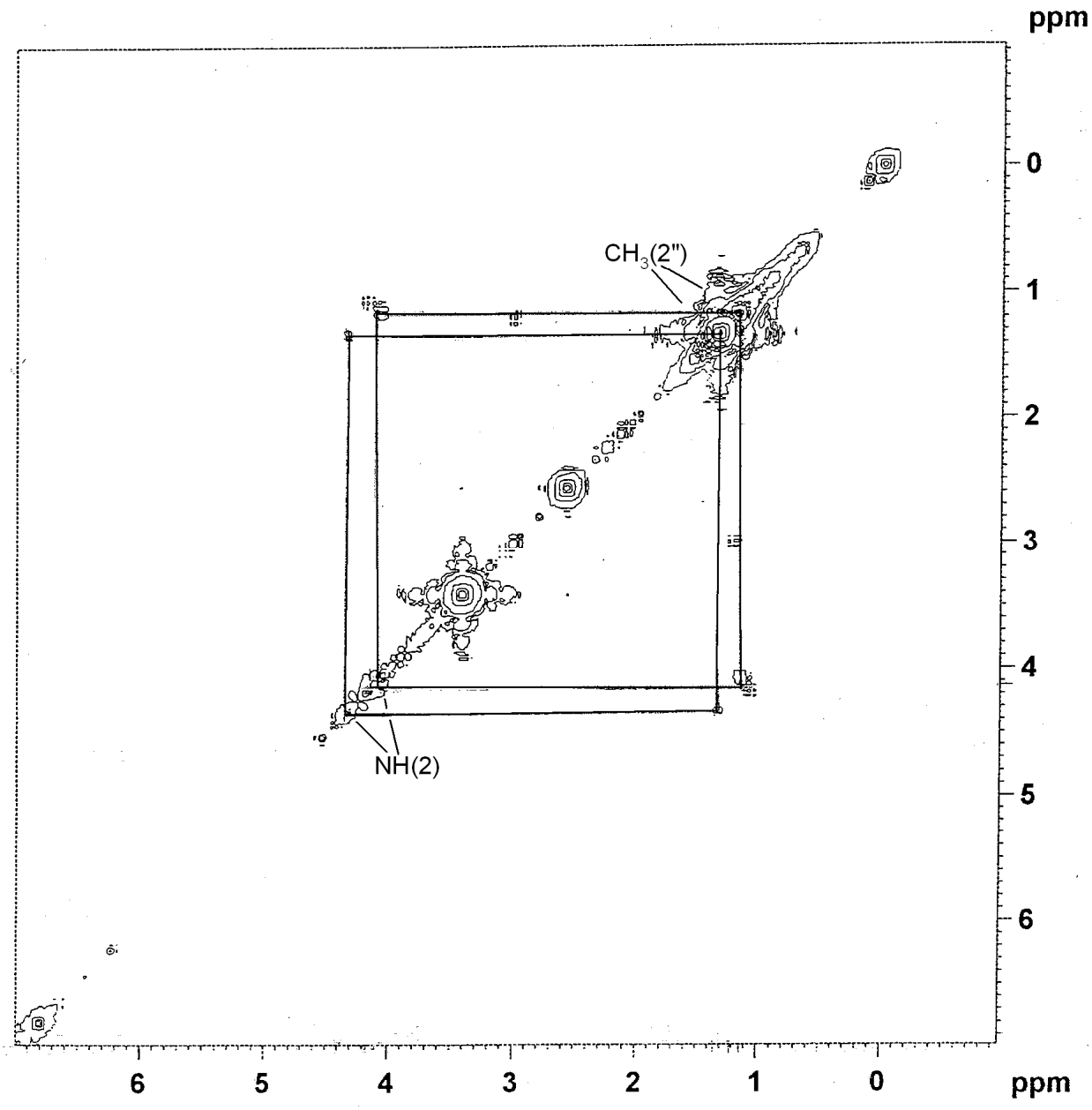

Fig. (V-35): ^1H-^1H COSY data (symmetrized) of compound **(6)** in DMSO-d_6 over the region δ6.0-0.0 (vide text for details).

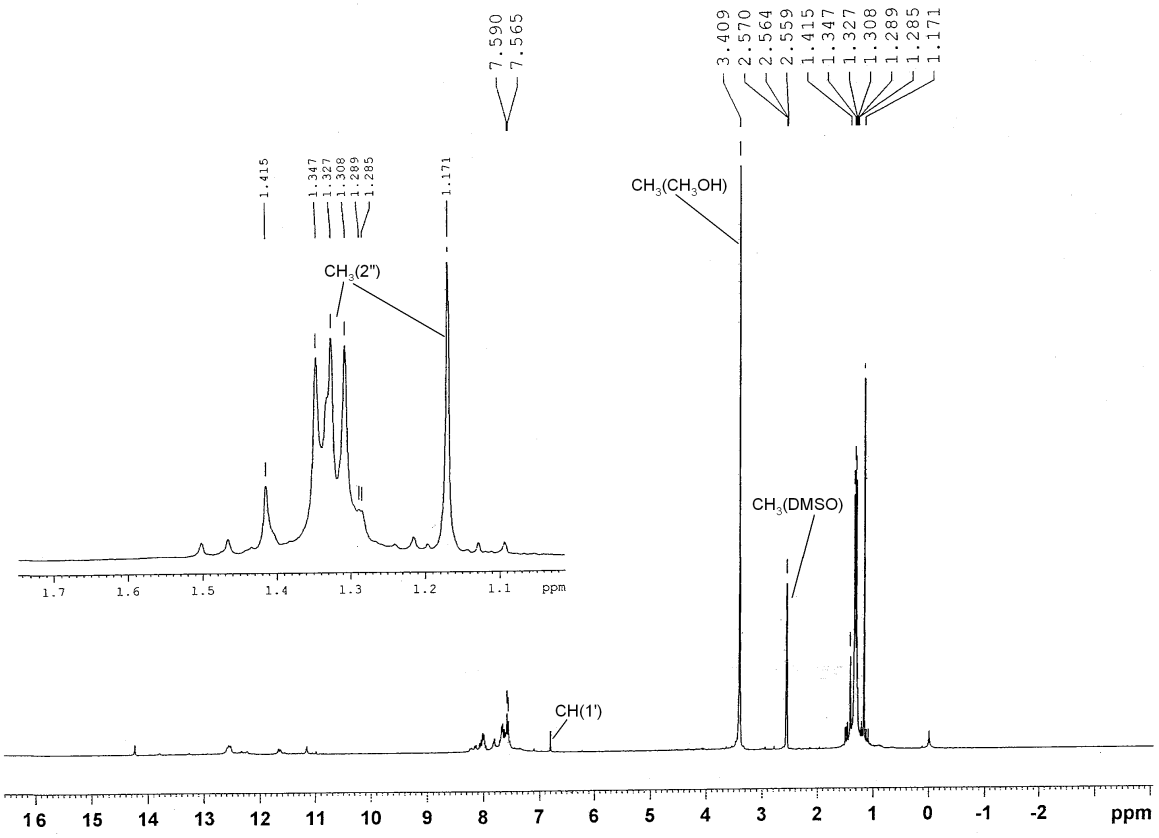

Fig. (V-36): ^{1}H-NMR data of compound **(6)** in DMSO-d_6 over the region δ16.0-0.0 (vide text for details).

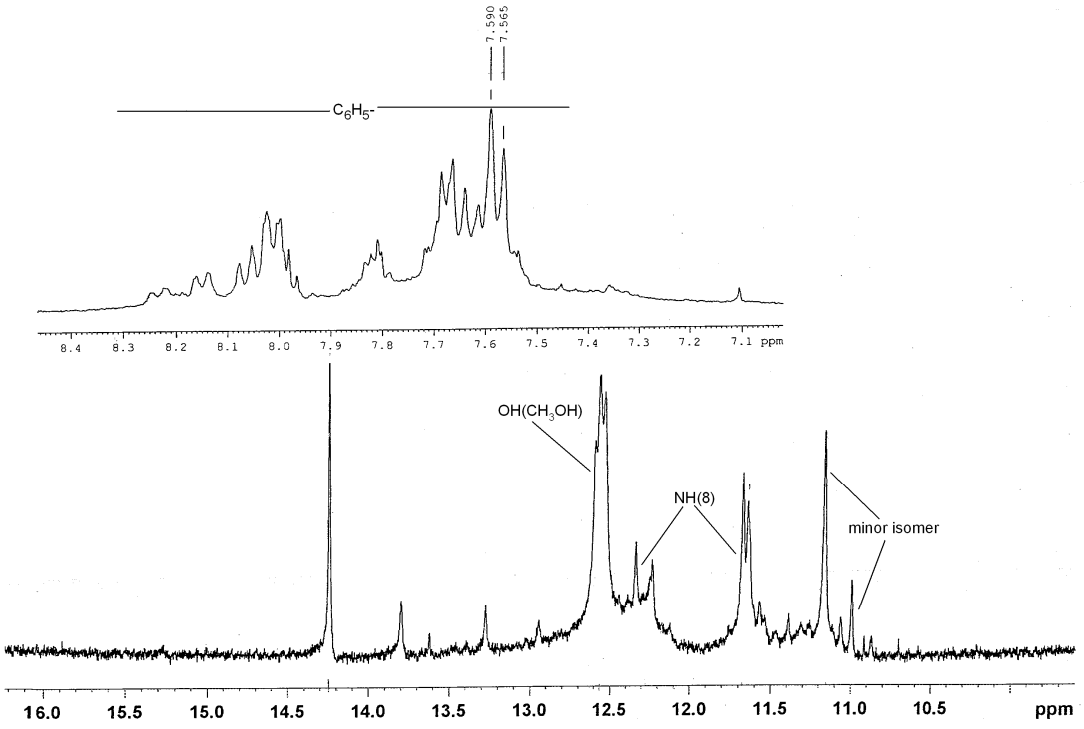

Fig. (V-37): ^{1}H-NMR data of compound **(6)** in DMSO-d_6 over the region δ16.0-11.0 (vide text for details).

Table (V-3): Relevant ^{1}H-NMR signals in DMSO-d_6 (300 MHz, δ ppm, internal TMS) of the free ligand H_2L^2, the corresponding compounds (**1**) – (**5**) and Δ ($=\delta_{complex} - \delta_{ligand}$) values.

Compound[a]	CH(1′)(δ) Δ*	NH(8) (δ) Δ*	NH(2) (δ) Δ*
(H_2L^3)	6.68	10.90	4.20; 3.96
(1) [b]	6.67;6.10 -0.01;-0.58	11.50 0.6	[e]
(2) [b,c,d]	6.80 0.12	12.25;11.65 1.35;0.75	3.25 -0.95
(3) [b,c,d]	6.84 0.16	12.25;11.10 1.35;0.2	3.25 -0.95
(4) [b,d]	6.81 0.13	12.30:11.10 1.4;0.2	4.02 -0.18
(5) [b,d]	6.81 0.13	12.30;11.60 1.4;0.7	4.06 -0.14
(6) [b,c,d]	6.80 0.12	12.30;11.60 1.4;0.7	4.07,4.38 -0.13;0.18
(7) [b]	7.37; 6.98; 6.81 0.69;0.3;0.13	12.28;11.55 1.38;0.65	[e]

Abbreviations : ss = sharp singlet ; wb = weak broad.

[a]vide Scheme (V-1) for the proton numbering system.

[b]CH_3OH signals of these complexes appear at δ 13.60 – 13.65 (-OH) and δ 3.41 – 3.40 (CH_3-) respectively.

[c]**the shielding of the NH(2) signal is associated with the electronic redistribution during complex formation process involving the redox non-innocent pterin ligand; concluding remarks of this thesis give a better picture**

[d]The phenyl ring proton signals of the Ph_4P^+ counter cation of compound **(2)**, appear at δ 8.0- δ 7.4. The 2D NMR data of PPh_4Br (in CH_3OH –d_4) is shown in Fig.(III-37).

[e]Here this signal could not be located with certainty.

Fluorescence spectra (in CH_3OH)

The electronic redistribution in the pterin ligand during the complex formation is further supported by fluorescence spectra. The free pterin ligand ($H_2L^3.H_2O$) is moderately fluorescent [Fig. (V-38)] due to the presence of aromatic phenyl ring (2′) [with both the pyrimidine and pyrazine rings are in the non-aromatic state, Scheme (V-1)] whereas the compound **(1)** is strongly fluorescent [Fig. (V-39)]. In case of compound **(1)** several factors contribute towards its more rigid framework, e.g. the pyrimidine ring of the pterin ligand residue $(L^3)^{2-}$ [Scheme (V-10)], achieves aromaticity and the chelation process makes the entire complex molecule rigid. As a result dissipation of the excitation energy in manners other than by the emission of fluorescent light is prevented [23].In fact, strong fluorescence property of pterins (essentially the oxidized forms with aromatic rings, e.g., pterin-6-carboxy-7-sulphonic acid) has served as a nice probe for their detection in the molybdenum-cofactor (of oxomolybdoenzymes) after oxidative degradation. Even pH dependence of fluorescence property of biopterin is interesting, e.g., no fluorescence of the protonated form and strong fluorescence for the anion is observed [24].

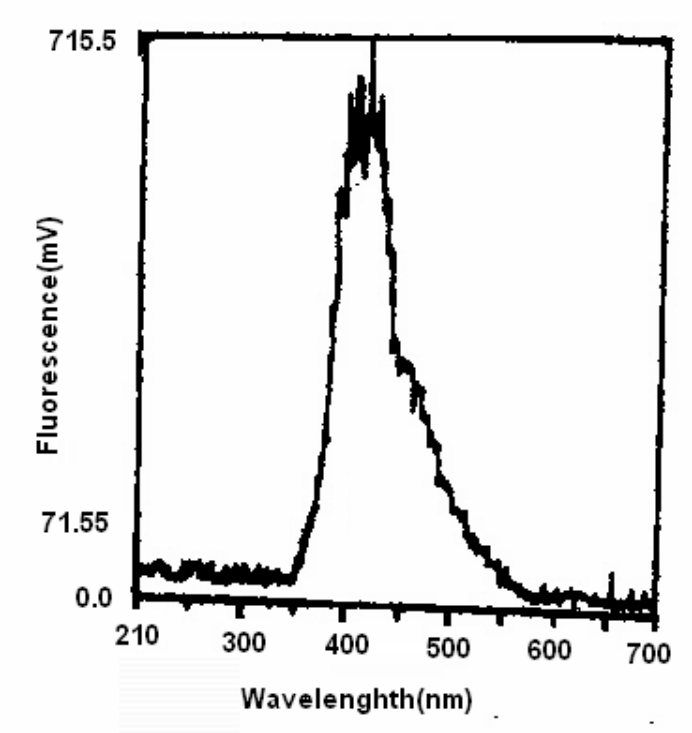

Fig. (V-38): Fluorescence spectra in methanol of free pterin ligand ($H_2L^3.H_2O$) (1.5 x 10^{-5} mol dm^{-3}).

For the compound **(2)** the fluorescence spectra is shown by the Fig. (V-40). In this case the decrease in intensity is observed. λ_{max} is observed at 410 nm along with shoulders at 440 and 430 nm.

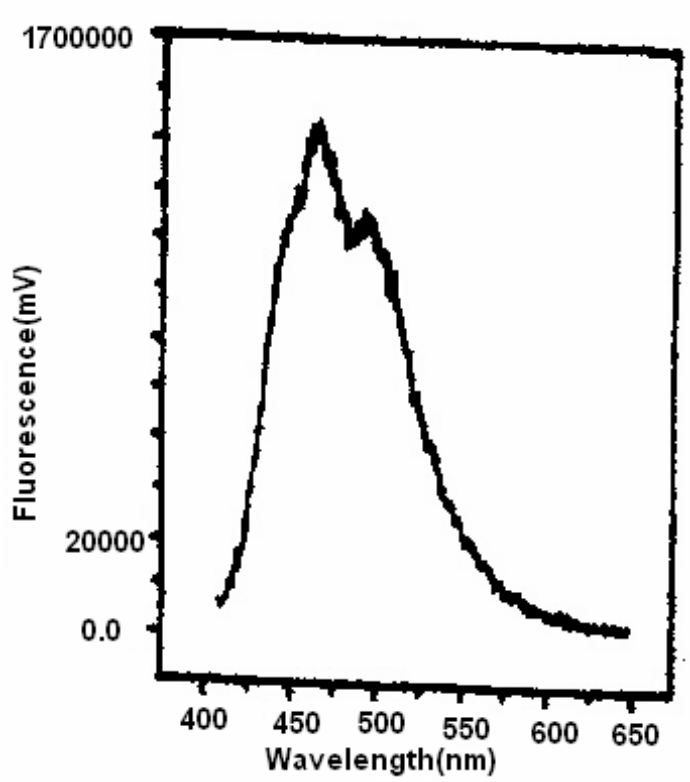

Fig. (V-39): Fluorescence spectra in methanol of compound **(1)** (4.8×10^{-6} mol dm^{-3}).

In case of compound **(3)** further decrease in intensity of florescence spectra [Fig. (V-41)] is observed. Here λ_{max} is observed at 499 nm along with two peaks at 459 and 445 nm.

The fluorescence spectra of compound **(4)** is represented in the Fig. (V-42). Here λ_{max} is observed at 450 nm with another peak at 430 nm.

Similar trend in fluorescence spectra is also in case of compound **(5)**, Fig. (V-43). Here also the intensity is decreased and λ_{max} is obtained at 430 nm with two shoulders at 455 and 494 nm.

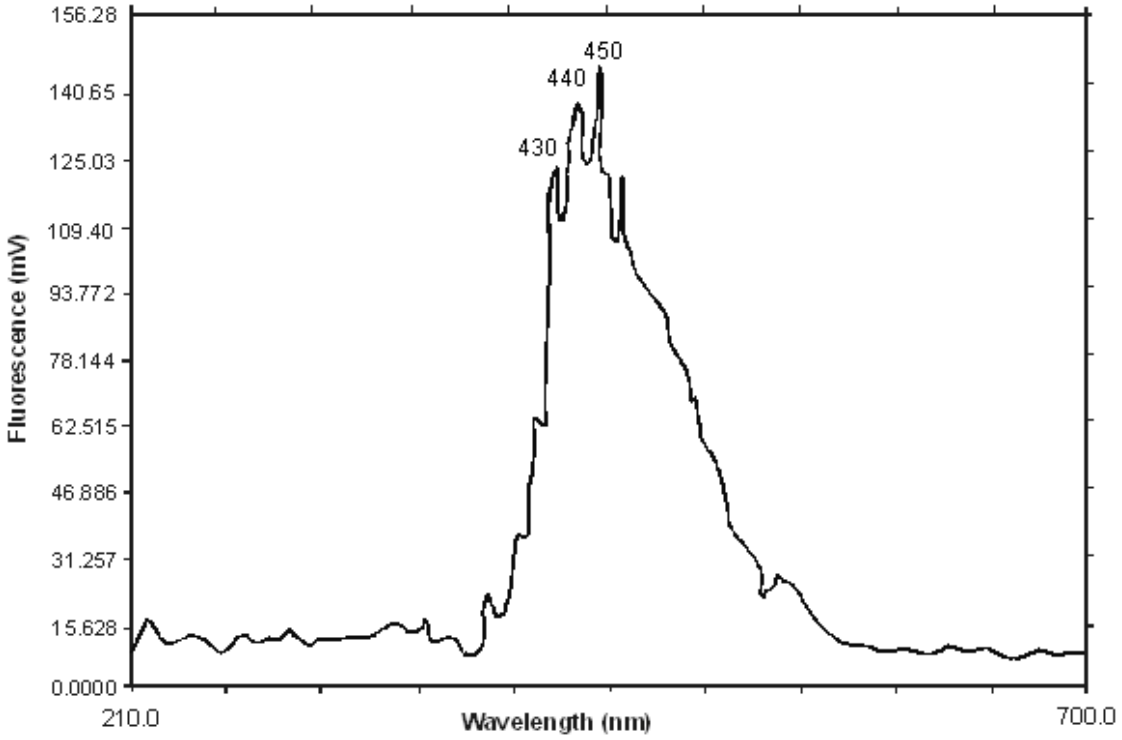

Fig. (V-40): Fluorescence spectra in methanol of compound **(2)** (6.0×10^{-5} mol dm^{-3}).

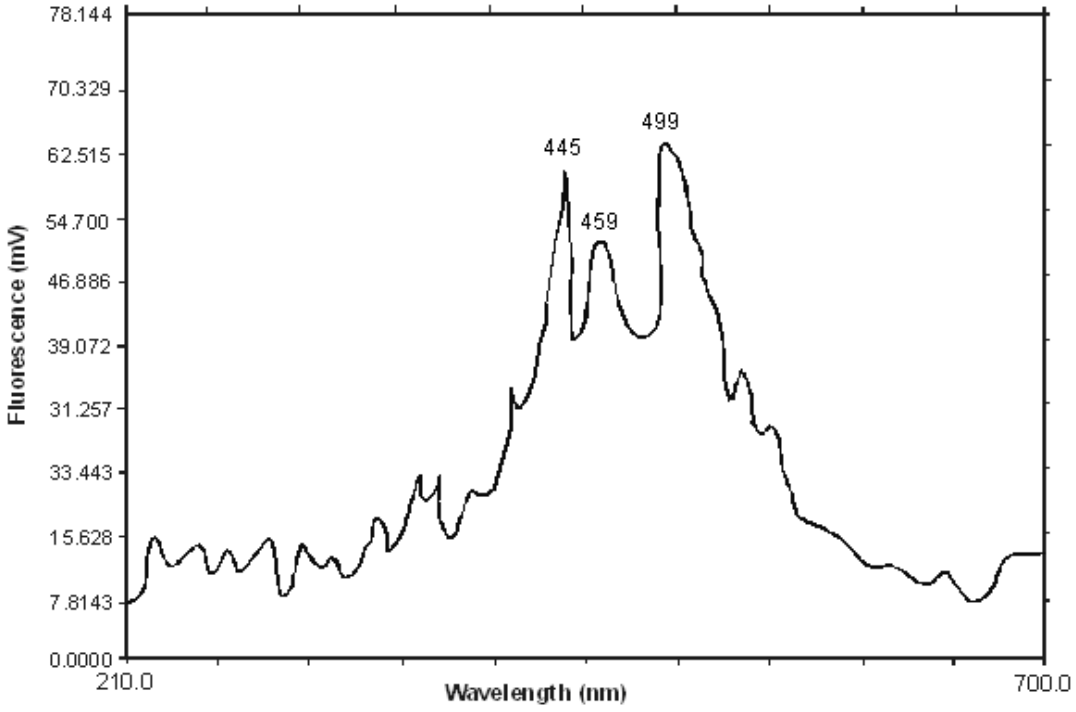

Fig. (V-41): Fluorescence spectra in methanol of compound **(3)** (1.3×10^{-5} mol dm^{-3}).

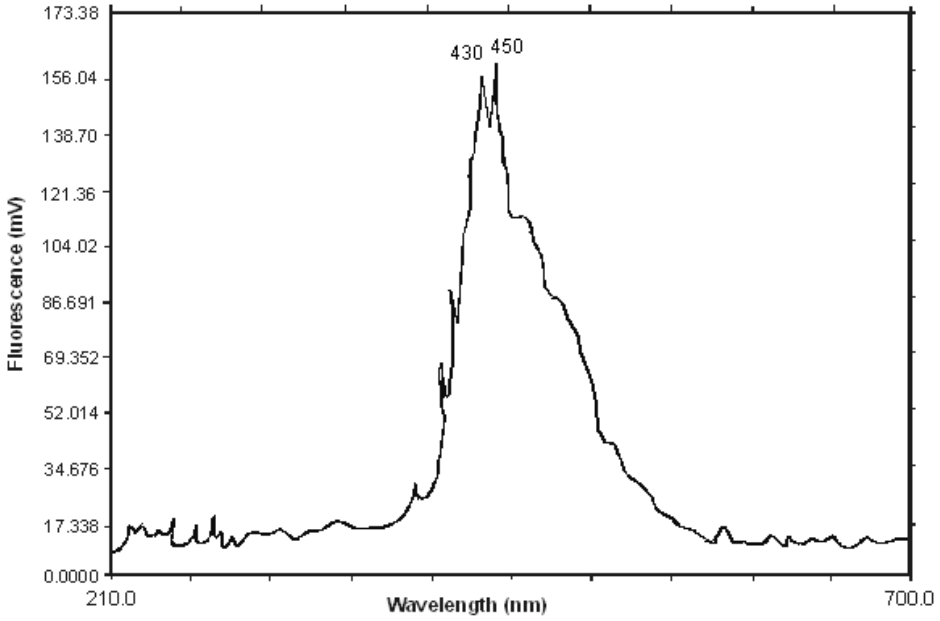

Fig. (V-42): Fluorescence spectra in methanol of compound **(4)** (5.8×10^{-5} mol dm^{-3}).

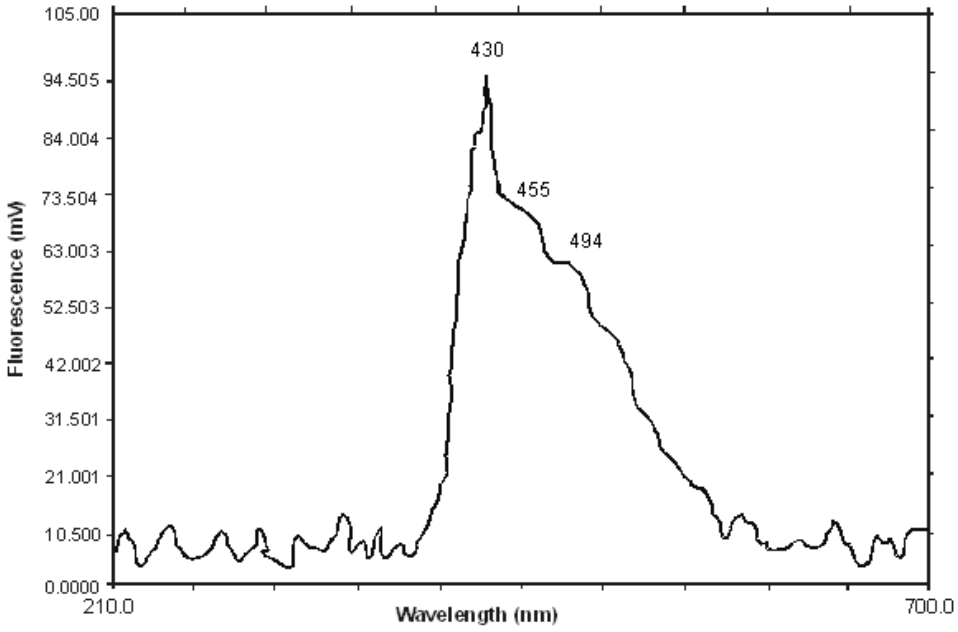

Fig. (V-43): Fluorescence spectra in methanol of compound **(5)** (1.5×10^{-5} mol dm^{-3}).

For the compound **(6)** [Fig. (V-44)] intensity is also decreased with λ_{max} at 445 nm and two shoulders found at 455 and 494 nm. Most likely formation of mixed ligand/ binuclear complexes leads to a decrease in fluorescence intensity, compared to that of compound **(1)**.

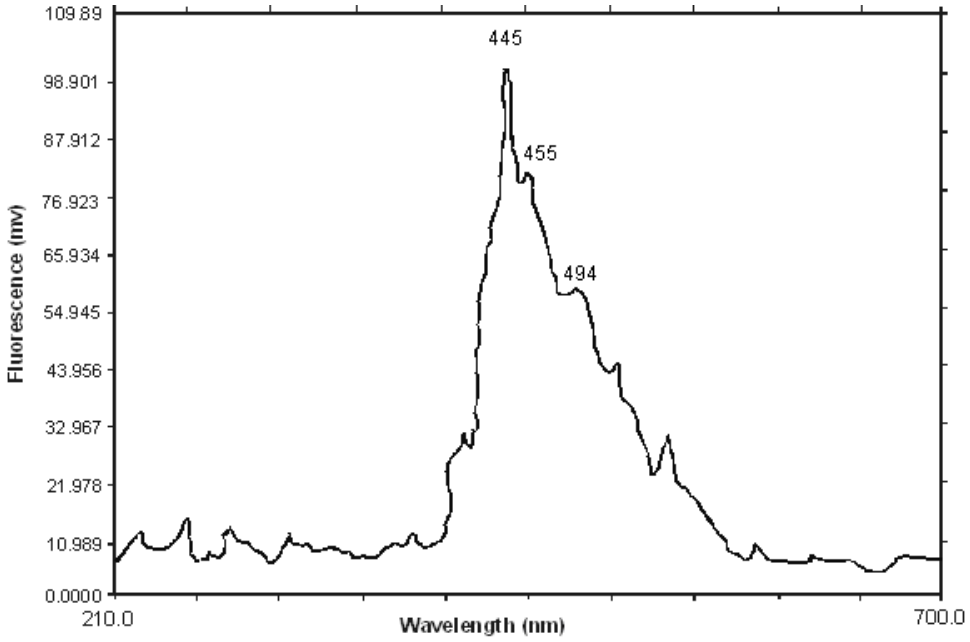

Fig. (V-44): Fluorescence spectra in methanol of compound (6) (6.0×10^{-5} mol dm^{-3}).

CHEM3D models

The possible schematic structures of the pertinent compounds were optimized by molecular mechanics calculations (MM2), giving the lowest steric energy (kcal/mol*)* CHEM3D models e.g., Fig. (V-45) for $H_2L^3.H_2O$ with a steric energy of 0.21 kcal/mol and a steric energy value of 29.6 kcal/mol for compound **(1)** with its CHEM3D model shown in the Fig. (V-46), thereby throwing light on their stability as well as geometry [19]. Besides this, other two basic parameters were evaluated, e.g., bond distances (Å) and bond angles (deg), the important of which are shown for compound **(1)** in Table (V-4), together with the literature data obtained through x-ray structural studies on molybdenum complexes with different pterin ligands and other relevant systems for comparison [16]. Here the Mo-N(5) distance [Scheme (V-10)] shows a fair agreement between the computed and experimental literature data. Concentrating on the chelating aspect of the pterin ligand towards molybdenum, the Mo-N(5) bond plays a pivotal role here; it has significant multiple bond character as verified through x-ray structural data [1]. Joule and coworkers concluded from both chemical and x-ray structural studies that sufficiently greater

basicity/ nucleophilicity resides at N(5) than at N(8), thereby supporting such coordination property [20]. Table (V-4) shows essentially four types of computed bond angles involving the [Mo(IV)] atom, in agreement with the four types of such bond angles (72^{o}-74^{o}, 80^{o}-88^{o}, 92^{o}-98^{o} and 158^{o}-170^{o}) found from x-ray structural studies in different molybdenum-pterin systems with distorted octahedral geometry around the Mo atom (in both mono and binuclear complexes) [1]. A good agreement is observed [Table (V-5)] between the selected optimized bond lengths (Å) of the CHEM3D model of $H_2L^3.H_2O$ and the corresponding literature x-ray structural data of several pterin compounds [20]. Table (V-5) also compares several optimized bond length data (Å) of $H_2L^3.H_2O$ and compound **(1)**, some of which undergo change during the complex formation process. It is evident that the pterin ring is attached to the Mo atom [in compound **(1)** through the O(4) and N(5) atoms resulting from the dianion formation [Scheme (V-10)] involving the amide function in position 3, 4 and the vinylogous amide in position 5 including the adjacent side-chain [i.e., the proton from C(1′) is located at N(5)]; [24a,b,d] each pterin ligand residue $(L^3)^{2-}$ in compound **(1)** acts as a tridentate one [Fig. (V-46)].

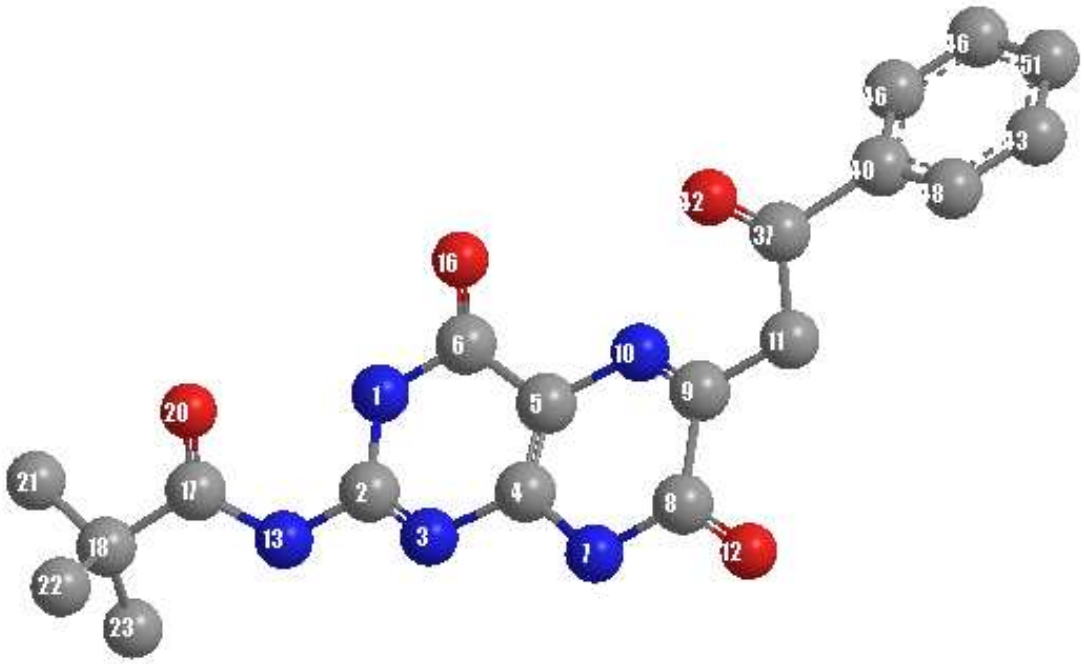

Fig. (V-45): The optimized geometry (CHEM3D model obtained through MM2 calculations) of free ligand i.e., $H_2L^3.H_2O$ with a steric energy of 0.21 kcal/mol.

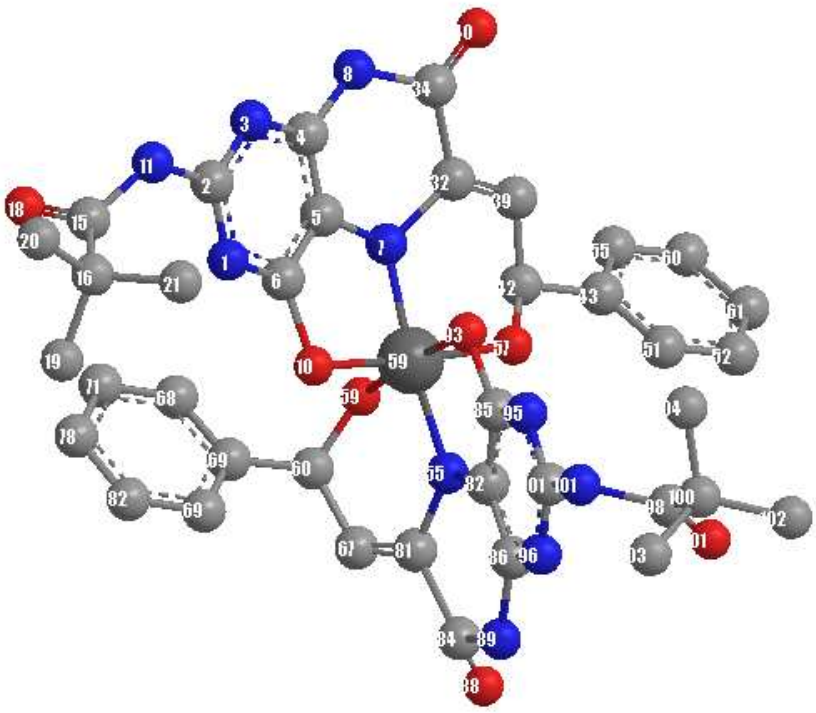

Fig. (V-46): The optimized geometry (CHEM3D model obtained through MM2 calculations) of compound **(1)** with a steric energy of 29.6 kcal/mol.

Table (V-4). Comparison of selected computed bond lengths (Å) and bond angles (deg) in compound **(1)** from the optimized geometry [Fig. (V-46), MM2 calculations] with the available literature data (in parentheses) from X-ray structural studies*

Bond distances (Å) [+,†]	**Bond angles (deg)** [+,≠]
Mo(59)-O(93) 1.965	O(10)-Mo(59)-O(59) 87.9
Mo(59)-O(10) 1.962	(80.16-88.0)
(2.081-2.302)	
Mo(59)-N(7)1.986	O(10)-Mo(59)-O(57) 161.1
Mo(59)-N(55) 1.980	(158.0-169.2)
(1.997-2.080)	N(55)-Mo(59)-O(10) 97.5
Mo(59)-O(57) 1.964	(92.1-98.8)
Mo(59)-O(59) 1.959	N(55)-Mo(59)-O(93) 77.5
(2.246-2.252)	(72-74)

*X-ray structural data have been collected from reference 1.

[+] Here O(10), O(93) and N(7), N(55) correspond to O(4) and N(5) donor atoms respectively, of the pterin ring as per Scheme (V-1), while O(57), O(59) correspond to O(2′) of the 6-substitutent.

[†] Bond length data for the two ligand residues in compound **(1)**.

[≠] One set of selected bond angle data involving Mo(59) for compound **(1)**, is presented here.

Table (V-5). Comparison of selected optimized bond lengths (Å) in the pterin ligand ($H_2L^3.H_2O$) and the molybdenum compound **(1)** from the respective optimized geometries (MM2 calculations). Available x-ray structural data on pterins are shown in parentheses.*

Bond[+]	**$H_2L^3.H_2O$**	**compound (1)**[±]
N(3)-C(4)	1.379 (1.390-1.400)	1.288, 1.283
C(4)-O(4)	1.234 (1.212-1.231)	1.366, 1.372
N(5)-C(6)	1.282[‡] (1.359-1.468)	1.462, 1.444
C(6)-C(1′)	1.512 (1.512-1.514)	1.401, 1.544
C(6)-C(7)	1.492 (1.467-1.535)	1.536, 1.530
C(7)-O(7)	1.219 (1.240)	1.206, 1.206
C(7)-N(8)	1.354 (1.303-1.443)	1.368, 1.368

[+] Scheme (V-1) indicates the atom numbering system.

[±] Data for the two ligand residues in compound **(1)**.

* X-ray structural data have been collected from reference 20.

[‡] The only exception to a reasonable agreement between the computed bond length data (Å) and related X-ray data, is the N(5)-C(6) distance; this is due to the presence of vinylogous amide in position 5 including the adjacent side-chain [i.e., the proton from C(1′) is located at N(5) through tautomerism, Schemes (V-1) and (V-10)] [24a,b,d].

The CHEM3D model of the compound **(2)** [Fig. (V-47)] can be obtained by the (MM2) calculations[19(a)] with the lowest steric energy 41.5 kcal/mol. It also indicates both the geometry and stability of the complex. Comparison of selected bond lengths and bond angels with the literature values are given in the Table (V-6). Concentrating on the bond length data,

obtained from the MM2 calculations [19(a)] of free pterin ligand (H_2 L^3.H_2O) and compound **(2)**, the chelating nature of the ligand can also be understood. Table (V-7) contains some of the comparison of bond length data of both free ligand as well as in the compound **(2)**.

Table (V-6). Comparison of selected computed bond lengths (Å) and bond angles (deg) in compound **(2)** from the optimized geometry [Fig. (V-47), MM2 calculations] with the available literature data (in parentheses) from x-ray structural studies*.

Bond distances (Å) [+]	**Bond angles (deg)** [+]
[±]Mo(59) - O(10) 1.960	N(7)-Mo(59)-O(10)
Mo(59) - O(93) 1.962	88.75 (72 - 74)
(2.081 - 2.302)	
Mo(59) - S(59) 2.363	N(7)-Mo(59)-N(55)
Mo (59) - S(62) 2.362	164.38 (158.0 - 169.2)
(2.393-2.460)	
[±]Mo(59) - N(7) 1.998	S(59)-Mo(59)-S(62)
Mo (59) - N(55) 1.998	73.96 (83.69 - 96.6)
(1.997 - 2.080)	

*X-ray structural data have been collected from the reference 1.

[+] Here O(10) and O(93) correspond to O(4) and N(7) and N(55) corresponds to N(5) donor atoms respectively, of the pterin ring as per Scheme (V-1).

[±] Bond length data for the two $(L^3)^{-2}$ ligand residues in compound **(2)**.

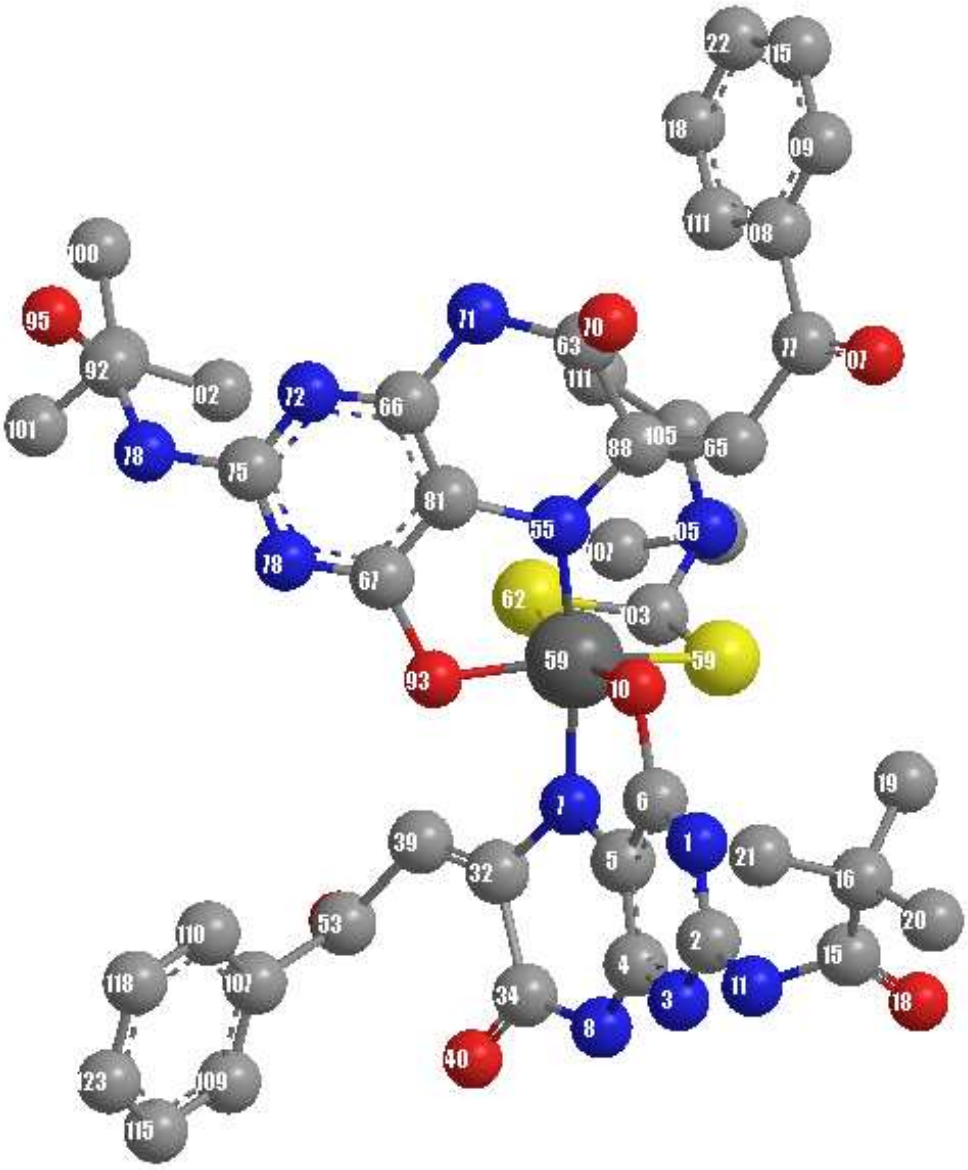

Fig. (V-47): The optimized geometry (CHEM3D model obtained through MM2 calculations) of compound **(2)** with a steric energy of 41.5 kcal/mol.

Table (V-7). Comparison of selected optimized bond lengths (Å) in the pterin ligand ($H_2L^3.H_2O$) and the molybdenum compound **(2)** from the respective optimized geometries (MM2 calculations). Available X-ray structural data on pterins are shown in parentheses.*

Bond[+]	**$H_2L^3.H_2O$**	**compound (2)**[±]
N(3)-C(4)	1.379 (1.390-1.400)	1.334, 1.336
C(4)-O(4)	1.234 (1.212-1.231)	1.558, 1.566

N(5)-C(6)	1.282‡ (1.359-1.468)	1.591, 1.596
C(6)-C(1′)	1.512 (1.512-1.514)	1.329, 1.328
C(7)-O(7)	1.219 (1.240)	1.211, 1.213
C(7)-N(8)	1.354 (1.303-1.443)	1.447, 1.342

+ Scheme (V-1) indicates the atom numbering system.

± Data for the two ligand residues in compound **(2)**.

* X-ray structural data have been collected from reference 20.

‡ The only exception to a reasonable agreement between the computed bond length data (Å) and related X-ray data, is the N(5)-C(6) distance; this is due to the presence of vinylogous amide in position 5 including the adjacent side-chain [i.e., the proton from C(1′) is located at N(5) through tautomerism, Schemes, V-1 and V-10] [24a,b,d].

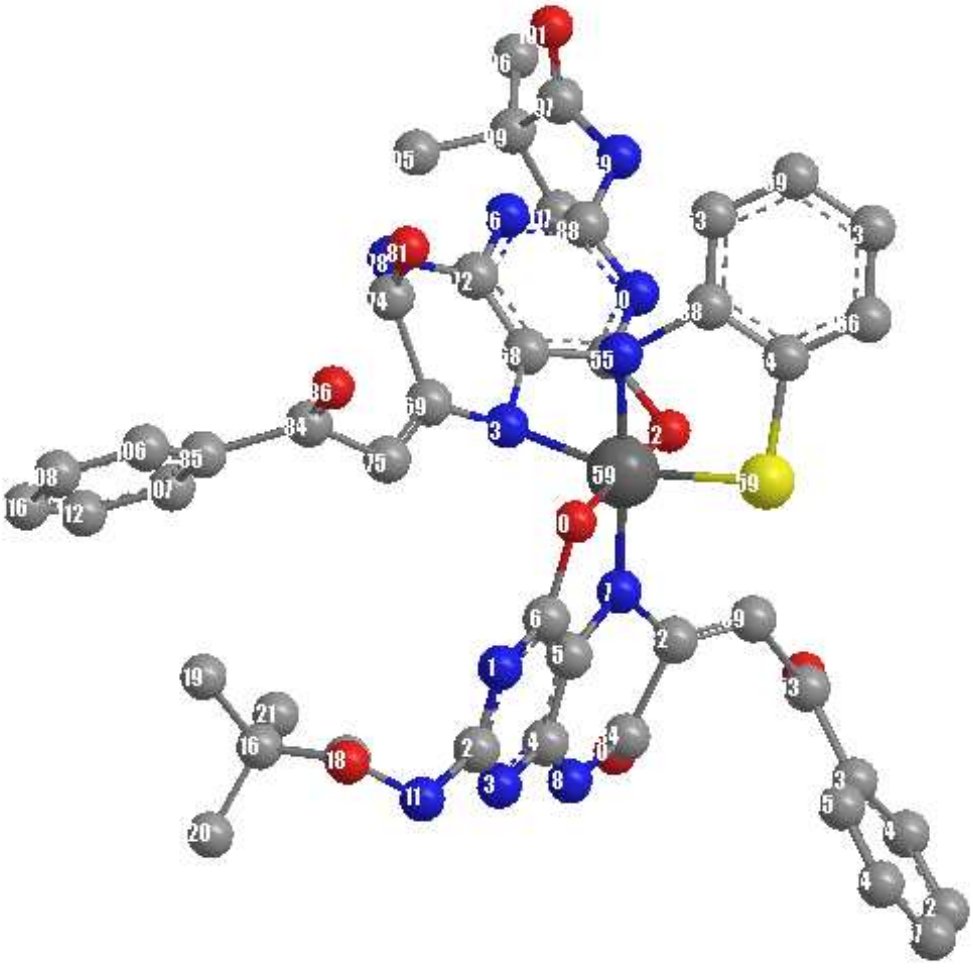

Fig. (V-48): The optimized geometry (CHEM3D model obtained through MM2 calculations) of compound **(3)** with a steric energy of 16.92 kcal/mol.

The corresponding CHEM3D model of compound **(3)** was obtained through MM2 calculation [19(a)] with the lowest steric energy 16.92 kcal/mol presented in Fig. (V-48). It indicates the stability of the coordination core. Some of the bond length and bond angle data is compared with standard literature data [1] and listed in the Table (V-8). Change of bond length data of the pterin ligand $(L^3)^{2-}$ in this complex due to the coordination with Mo atom may be a valuable information to interpret the coordination mode of the ligand. Selected bond length data are compared and listed in the Table V-9.

Table (V-8). Comparison of selected computed bond lengths (Å) and bond angles (deg) in compound (3) from the optimized geometry [Fig. (V-48), MM2 calculations] with the available literature data (in parentheses) from X-ray structural studies*.

Bond distances (Å) [+]	**Bond angles (deg)** [+]
[±]Mo(59) - O(10) 1.963	N(7)-Mo(59)-O(10)
Mo(59) - O(62) 1.960	87.44(72 - 74)
(2.081 - 2.302)	
Mo(59) - S(59) 2.345	N(7)-Mo(59)-N(55)
(2.393-2.460)	175.38 (158.0 - 169.2)
[±]Mo(59) - N(7) 1.991	
Mo (59) - N(55) 1.998	
(1.997 - 2.080)	

*X-ray structural data have been collected from the reference 1.

[+] Here O(10) and O(62) correspond to O(4) and N(7) and N(55) corresponds to N(5) donor atoms respectively, of the pterin ring as per Scheme (V-1).

[±] Bond length data for the two $(L^3)^{-2}$ ligand residues in compound **(3)**.

A CHEM3D model with lowest steric energy (18.88 kcal/mol) of the compound **(4)** was obtained through MM2 calculations [19(a)] is presented in the Fig. (V-49). The compactness of the coordination geometry of this compound is reflected from the steric energy value. The comparison of some selected bond lengths and bond angles data given in the following Table (V-10). Some of the bond lengths of pterin ligand coordinated to Mo atom in this complex, undergoes change during the complex formation process. Some of the selected bond length data are given in the Table (V-11).

Table (V-9). Comparison of selected optimized bond lengths (Å) in the pterin ligand ($H_2L^3.H_2O$) and the molybdenum compound **(3)** from the respective optimized geometries (MM2 calculations). Available x-ray structural data on pterins are shown in parentheses.*

Bond[+]	**$H_2L^3.H_2O$**	**compound (3)**[±]
N(3)-C(4)	1.379 (1.390-1.400)	1.334, 1.336
C(4)-O(4)	1.234 (1.212-1.231)	1.567, 1.562
N(5)-C(6)	1.282[‡] (1.359-1.468)	1.588, 1.608
C(6)-C(1′)	1.512 (1.512-1.514)	1.327, 1.327
C(7)-O(7)	1.219 (1.240)	1.212, 1.213
C(7)-N(8)	1.354 (1.303-1.443)	1.451, 1.585

[+] Scheme (V-1) indicates the atom numbering system.

[±] Data for the two ligand residues in compound **(3)**.

* X-ray structural data have been collected from reference 20.

[‡] The only exception to a reasonable agreement between the computed bond length data (Å) and related X-ray data, is the N(5)-C(6) distance; this is due to the presence of vinylogous amide in position 5 including the adjacent side-chain [i.e., the proton from C(1′) is located at N(5) through tautomerism, Schemes, V-1 and V-10] [24a,b,d].

Possible schematic structure of compound **(5)** was optimized by molecular mechanics calculations (MM2) [19(a)] giving the lowest steric-energy (17.20 kcal /mol) [Fig. (V-50)], indicating both its stability and geometry. Some of the bond length and bond angle data are compared with the literature data in Table (V-12) below. Comparison of bond length data of free pterin ligand ($H_2L^3.H_2O$) and to that of complex is listed in the Table (V-13).

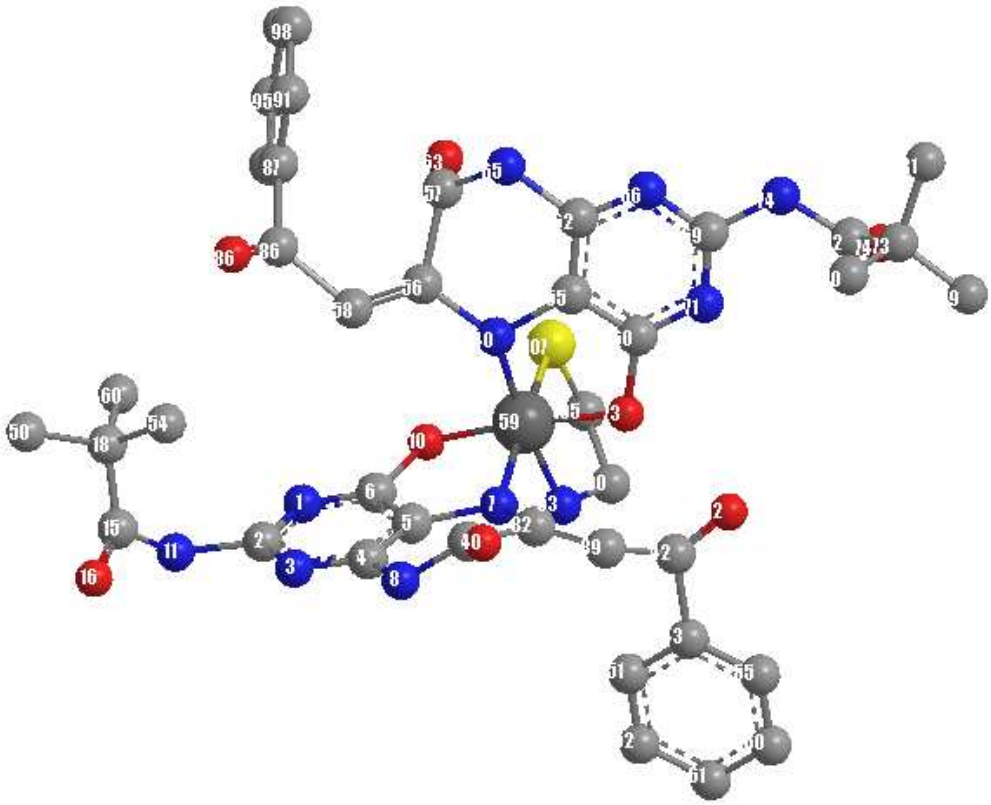

Fig. (V-49): The optimized geometry (CHEM3D model obtained through MM2 calculations) of compound **(4)** with a steric energy of 18.88 kcal/mol.

Table (V-10). Comparison of selected computed bond lengths (Å) and bond angles (deg) in compound **(4)** from the optimized geometry [Fig. (V-49), MM2 calculations] with the available literature data (in parentheses) from X-ray structural studies*.

Bond distances (Å) [+]	**Bond angles (deg)** [+]
[±]Mo(59) - O(10) 1.963	N(7)-Mo(59)-O(10)
Mo(59) - O(73) 1.959	87.89(72 - 74)
(2.081 - 2.302)	
Mo(59) - S(59) 2.336	N(7)-Mo(59)-N(55)
(2.393-2.460)	174.01 (158.0 - 169.2)
[±]Mo(59) - N(7) 1.994	
Mo (59) - N(40) 1.995	
(1.997 - 2.080)	

*X-ray structural data have been collected from the reference 1.

[+] Here O(10) and O(73) correspond to O(4) and N(7) and N(40) corresponds to N(5) donor atoms respectively, of the pterin ring as per Scheme (V-1).

[±] Bond length data for the two $(L^3)^{2-}$ ligand residues in compound **(4)**.

Table (V-11). Comparison of selected optimized bond lengths (Å) in the pterin ligand ($H_2L^3.H_2O$) and the molybdenum compound **(4)** from the respective optimized geometries (MM2 calculations). Available x-ray structural data on pterins are shown in parentheses.*

Bond[+]	**$H_2L^3.H_2O$**	**compound (4)**[±]
N(3)-C(4)	1.379 (1.390-1.400)	1.335, 1.337
C(4)-O(4)	1.234 (1.212-1.231)	1.555, 1.552
N(5)-C(6)	1.282[‡] (1.359-1.468)	1.596, 1.600
C(6)-C(1′)	1.512 (1.512-1.514)	1.328, 1.328
C(7)-O(7)	1.219 (1.240)	1.211, 1.214
C(7)-N(8)	1.354 (1.303-1.443)	1.449, 1.591

[+] Scheme (V-1) indicates the atom numbering system.

[±] Data for the two ligand residues in compound **(4)**.

* X-ray structural data have been collected from reference 20.

[‡] The only exception to a reasonable agreement between the computed bond length data (Å) and related X-ray data, is the N(5)-C(6) distance; this is due to the presence of vinylogous amide in position 5 including the adjacent side-chain [i.e., the proton from C(1′) is located at N(5) through tautomerism, Schemes, V-1 and V-10] [24a,b,d].

For compound **(6)** the CHEM3D model with the lowest seric energy of 39.84 kal/mol is represented in Fig. (V-51). The comparison of few selected bond length and bond angle data (with literature value) is given in the following Table (V-14). The bond length data of pterin ligand residue $(L^3)^{2-}$ obtained from MM2 calculation compared with the free ligand ($H_2L^3.H_2O$) value and listed in Table (V-15) below.

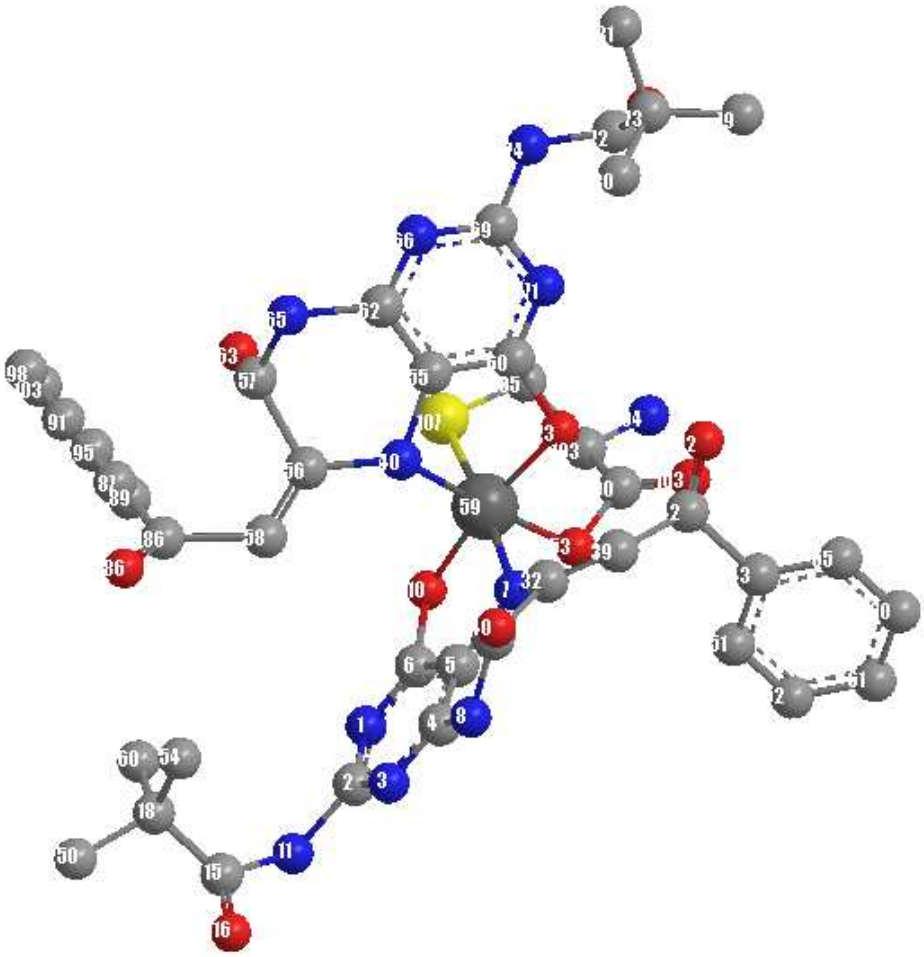

Fig. (V-50): The optimized geometry (CHEM3D) model obtained through MM2 calculations) of compound **(5)** with a steric energy of 17.20 kcal/mol.

Table V-12. Comparison of selected computed bond lengths (Å) and bond angles (deg) in compound **(5)** from the optimized geometry [Fig. (V-50), MM2 calculations] with the available literature data (in parentheses) from X-ray structural studies*.

Bond distances (Å) [+]	**Bond angles (deg)** [+]
[±]Mo(59) - O(10) 1.963	N(7)-Mo(59)-O(10)
Mo(59) - O(73) 1.959	87.89(72 - 74)
(2.081 - 2.302)	
Mo(59) - S(59) 2.336	N(7)-Mo(59)-N(55)
(2.393-2.460)	174.01 (158.0 - 169.2)
[±]Mo(59) - N(7) 1.994	

Mo (59) - N(40) 1.995

(1.997 - 2.080)

*X-ray structural data have been collected from the reference 1.

[+] Here O(10) and O(73) correspond to O(4) and N(7) and N(40) corresponds to N(5) donor atoms respectively, of the pterin ring as per Scheme (V-1).

[±] Bond length data for the two $(L^3)^{-2}$ ligand residues in compound **(5)**.

Table (V-13). Comparison of selected optimized bond lengths (Å) in the pterin ligand ($H_2L^3.H_2O$) and the molybdenum compound **(5)** from the respective optimized geometries (MM2 calculations). Available x-ray structural data on pterins are shown in parentheses.*

Bond[+]	**H_2 L^3.H_2O**	**compound (5)**[±]
N(3)-C(4)	1.379 (1.390-1.400)	1.335, 1.337
C(4)-O(4)	1.234 (1.212-1.231)	1.555, 1.552
N(5)-C(6)	1.282[‡] (1.359-1.468)	1.596, 1.600
C(6)-C(1′)	1.512 (1.512-1.514)	1.328, 1.328
C(7)-O(7)	1.219 (1.240)	1.211, 1.214
C(7)-N(8)	1.354 (1.303-1.443)	1.449, 1.591

[+] Scheme (V-1) indicates the atom numbering system.

[±] Data for the two ligand residues in compound **(5)**.

* X-ray structural data have been collected from reference 20.

[‡] The only exception to a reasonable agreement between the computed bond length data (Å) and related X-ray data, is the N(5)-C(6) distance; this is due to the presence of vinylogous amide in position 5 including the adjacent side-chain [i.e., the proton from C(1′) is located at N(5) through tautomerism, Schemes, V-1 and V-10] [24a,b,d].

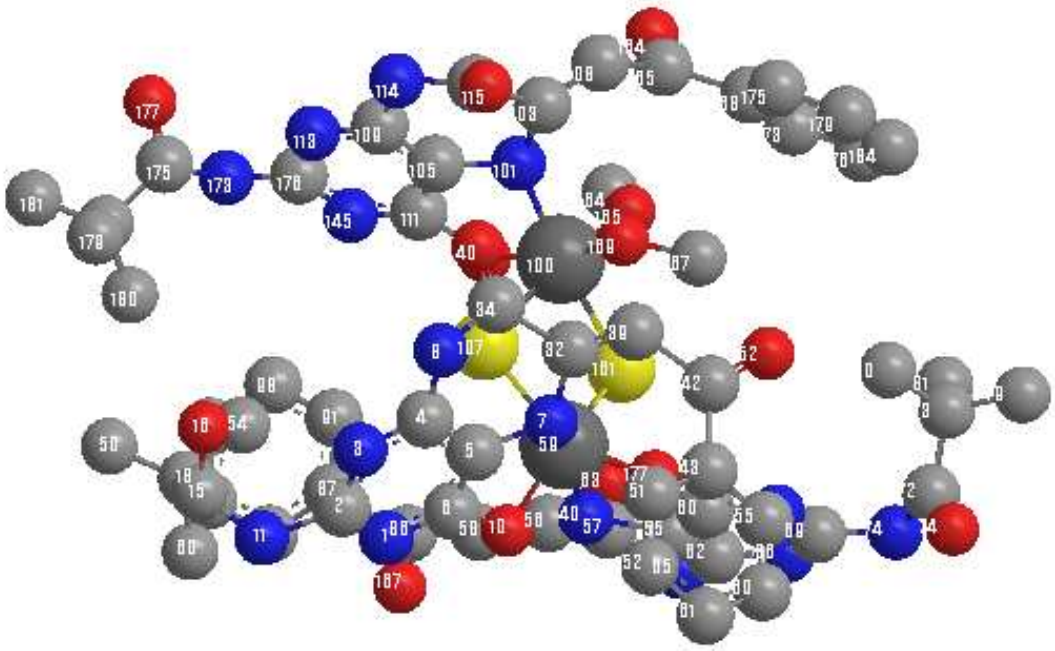

Fig. (V-51): The optimized geometry (CHEM3D) model obtained through MM2 calculations) of compound **(6)** with a steric energy of 39.84 kcal/mol.

A CHEM3D representation [MM2 calculations; steric energy : 32.02 kcal/mol, Fig. (V-52)] of compound **(7)** shows a bent μ-oxo bridge between the two Mo(V) atoms, each of which exhibits distorted octahedral geometry; out of the four pterin ligand residues, two act as tridentate ones as earlier and the other two act as bidentate ones [using the O(4), N(5) donor atoms]. Existence of such a bent μ-oxo bridge is supported by x-ray structure data [14]. The comparison of some selected bond length and bond angle data (with literature value) is given in the following Table V-16. The bond length data of pterin ligand residue $(L^3)^{2-}$ obtained from MM2 calculation compared with the free ligand ($H_2L^3.H_2O$) value and listed in Table (V-17) below.

Table (V-14). Comparison of selected computed bond lengths (Å) and bond angles (deg) in compound **(6)** from the optimized geometry [Fig. (V-51), MM2 calculations] with the available literature data (in parentheses) from X-ray structural studies*.

Bond distances (Å) [+]	**Bond angles (deg)** [+]
[±]Mo(59) - O(10) 1.969	N(7)-Mo(59)-O(10)
Mo(59) - O(177) 1.961	81.80 (72 - 74)
Mo(100) – O(147) 1.970	
(2.081 - 2.302)	
Mo(59) - S(161) 2.355	N(40)-Mo(59)-O(177)
Mo(59) – S(107) 2.354	86.32 (72 - 74)
Mo(100) – S(107) 2.352	O(147)-Mo(100)-S(161)
Mo(100) – S(161) 2.343	91.31 (92.2 – 94.8)
(2.393-2.460)	
[±]Mo(59) - N(7) 2.015	S(107)-Mo(100)-O(147)
Mo (59) - N(40) 2.015	84.90 (92.2 – 94.8)
Mo(100) – N(101) 1.998	
(1.997 - 2.080)	

*X-ray structural data have been collected from the reference 1.

[+] Here O(10) and O(73) correspond to O(4) and N(7) and N(40) corresponds to N(5) donor atoms respectively, of the pterin ring as per Scheme (V-1).

[±] Bond length data for the three $(L^3)^{-2}$ ligand residues in compound (6).

Table (V-15). Comparison of selected optimized bond lengths (Å) in the pterin ligand ($H_2L^3.H_2O$) and the molybdenum compound **(6)** from the respective optimized geometries (MM2 calculations). Available x-ray structural data on pterins are shown in parentheses.*

Bond[+]	**$H_2L^3.H_2O$**	**compound (6)**[±]
N(3)-C(4)	1.379 (1.390-1.400)	1.334, 1.334, 1.338
C(4)-O(4)	1.234 (1.212-1.231)	1.548, 1.560, 1.565
N(5)-C(6)	1.282[‡] (1.359-1.468)	1.602, 1.602, 1.598
C(6)-C(1′)	1.512 (1.512-1.514)	1.326, 1.328, 1.327

C(7)-O(7)	1.219 (1.240)	1.211, 1.213, 1.212
C(7)-N(8)	1.354 (1.303-1.443)	1.450, 1.578, 1.571

[+] Scheme (V-1) indicates the atom numbering system.

[±] Data for the three ligand residues in compound **(6)**.

* X-ray structural data have been collected from reference 1.

[‡] The only exception to a reasonable agreement between the computed bond length data (Å) and related X-ray data, is the N(5)-C(6) distance; this is due to the presence of vinylogous amide in position 5 including the adjacent side-chain [i.e., the proton from C(1′) is located at N(5) through tautomerism, Schemes, V-1 and V-10] [24a,b,d].

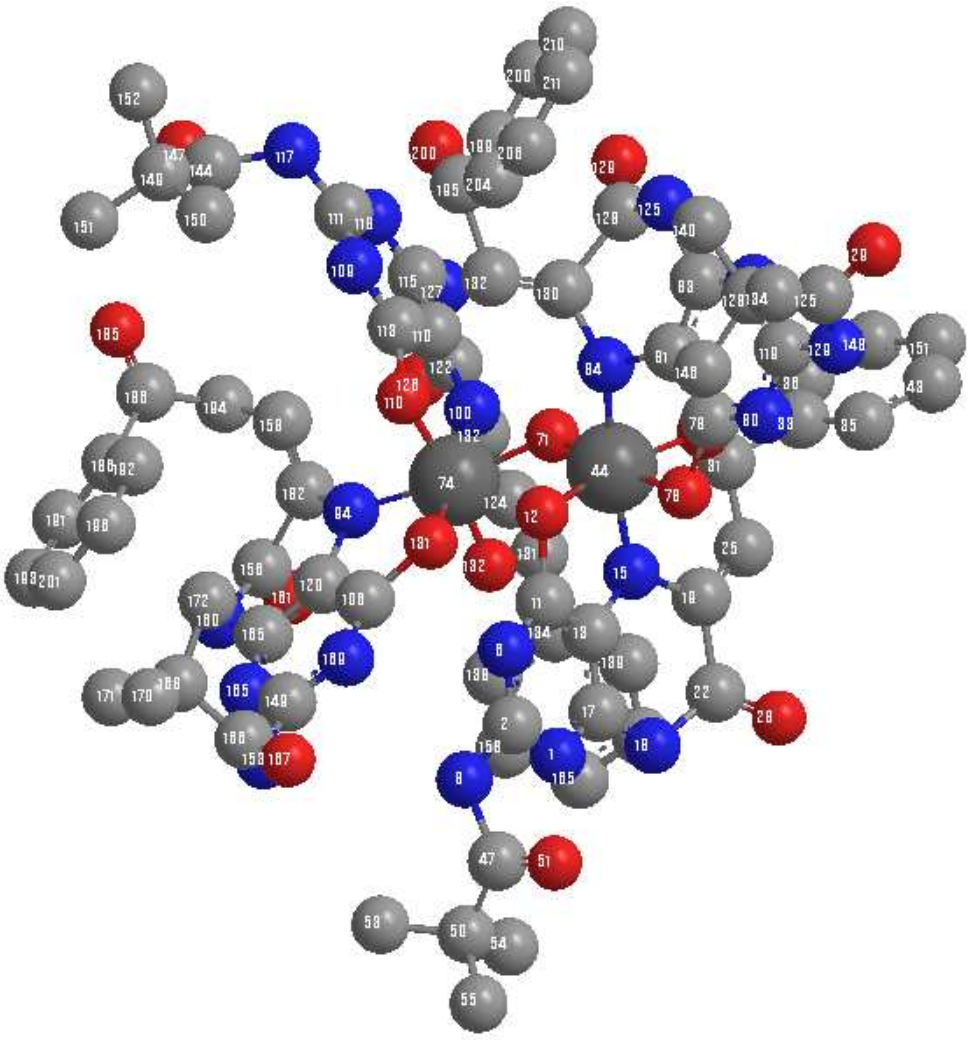

Fig. (V-52): The optimized geometry (CHEM3D model obtained through MM2 calculations) of compound **(7)** with a steric energy of 32.02 kcal/mol.

Table (V-16). Comparison of selected computed bond lengths (Å) and bond angles (deg) in compound **(6)** from the optimized geometry [Fig. (V-52), MM2 calculations] with the available literature data (in parentheses) from X-ray structural studies*.

Bond distances (Å) [+]	**Bond angles (deg)** [+]
[±]Mo(44) - O(12) 1.965	O(12)-Mo(44)-N(15)
Mo(44) - O(32) 1.965	88.11(72 - 74)
Mo(44) – O(78) 1.974	
Mo(74) – O(110) 1.958	O(78)-Mo(44)-N(84)
Mo(74) – O(131) 1.960	86.31 (72 - 74)
Mo(74) – O(132) 1.960	O(131)-Mo(74)-N(94)
(2.081 - 2.302)	84.86 (72 - 74)
[±]Mo(44) - N(15) 1.984	
Mo (44) - N(84) 1.990	O(110)-Mo(74)-N(100)
Mo(74) – N(94) 2.001	88.05 (72 - 74)
Mo(74) – N(100) 1.985	
(1.997 - 2.080)	
Mo(44) – O(71) 1.956	
Mo(74) – O(71) 1.965	
(1.91 – 1.95)	

*X-ray structural data have been collected from the reference 1.

[+] Here O(12), O(78), O(110) and O(131) correspond to O(4) and N(15), N(84), N(94) and N(100) correspond to N(5) donor atoms respectively, of the pterin ring as per Scheme (V-1).

[±] Bond length data for the four $(L^3)^{-2}$ ligand residues in compound **(7)**.

The distorted octahedral geometry of compound **(1)** (as per bond angles data in Table (V-4) leads to ligand field splitting of d-orbitals (e_g and t_{2g} levels of O_h symmetry) and favours spin pairing in the $(d_{xy})^2[(b_2)^2]$ levels of this Mo(IV)-d^2 system [9]. Out of the three biologically relevant oxidation states of molybdenum [e.g., Mo(VI), Mo(V) and Mo(IV)], during catalysis only the Mo(V) (d^1) state could be detected as a transient species by EPR spectroscopy in oxomolybdoenzymes; the Mo(IV) (d^2) state is consistently diamagnetic in such cases [27(a)]. Almost all the synthetic molybdenum-pterin complexes reported so far are diamagnetic, including one formulated as containing a Mo(V) centre; diamagnetic behaviour of the later

system is explained by invoking a strong coupling between the d^1[Mo(V)] electron and the delocalized electron system of the redox 'non-innocent' pterin ligand [1(b)]. This unique nature of pterin ligand ($H_2L^3.H_2O$) is responsible for the observed diamagnetism.

Table (V-17). Comparison of selected optimized bond lengths (Å) in the pterin ligand ($H_2L^3.H_2O$) and the molybdenum compound **(7)** from the respective optimized geometries (MM2 calculations). Available X-ray structural data on pterins are shown in parentheses.*

Bond[+]	**$H_2L^3.H_2O$**	**compound (7)**[±]
N(3)-C(4)	1.379 (1.390-1.400)	1.337, 1.336, 1.331, 1.334
C(4)-O(4)	1.234 (1.212-1.231)	1.568, 1.566, 1.555, 1.563
N(5)-C(6)	1.282[‡] (1.359-1.468)	1.575, 1.599, 1.600, 1.568
C(6)-C(1′)	1.512 (1.512-1.514)	1.325, 1.327, 1.328, 1.325
C(7)-O(7)	1.219 (1.240)	1.213, 1.211, 1.212, 1.212
C(7)-N(8)	1.354 (1.303-1.443)	1.576, 1.594, 1.622, 1.455

[+] Scheme (V-1) indicates the atom numbering system.

[±] Data for the four ligand residues in compound **(7)**.

* X-ray structural data have been collected from reference 1.

[‡] The only exception to a reasonable agreement between the computed bond length data (Å) and related X-ray data, is the N(5)-C(6) distance; this is due to the presence of vinylogous amide in position 5 including the adjacent side-chain [i.e., the proton from C(1′) is located at N(5) through tautomerism, Schemes, V-1 and V-10] [24a,b,d].

The observed changes in different spectral properties of the pterin ligand [$H_2L^3.H_2O$] (e.g, IR, ^{1}H-NMR, fluorescence spectra) on complex formation here, can be interpreted in terms of the changes in the computed bond length data, shown in Table (V-5), (V-7), (V-9), (V-11), (V-13), (V-15), and (V-17).

The visualized frontier orbitals with energies (eV) of the complexes

In recent years, synthetic molecules with exceptionally small (< 0.5 eV) gaps in frontier orbitals have received considerable attention due to their interesting properties e.g., electrochemical / redox amphoteric behaviour [86]. The different locations of the frontier orbitals in a single molecule hinders the electron transition between them, unlike systems with extended conjugation. However, facile electron transfer may occur between two such covalently linked centers in solution with thermal excitation, when small energy gaps between frontier orbitals levels as stated above exist. The foregoing CHEM3D models have been utilized in obtaining information about the relevant frontier orbitals with energies (eV) as shown in Fig. (V-53) and Fig. (V-54).

UV – VIS spectroscopy (in CH_3OH)

The UV/VIS spectra of free ligand is consisted with a band at 284 nm due to ($\pi \rightarrow \pi^*$) transition. For compound **(1)** the 261nm band is due to an intraligand ($\pi \rightarrow \pi^*$) transition, the bands at 386 nm and 439 nm (broad shoulder) with large molar exinction coefficient values are assigned to charge transfer [L→Mo(IV)] transition and intensity stealing respectively. The last two bands account for the orange-yellow colour of compound **(1)** [1(a)].

For the compound **(2)** the intraligand ($\pi \rightarrow \pi^*$) transition is observed at 288 nm and charge transfer [L→Mo(IV)] transition occurred at 388 and 450 nm with moderate intensity and shoulder. The orange red colour of this compound is due to the later transition. On the other hand the UV/VIS spectra of the compound **(3)** is characterized by intraligand ($\pi \rightarrow \pi^*$) transition at 297 nm. The charge transfer [L→Mo(IV)] transition of this compound is occurred at 390 and 483 nm causes the reddish yellow colour.

In a similar fashion in case of compound **(4)** the intraligand ($\pi \rightarrow \pi^*$) transition occurred at 294 nm and charge transfer [L→Mo(IV)] transition occurred at 384 and 460 nm. That is why the compound is reddish in colour. The brown colour of compound **(5)** is due to charge transfer [L→Mo(IV)] transition at 385 and 470 nm whereas intraligand ($\pi \rightarrow \pi^*$) transition remain essentially unchanged at 297 nm. Similar trend is also observed in compound **(6)**. The reddish colour is due to charge transfer [L→Mo(VI)] transition at 380 and 470 nm and intraligand ($\pi \rightarrow \pi^*$) transition occurs at 470 nm.

Compound **(1)**	Compound **(2)**	Compound **(3)**
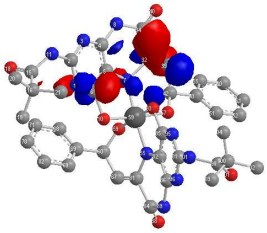	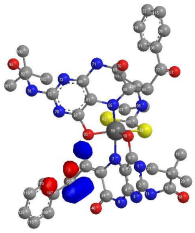	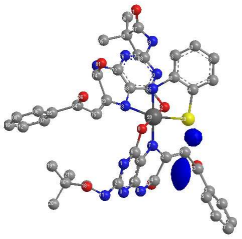
E_4(LUMO+1)= -2.031	E_4(LUMO+1)= -3.982	E_4(LUMO+1)= -4.649
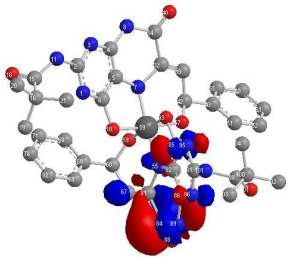	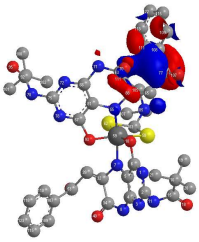	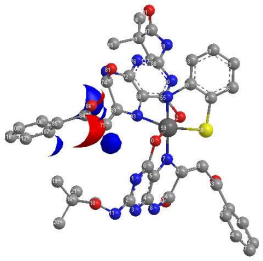
E_3(LUMO)= -2.389	E_3(LUMO)= -4.777	E_3(LUMO)= -4.682
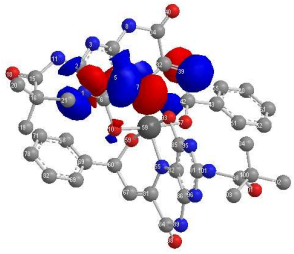	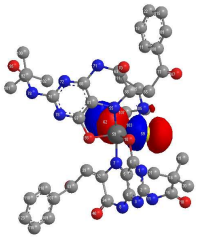	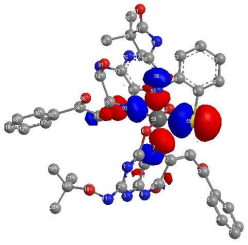
E_2(HOMO)= -8.873	E_2(HOMO)= -5.890	E_2(HOMO)= -8.123
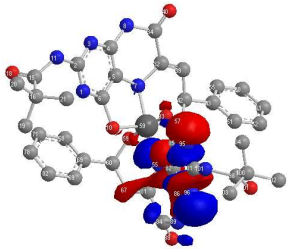	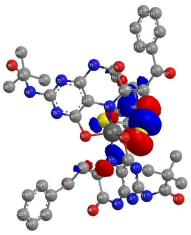	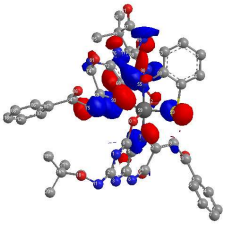
E_1(HOMO-1)= -9.229	E_1(HOMO-1)= -7.189	E_1(HOMO-1)= -8.973
$\Delta(E_2-E_1)$ = 0.356 eV	$\Delta(E_2-E_1)$ = 1.299eV	$\Delta(E_2-E_1)$ = 1.299eV
$\Delta(E_3-E_2)$ = 6.484 eV	$\Delta(E_3-E_2)$ = 1.113 eV	$\Delta(E_3-E_2)$ = 3.441 eV
$\Delta(E_4-E_3)$ = 0.358 eV	$\Delta(E_4-E_3)$ = 0.795 eV	$\Delta(E_4-E_3)$ = 0.850 eV

Fig. (V-53): The visualized frontier orbitals with energies (E, eV) of (**1**), (**2**) and (**3**) (using Chem Office 2004, version 8.0).

Compound **(4)**	Compound **(5)**	Compound **(6)**	Compound **(7)**
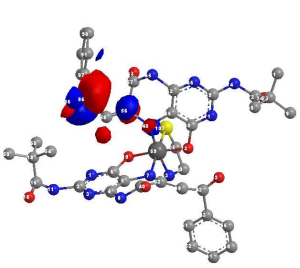	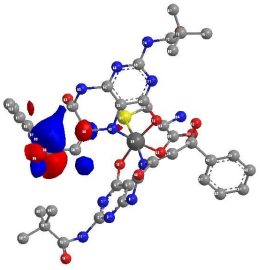	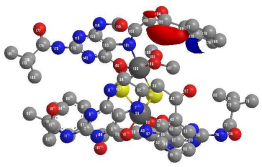	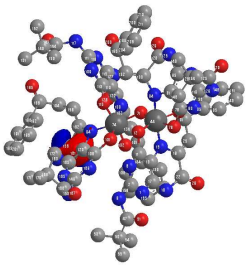
E_4(LUMO+1)= -3.681	E_4(LUMO+1)= -3.810	E_4(LUMO+1)= -4.320	E_4(LUMO+1)= -2.969
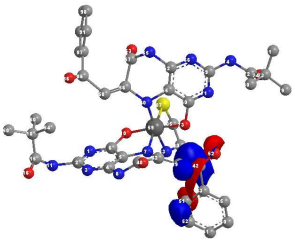	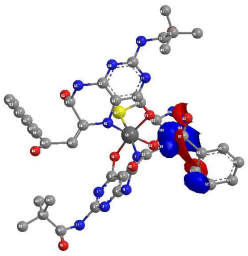	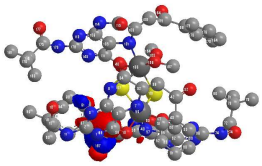	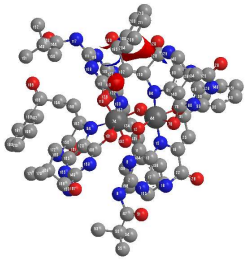
E_3(LUMO)= -4.217	E_3(LUMO)= -4.228	E_3(LUMO)= -4.393	E_3(LUMO)= -4.282
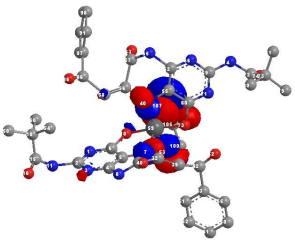	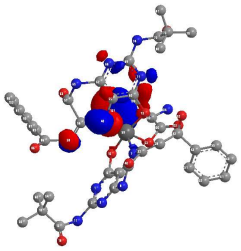	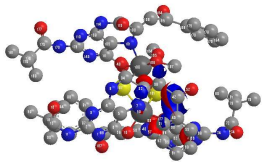	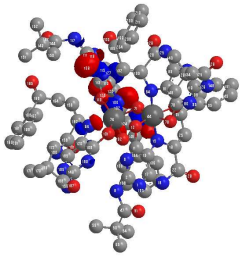
E_2(HOMO)= -7.965	E_2(HOMO)= -8.506	E_2(HOMO)= -4.584	E_2(HOMO)= -8.707
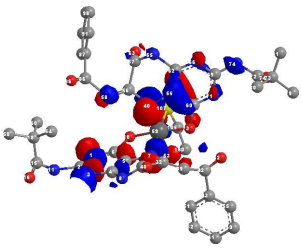	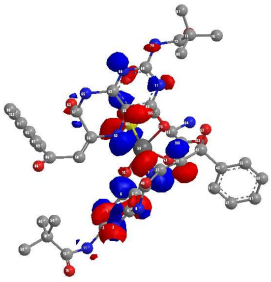	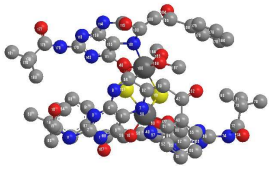	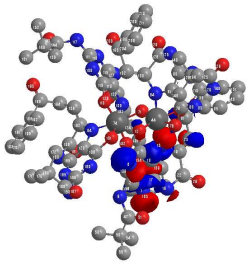
E_1(HOMO-1)= -8.967	E_1(HOMO-1)= -8.990	E_1(HOMO-1)= -7.395	E_1(HOMO-1)= -9.164
$\Delta(E_2-E_1)$ = 1.002 eV	$\Delta(E_2-E_1)$ = 0.484eV	$\Delta(E_2-E_1)$ = 2.811eV	$\Delta(E_2-E_1)$ = 0.457eV
$\Delta(E_3-E_2)$ = 3.748 eV	$\Delta(E_3-E_2)$ = 4.278 eV	$\Delta(E_3-E_2)$ = 0.191 eV	$\Delta(E_3-E_2)$ = 4.425 eV
$\Delta(E_4-E_3)$ = 0.536 eV	$\Delta(E_4-E_3)$ = 0.418 eV	$\Delta(E_4-E_3)$ = 0.073 eV	$\Delta(E_4-E_3)$ = 1.313 eV

Fig. (V-54): The visualized frontier orbitals with energies (E, eV) of **(4)**, **(5)**, **(6)** and **(7)** (using Chem Office 2004, v 8.0).

A slight deviation is observed in compound **(7)**. The intraligand ($\pi \rightarrow \pi^*$) transition occurred at 292 nm and that of charge transfer [L→Mo(V)] transition at 383 and 445 nm. The colour of the compound is reddish yellow.

Some of the reactivity data presented in the next section highlight interesting redox behaviour of the present complexes.

Reactivity: UV – VIS spectroscopy (in CH_3OH)

Different oxomolybdenum enzymes like dimethylsulfoxide reductase (DMSOR), trimethyl N-oxide reductase (TMAOR), sulphite oxidase, etc., undergo reactions with suitable substrates. When the free ligand ($H_2L^3.H_2O$) is allowed to react with substrates like $Me_3N \rightarrow O$ at 318K [Fig. (V-55)] and PPh_3 [Fig. (V-56)], no reaction occurs at same condition.

Fig. (V-57) represents the spectrophotometric monitoring of the reaction of compound **(1)** with $Me_3N \rightarrow O$ in MeOH at 313K; continuous increase in optical density with time is observed at 261nm and 386nm respectively. Near approach to isosbestic points is observed at 273nm and 413nm; this reaction involving a mononuclear → binuclear complex conversion [Equation. (V-1)], prevents the appearance of perfect isosbestic points. Kinetics of this reaction was followed at 386nm under pseudo first order conditions (maintaining ca. 3-50 times excess of $Me_3N \rightarrow O$) in MeOH. The observed rate constants were determined by least square method from the plots of $\log(A_\alpha - A_t)$ versus time, which are found to be linear for more than two half lives. Fig. (V-58) reflects the changes of $k_{obs}(s^{-1})$ values for this reaction with increasing substrate ($Me_3N \rightarrow O$) concentration; it indicates neither a substrate saturation kinetics nor a second order reaction [28,29]. Initially, the k_{obs} value falls off with increasing substrate concentration, only to achieve a steady value at high concentration. Most likely, an optimum balance is achieved at this stage among the oxygen atom transfer from $Me_3N \rightarrow O$, the binuclear complex formation process and the ultimate release of Me_3N from the reaction site. Activation parameters [$\Delta H^{\neq}$ =33.3 k J mol^{-1}; $\Delta S^{\neq}$ = -282.8 J K^{-1} mol^{-1}] were obtained from the Eyring plot [ln(k/T) versus 1/T], using pseudo first order rate constants data determined (keeping a three fold excess of $Me_3N \rightarrow O$) at four different temperatures. The $k_{obs}(s^{-1})$ values are within the range of existing data for oxygen atom transfer reactions of different Mo(IV) complexes [28, 29]. The negative $\Delta S^{\neq}$ values indicates an associative type pathway.

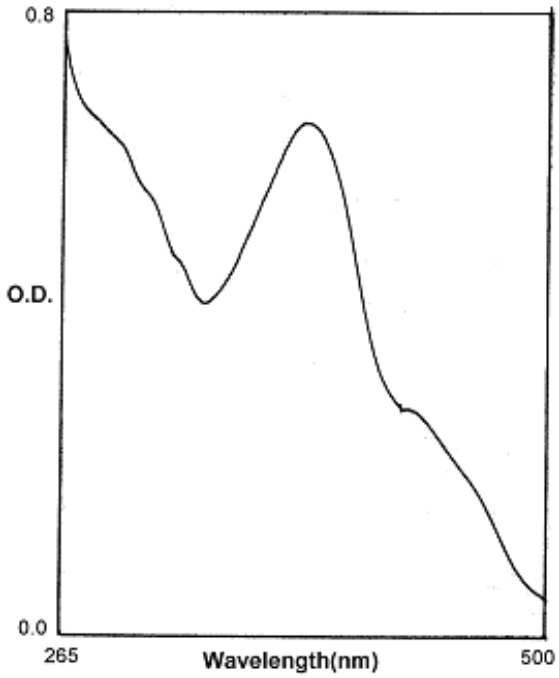

Fig. (V-55): Spectrophotometric monitoring of the reaction between ligand ($H_2L^3.H_2O$) (5.3×10^{-5} mol) and $Me_3N \rightarrow O$ (3.2×10^{-3} mol) at 318K.

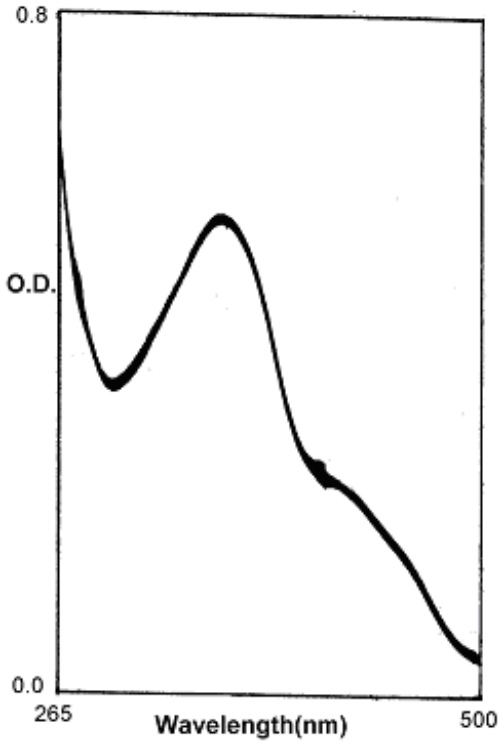

Fig. (V-56): Spectrophotometric monitoring of the reaction between ligand ($H_2L^3.H_2O$) (5.3×10^{-5} mol) and PPh_3 (2.08×10^{-3} mol) at 318K.

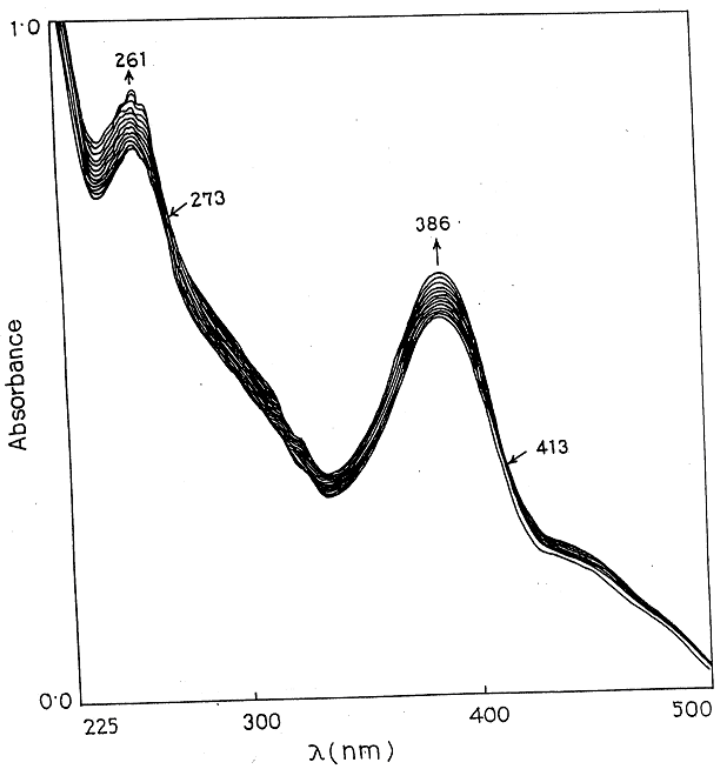

Fig. (V-57): Absorption spectral changes recorded at 10 min interval during the reaction of compound (1) (1.0 x 10^{-4} mol) with $Me_3N\rightarrow O$ (1.5 x 10^{-2} mol) in CH_3OH at 301K.

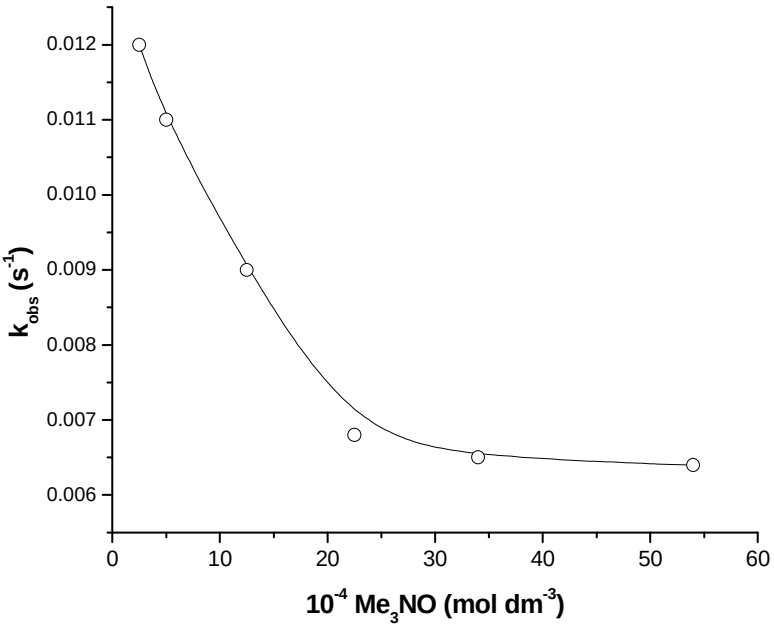

Fig. (V-58): Plot of k_{obs} (s^{-1}) at different concentrations of $Me_3N\rightarrow O$ at 313K, for the reactivity stated in Fig. (V-57).

The compound **(2)** was found to react with $Me_3N\rightarrow O$ at 319K. A spectroscopic monitoring of this reaction was done by UV-VIS spectra and represented in the Fig. (V-59). An isosbestic point at 296 nm is observed. The decrease in the optical density is observed from 296 nm to 410 nm where as an increase in optical density is observed from 265 nm to 296 nm.

The reaction between $Me_3N\rightarrow O$ and compound **(3)** takes place at 319K. The spectroscopic monitoring of this reaction was done and represented in the Fig. (V-60). A regular decrease in the optical density from 265 nm to 500 nm wavelength is observed in the reaction. A near isosbestic-like point is observed at 316 nm.

The decay kinetics for the reaction of $Me_3N\rightarrow O$ with compound **(3)** is studied at 347 nm under pseudo first order condition (maintaining c.a., 13-101 times excess of $Me_3N\rightarrow O$ in CH_3OH). The least square method [plotting of $\log(A_\infty - A_t)$ versus time at 319K] was employed to determine the pseudo first order rate constant,(k_{obs}, s^{-1}). The rate constants are plotted against the different $Me_3N\rightarrow O$ concentration and a curve is obtained giving a maximum at 3.5×10^{-4} mole dm^{-3} of $Me_3N\rightarrow O$ concentration [Fig. (V-61)].

The pseudo first order rate constants are also determined at different temperature (313.15 – 328.15K) keeping the $Me_3N\rightarrow O$ concentration unchanged (keeping thirteen fold excess) to obtain the activation parameters ($\Delta S^{\neq}$ = - 197.52 J K^{-1} mol^{-1}) (obtained from the Eyring Plot [ln(k/T) versus 1/T]). The negative $\Delta S^{\neq}$ value indicates the associative nature of the complex during the reaction.

The compound **(4)** is reactive towards $Me_3N\rightarrow O$ and was followed spectrophotometrically at 318K [Fig. (V-62)]. An isosbestic like point is observed at 302.7 nm and optical density decreases at longer wavelength.

A decay kinetics of the reaction with compound **(4)** and $Me_3N\rightarrow O$ was studied at 384 nm at 318K under pseudo-first order condition with substrate concentration 20-52 times excess to that of the complex. The pseudo first order rate constants (k_{obs}, s^{-1}) is plotted against the concentration of $Me_3N\rightarrow O$ and is given by the Fig. (V-63). The k_{obs} values first undergoes a decrease with the increase in concentration of $Me_3N\rightarrow O$ up to 2.91×10^{-3} mole dm^{-3} then undergoes gradual increase up to 4.25×10^{-3} mole dm^{-3} concentration of $Me_3N\rightarrow O$, then again decreased.

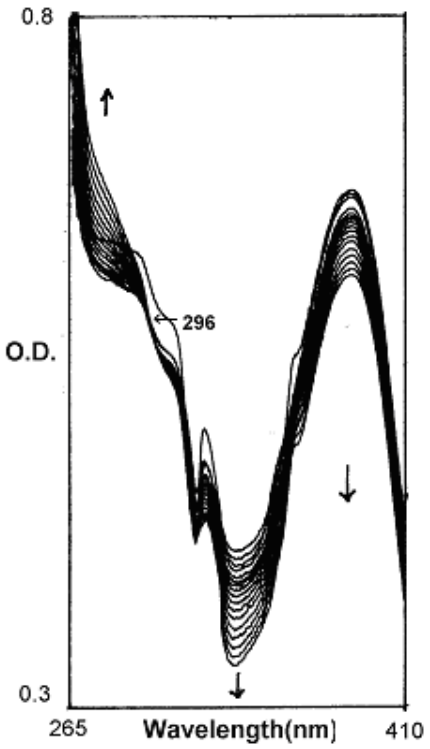

Fig. (V-59): Absorption spectral changes recorded at 10 min interval during the reaction of compound **(2)** (4.74×10^{-5} mol) with $Me_3N \rightarrow O$ (3.46×10^{-3} mol) in CH_3OH at 319K.

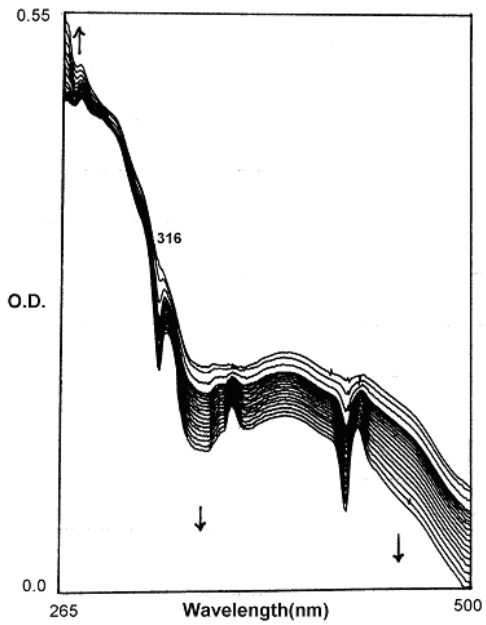

Fig. (V-60): Absorption spectral changes recorded at 10 min interval during the reaction of compound **(3)** (2.77×10^{-5} mol) with $Me_3N \rightarrow O$ (3.46×10^{-3} mol) in CH_3OH at 319K.

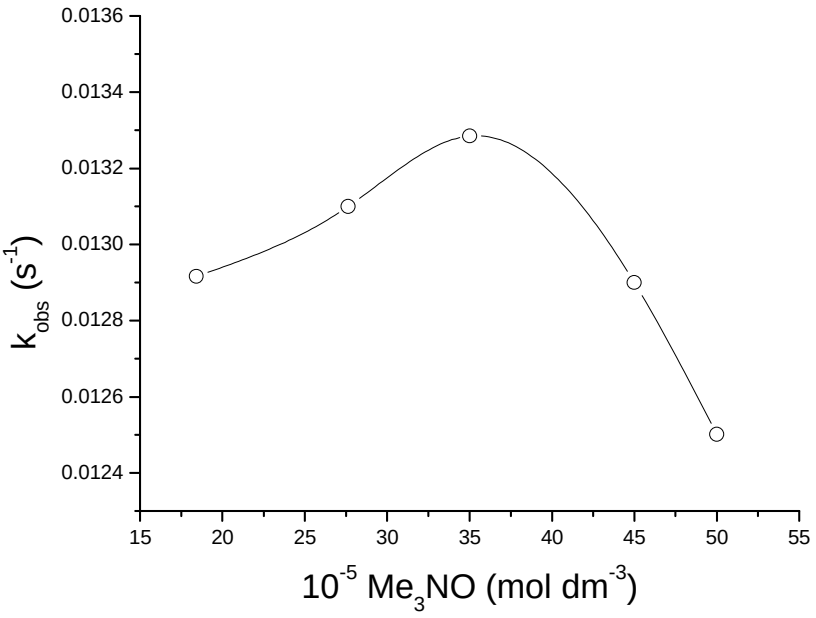

Fig. (V-61): Plot of k_{obs} (s^{-1}) at different concentrations of $Me_3N\rightarrow O$ at 319K, for the reactivity stated in Fig. (V-60).

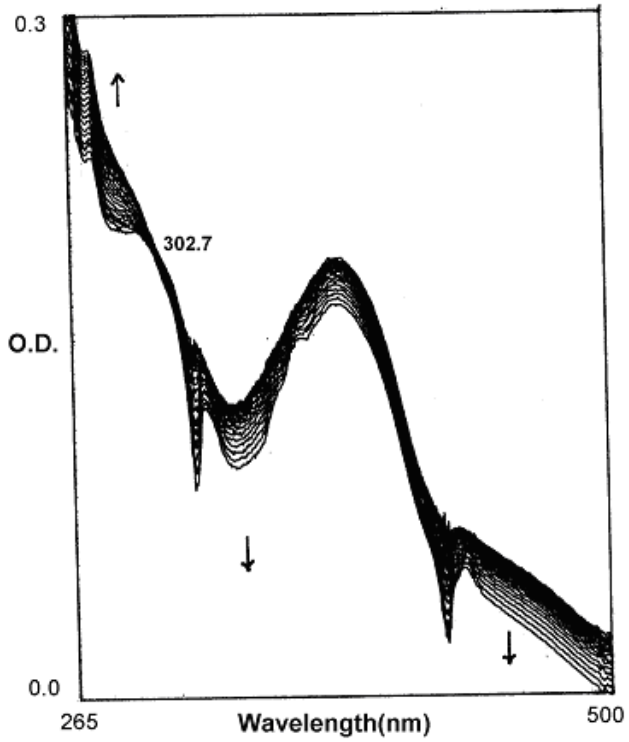

Fig. (V-62): Absorption spectral changes recorded at 10 min interval during the reaction of compound **(4)** (2.65 x 10^{-5} mol) with $Me_3N\rightarrow O$ (3.2 x 10^{-3} mol) in CH_3OH at 318K.

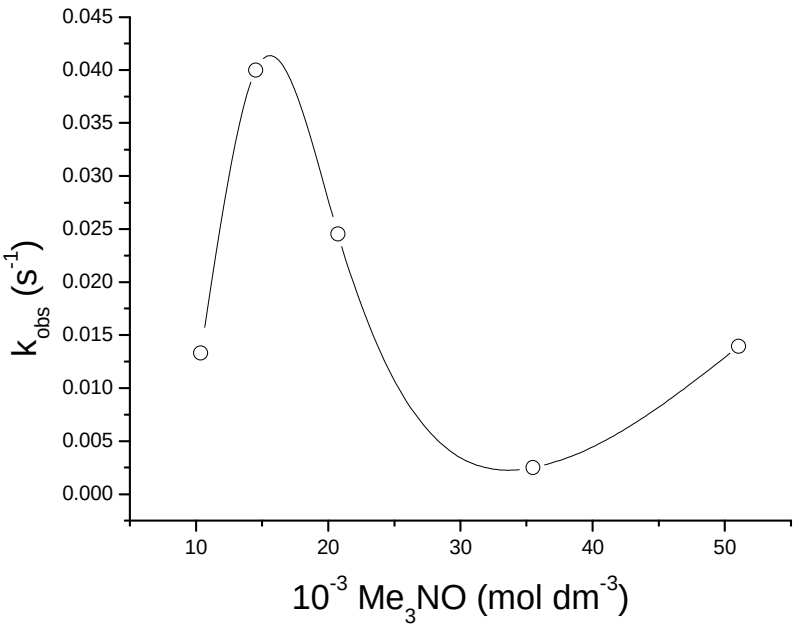

Fig. (V-63): Plot of k_{obs} (s^{-1}) at different concentrations of $Me_3N\rightarrow O$ at 319K, for the reactivity stated in Fig. (V-62).

Fig. (V-64) represents the spectrophotometric monitoring of the reaction between compound **(5)** and $Me_3N\rightarrow O$, in CH_3OH at 318K. A closer look to this figure reveals that a continuous decrease in optical density is occurred from 361.6 nm to 500 nm and a continuous increase in optical density at lower wavelength of 361.6 nm. A near approach to an isosbestic point is observed at 361.6 nm.

The rate constants (k_{obs}, s^{-1}) of this reaction were determined under pseudo first order condition by least-square method by plotting $\log(A_t-A_\infty)$ versus time maintaining 16-114 times excess of $Me_3N\rightarrow O$ concentration at 319K. A plotting of k_{obs} (s^{-1}) versus concentration of $Me_3N\rightarrow O$ is illustrated in the Fig. (V-65). First the rate constants increase with increase in concentration of $Me_3N\rightarrow O$ to reach a saturation level. The values of k_{obs} obtained are within the range of other oxygen atom transfer reaction by Mo(IV) complexes. The rate constants were also determined at four different temperatures (314 - 329K) maintaining sixteen fold excess concentration of $Me_3N\rightarrow O$ to obtain activation parameter ($\Delta S^{\neq}$ = - 196.77 J K^{-1} mol^{-1}) from Eyring plot [ln(k/T) versus 1/T]. The negative $\Delta S^{\neq}$ value indicates the associative nature of the reaction.

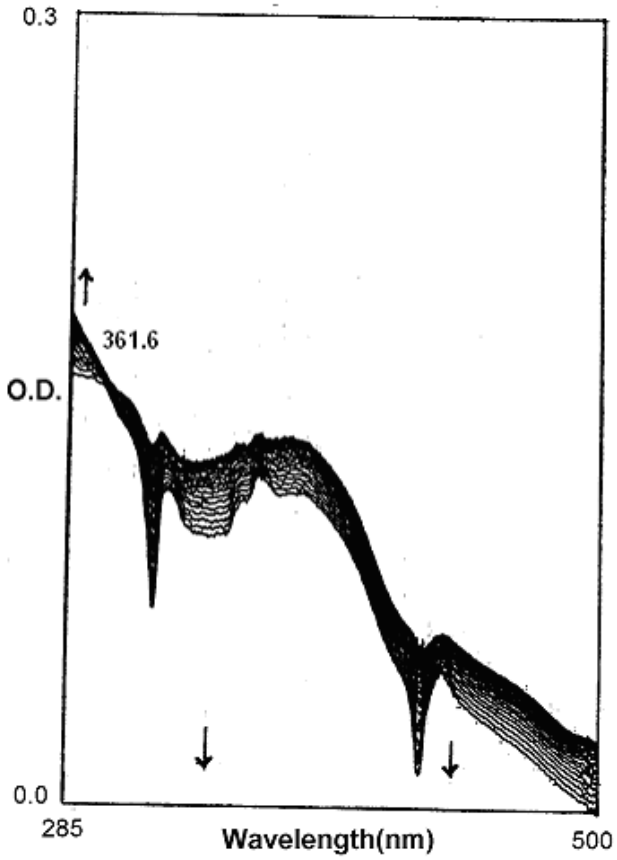

Fig. (V-64): Absorption spectral changes recorded at 10 min interval during the reaction of compound **(5)** (3.2 x 10^{-5} mol) with $Me_3N\rightarrow O$ (3.2 x 10^{-3} mol) in CH_3OH at 318K.

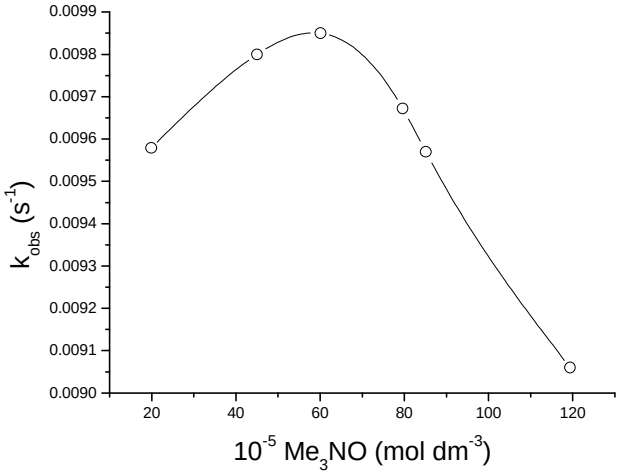

Fig. (V-65): Plot of k_{obs} (s^{-1}) at different concentrations of $Me_3N\rightarrow O$ at 318K, for the reactivity stated in Fig. (V-64).

In case of compound **(6)** it has been observed that the compound is active towards PPh_3. Spectrophotometric monitoring of this reaction from 300 nm to 500 nm at 318K is presented in the Fig. (V-66). A continious increment in optical density is observed in this course of reaction. Abstraction of the bridging sulfur atom can be inferred [Scheme (V-8)]. On the other hand the compound is found to inactive towards $Me_3N \rightarrow O$, as revealed from the Fig. (V-67). No change in optical density is observed in this region under the same condition confirms the oxidation state of Mo atoms in this compound is +VI. The above reactivities data verify the chemical formulation / schematic structure of compound **(6)**.

Cyclic voltammetry (in DMF)

Cyclic voltammetry data of ($H_2L^3.H_2O$) and compound **(1)** are shown in Fig. (V-68a) and Fig. (V-68b) respectively. The pterin ligand ($H_2L^3.H_2O$) is characterized by a single irreversible reduction peak at –0.86V [7]. For compound **(1)**, the Mo(IV)→Mo(III) reduction step is observed at –0.59V as an irreversible process. Further the appearance of ligand reduction peaks at –1.10V and –1.44V respectively for compound **(1)** is interesting. As evident from ^{1}H-NMR and fluorescence spectra, the introduction of extended conjugation in the pterin ligand residues in compound **(1)** affords a good deal of stability for them, making them less susceptible to reduction as compared to the corresponding free ligand reduction potential value [30].

In case of compound **(2)** the (i.e., Mo(IV) →Mo(III) reduction peak has been shifted to -0.95 V. Two other peak at -1.38 V and at -1.44 V may be due to pterin ligand and ancillary ligand reduction peak.

For the compound **(3)**, a single slightly reversible reduction peak at -1.0V is observed due to ligand reduction as in Fig. (V-70). The metal centered reduction [Mo(IV) →Mo(III)] could be detected at -0.8V at faster scan rates.

The similar trend is observed in case of compound **(4)** [Fig. (V-71)]. Here also the Mo(IV) →Mo(III) reduction peak is observed at -1.0V and the ligand reduction peak at -1.44V respectively.

For compound **(5),** the Mo(IV) →Mo(III) reduction peak is shifted to -1.08 V as revealed by the cyclic voltammetric data [Fig. (V-72)] and ligand reduction peak is obtained at -1.52V.

In case of compound **(6) t**he Mo(VI)→Mo(V) reduction peak is observed at -0.96 V [Fig. (V-73)] while the ligand reduction peaks are at -1.38 and -1.54V .

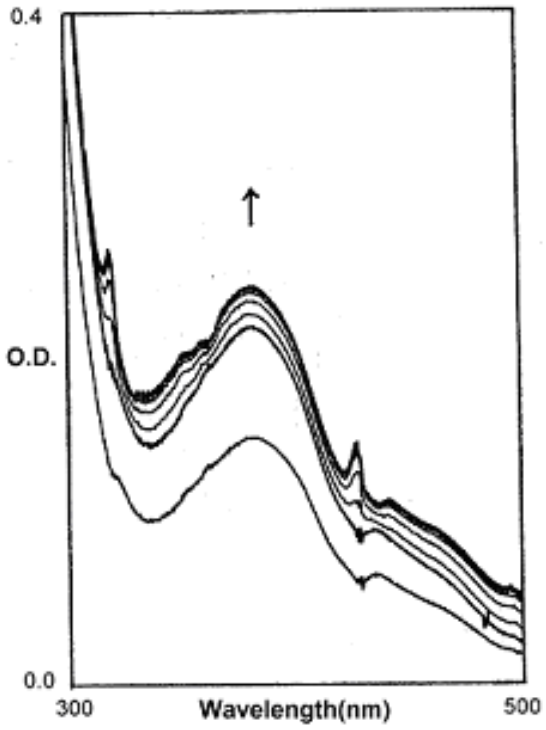

Fig. (V-66): Absorption spectral changes recorded at 10 min interval during the reaction of compound **(6)** (3.33×10^{-5} mol) with PPh_3 (2.08×10^{-3} mol) in CH_3OH at 318K.

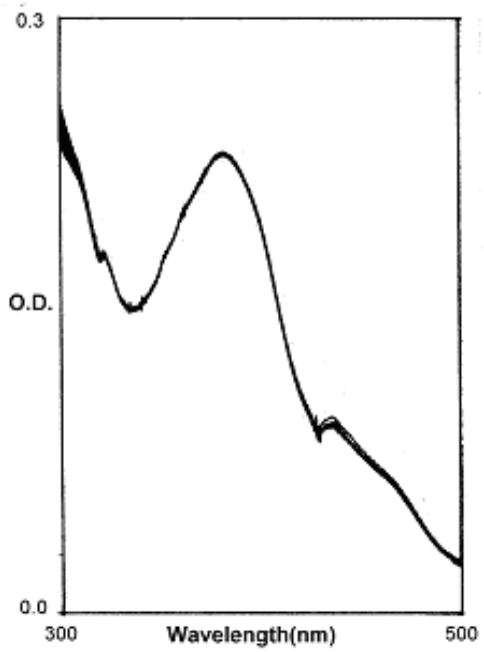

Fig. (V-67): Spectrophotometric monitoring of the reaction between compound **(6)** (1.42×10^{-5} mol) and $Me_3N \rightarrow O$ (2.08×10^{-3} mol) under the same condition as in Fig. (V-66).

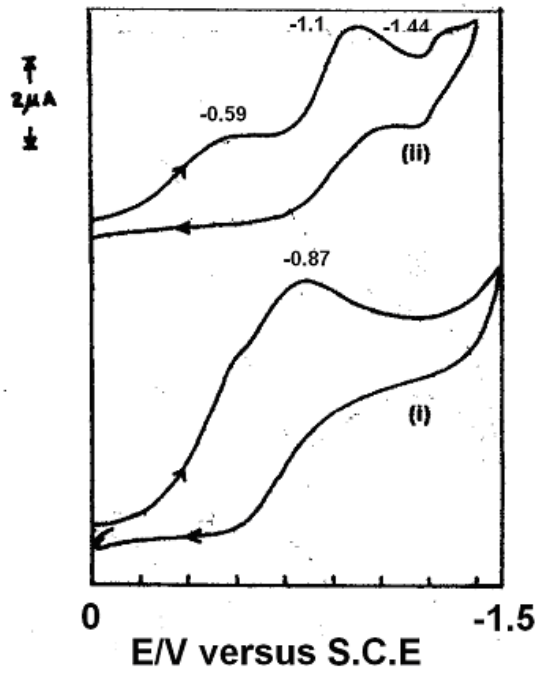

Fig. (V-68): Cyclic voltammograms of the (i) free ligand ($H_2L^3.H_2O$) (1.06 x 10^{-3} mol); (ii) the compound **(1)** (0.5 x 10^{-3} mol) in DMF (0.1 mol TBAP) at 50 mVs^{-1}.

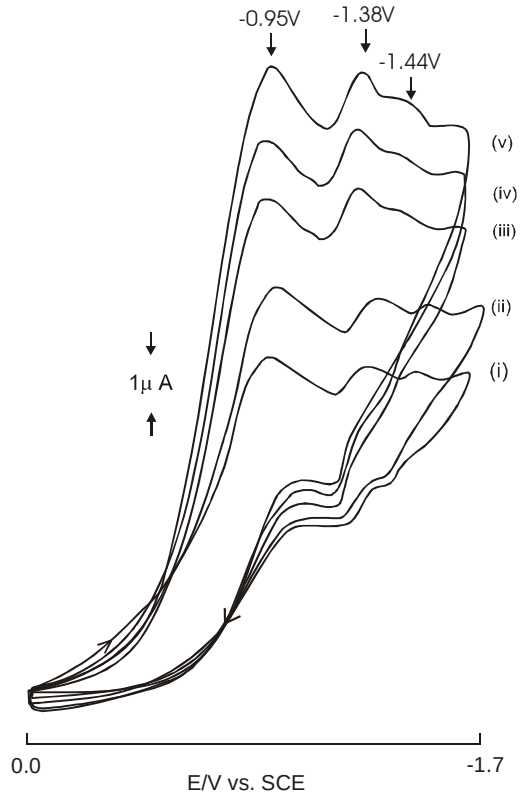

Fig. (V-69): Cyclic voltammograms of the compound **(2)** (1.00 x 10^{-3} mol) in DMF (0.1 mol TBAP) at (i) 50 mVs^{-1}, (ii) 100 mVs^{-1}, (iii) 150 mVs^{-1}, (iv) 200 mVs^{-1} and (v) 250 mVs^{-1}.

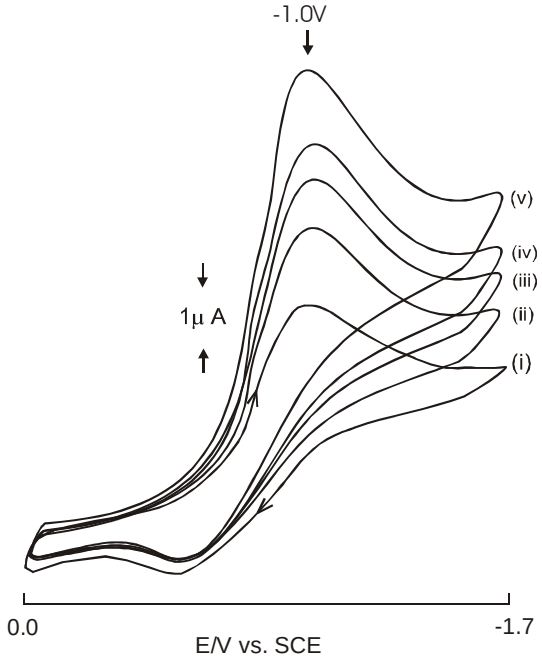

Fig. (V-70): Cyclic voltammograms of the compound **(3)** (1.00×10^{-3} mol) in DMF (0.1 mol TBAP) at (i) 50 mVs^{-1}, (ii) 100 mVs^{-1}, (iii) 150 mVs^{-1}, (iv) 200 mVs^{-1} and (v) 250 mVs^{-1}.

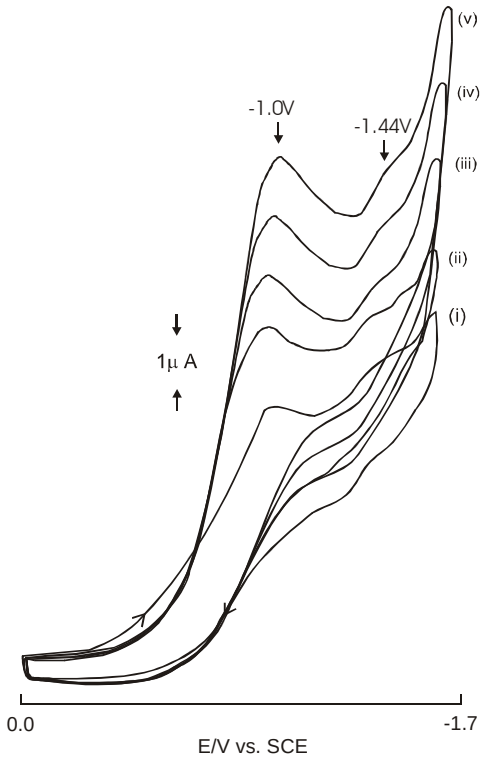

Fig. (V-71): Cyclic voltammograms of the compound **(4)** (1.14×10^{-3} mol) in DMF (0.1 mol TBAP) at (i) 50 mVs^{-1}, (ii) 100 mVs^{-1}, (iii) 150 mVs^{-1}, (iv) 200 mVs^{-1} and (v) 250 mVs^{-1}.

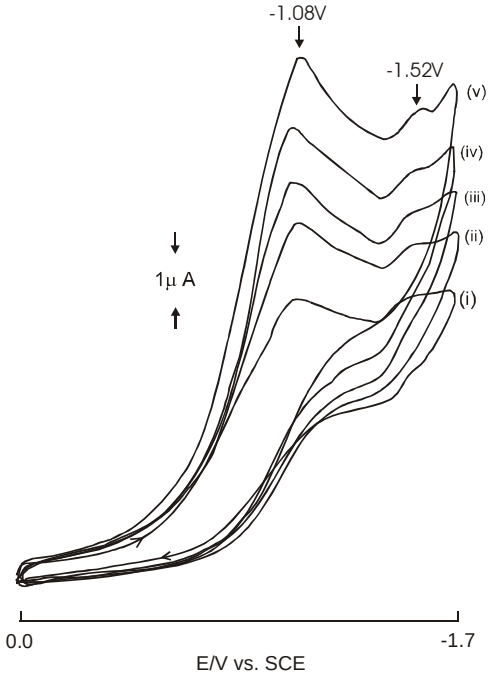

Fig. (V-72): Cyclic voltammograms of the compound **(5)** (1.17 x 10^{-3} mol) in DMF (0.1 mol TBAP) at (i) 50 mVs^{-1}, (ii) 100 mVs^{-1}, (iii) 150 mVs^{-1}, (iv) 200 mVs^{-1} and (v) 250 mVs^{-1}.

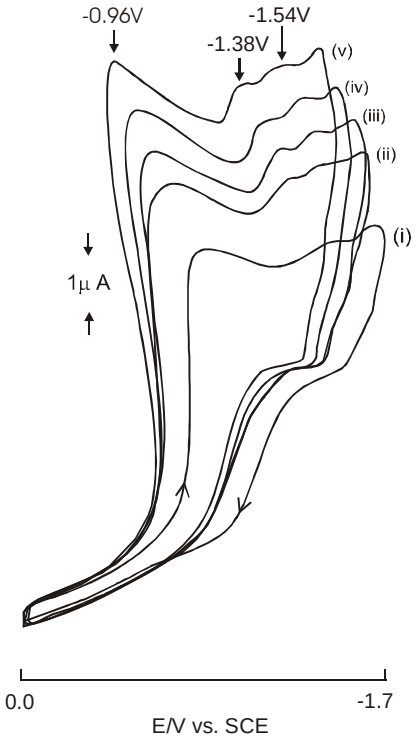

Fig. (V-73): Cyclic voltammograms of the compound **(6)** (1.04 x 10^{-3} mol) in DMF (0.1 mol TBAP) at (i) 50 mVs^{-1}, (ii) 100 mVs^{-1}, (iii) 150 mVs^{-1}, (iv) 200 mVs^{-1} and (v) 250 mVs^{-1}.

In each of the above cases, the metal-centered reduction step makes the complex molecules susceptible to further decomposition through solvent attack.

Conclusion

The foregoing discussions are summarized in Table (V-18).

Here a new series of molybdenum (IV, V, VI) complexes with the pterin ligand ($H_2L^3.H_2O$) have been carefully synthesized and thoroughly characterized through CHN analysis, ESIMS, UV-VIS, FT-IR, NMR and cyclic voltammetry. Their reactivity aspects towards an enzyme substrate like $Me_3N\rightarrow O$ and substrate analogue like PPh_3 have been studied. Isolation of one of the products [compound **(7)**] helps us to understand the oxygen atom transfer (OAT) nature of the reactions. Thus these compounds can be treated as model systems of oxoxmolybdoenzymes. These reactivities help to aertain the presence of a Mo(IV) center in compounds **(1)** to **(5)**.Reactivity of compound **(6)** towards PPh_3 verifies the presence of abstractable S-atom in this compound. Failure of compound **(6)** to with Me_3NO acertain an oxidation state Mo(VI) for this complex. IR spectral data of compound **(7)** [Fig. (V-10)] indicate the presence of a μ-oxo group corresponding to a intense band at 804.3 cm^{-1}[ν(Mo-O_b-Mo) mode]. These physicochemical data (fluorescence, ^{1}H-NMR etc) indicate Scheme (V-10) as the possible pterin ligand anion present in these complexes. The ESIMS data point towards the exceptional stability of the desolvated molecular ions in most cases as well as the binuclear nature of compounds **(6)** and **(7)**. Although no x-ray structural data could be obtained for the above complexes, the above physicochemical data give a comprehensive description of their chemical compositions. The low steric energy values of their CHEM3D models are noteworthy. Here all the three biologically relevant oxidation states (IV, V,VI) of molybdenum have been touched upon, highlighting their relevance to present content. Their reactivity and cyclic voltammetric studies will stand as benchmark data for investigation the oxomolybdoenzymes in future.

Shielding of the NH(2) signal in compounds **(2)** and **(3)** highlight the redox non-innocent behaviour of the pterin ligand of such complexes; during the complex formation process a redistribution of electron density occurs extending all the way from the ancillary ligand through the Mo(IV) atom [$4d_{xy}$/ $4d_y^2$/ $4d_{xz}$ – t_{2g} type orbitals] upto the NH(2) functional group. Significant deshielding of the NH(8) signal on complex formation in most cases, support this view.

Table (V-18) Comparison of different parameters of molybdenum compounds of pterin ($H_2L_1.H_2O$) as primary ligand and the secondary ligand containing sulfur-sulfur and sulfur-nitrogen as donor atoms.

Compounds→ / Parameters ↓	Compound **(1)** of Chapter III	Compound **(1)**	Compound **(2)**	Compound **(3)**	Compound **(4)**	Compound **(5)**	Compound **(6)**	Compound **(7)**
1.Colour	dark brown	orange-yellow	red	reddish yellow	reddish	brown	reddish	reddish yellow
2.UV-VIS	280(4.38), 346(4.69), 376sh(4.58), 415(4.48), 450sh(4.21).	218(4.14), 261 (3.91), 311sh(3.61), 325sh(3.52), 386(3.74), 439sh(3.27)	255(4.52), 288sh(4.21), 388(4.14), 450sh(3.69)	231 sh(3.98), 256 (3.95), 297 sh(3.77), 390 (3.34) 483 sh (3.01)	258 sh(4.18), 294 sh(4.05), 384.5 (4.02), 460 sh(3.49)	234 sh(3.83), 258 sh(3.55), 297 sh(3.39), 385 (3.36), 470 sh(2.90)	255(4.44), 260 sh(4.34), 294(4.14), 380(4.02) ,470 sh (3.57)	210 (5.29), 249.5sh (5.22), 292sh (5.01), 346 (4.93), 383.5 (5.08), 445sh (4.28)
3.Fluorescense (λ_{max}/ nm)	402	475.5	450; 440(sh) 430(sh)	499; 459(sh) 445(sh)	450; 430(sh)	430; 455(sh); 494(sh)	445; 455(sh); 494(sh)	†
4.Steric energy (Kcal/mol)	39.82	29.6	41.5	16.92	18.88	17.20	39.84	32.02
5. C.V [Epc(V) of Mo(IV) →Mo(III)]	-0.98	-1.10	–0.95	–1.0	–1.0	-1.08	-0.96*	†
6. Substrate with which react	$Me_3N\rightarrow O$	$Me_3N\rightarrow O$	$Me_3N\rightarrow O$	$Me_3N\rightarrow O$	$Me_3N\rightarrow O$	$Me_3N\rightarrow O$	PPh_3	†
7.ΔE (HOMO-LUMO) eV	5.66	6.48	1.11	3.44	3.74	4.27	0.19	4.25

*Corresponds to Mo(VI) → Mo(V) reduction peak. † Data cannot be obtained due to unavailability of the compound.